Targeting the interaction between p38α and TAB1

Thapa, Dibesh

Awarding institution:
King's College London

Targeting the interaction between p38α and TAB1

Dibesh Thapa

Thesis submitted for the degree of Doctor of Philosophy

2016

Department of Cardiology
Cardiovascular Division
Rayne Institute, BHF Centre
4th Floor Lambeth Wing
St Thomas' Hospital
London, SE1 7EH

Abstract

p38α, a member of the mitogen activated protein kinase family, is a stress activated serine/threonine kinase which plays an important role in signalling pathways mediating fundamental processes such as inflammation, apoptosis, autophagy, and cell division, differentiation and death. Over the last two decades, its prominence in ischaemic heart disease has risen rapidly with several studies providing overwhelming evidence that p38α activation aggravates lethal injury during myocardial ischaemia. Several inhibitors have been tested to prevent p38α activation and although they have performed well in the laboratory; unfortunately the results have not translated to clinical trials in patients. This has mainly been due to toxicity such as liver injury, skin rashes, gastrointestinal disorders, and flares-ups of rheumatoid arthritis. These adverse effects are shared by different inhibitors, the majority of which belong to the ATP-mimetic, type I group, suggesting they result from an on-target effect of inhibiting ubiquitously expressed p38α. As a result, an alternative therapeutic strategy, other than the blanket inhibition of p38, is required. TAB1 mediated p38α activation appears to be the culprit behind the detrimental p38α signalling during myocardial ischaemia and selectively targeting this branch of p38α activation, without affecting prototypical p38α activation, is highly desirable. In this thesis I studied the structural features of p38α and TAB1 which contribute to the TAB1-mediated p38α autoactivation mechanism. Using various biochemical and biophysical tools in *in-vitro* and *ex-vivo* systems, I have identified the key residue in p38α, and TAB1, which contribute to the auto-activation of p38α by TAB1. The results from my investigations suggest that targeting these residues impairs the autoactivation process and these structural features may be exploited to elucidate p38α's role in myocardial ischaemia. Ischaemic heart disease continues to be the biggest killer in the world, and the search for p38α inhibitors still continues without any fruitful outcomes. A new direction and strategy focusing on circumstance selective inhibition is required in p38α therapeutics, and hopefully the results in my thesis will contribute to that search.

Acknowledgements

First and foremost, I would like to sincerely thank my principal supervisor Professor Michael Marber for giving me this amazing opportunity to work with him. For his limitless knowledge, and encouragement, which helped me become a better scientist, and for his guidance and unrestrained support from the first to the last day, which helped me sail this 3 years of PhD without any problems; I will forever be grateful to him.

I would like to thank Dr Gian De Nicola and Dr Rekha Bassi, both of you trained me everyday to be a competent researcher. I am extremely grateful to you both as I learned several lab skills and gained tremendous amount of knowledge. Next, I would like to thank everyone in the Marber group and Conte group; Dr Denise Eva Martin, Dr Charles Nichols, Dr Asvi Francois, Dr Aminah Loonat, Dr Pelin Arabacilar, Vittorio De Santis, Giancarlo Abis. Each one of you has helped me throughout my PhD, whether it was a helpful suggestion, discussion of my work, splitting my cells or just having a laugh, thank you to all.

Thank you Shreeju Rai for encouraging me to embark on this journey and then for being at my side through thick and thin. It was your words after long day of work that helped me get by, especially on tough days. Dhanyabad to my yaars Kushal, Bishal, Ranjana and Rishu, you guys are my chill-pill, 10 years and counting.

Finally, a very special thank you to my parents and my brother. Without them I would not be here today. Their unconditional love and continuous support is the reason I was in a position that enabled me to apply for this PhD. Nothing I will ever do would repay the sacrifices my parents have made for me, but I would like to start now by dedicating this thesis to them.

Table of contents

List of Figures

List of Tables

Abbreviations

^{o}C	Degree Celsius
µg	Microgram
µl	Microlitre
µM	Micromolar
ADP	Adenosine diphosphate
AMP	Adenosine monophosphate
ANOVA	Analysis of variance
APS	Ammonium persulphate
ASK1	Apoptosis signal-regulating kinase 1
ATF2	Activating transcription factor 2
ATP	Adenosine triphosphate
BSA	Bovine serum albumin
cDNA	Complimentary DNA
CHF	Chronic heart failure
CICR	Calcium induced calcium release
CMV	Cytomegalovirus
C-terminal	Carboxyl terminal
DAPI	4',6-diamidino-2-phenylindole
DMEM	Dulbecco's modified eagle medium
DMSO	Dimethyl sulfoxide
DNA	Deoxyribonucleic acid
dNTP	Deoxynucleotide
DTT	Dithiothreitol
E.coli	Escherichia coli
ECL	Enhanced chemiluminescence
ECM	Extracellular matrix

EDTA	Ethylene diaminetetraacetic acid
EGTA	Ethylene glycol tetraacetic acid
ERK	Extracellular signal regulated kinase
FBS	Foetal bovine serum
g	Gram
GPCR	G-protein coupled receptors
H9C2	Rat heart-derived embryonic myocyte
HEK	Human embryonic kidney
HEPES	4-(2-hydroxyethyl)-1-piperazineethanesulfonic acid
IEC	Ion exchange chromatography
IL-6	Interleukin 6
IPTG	Isopropyl β-D-1 thiogalactopyranoside
ITC	Isothermal titration calorimetry
IVK	In vitro kinase
JNK	c-Jun N-terminal kinase
kDa	Kilo Dalton
KI	Knock in
LB	Luria-Bertani
LDH	Lactate dehydrogenase
LPS	Lipopolysaccharide
LTCC	L-type calcium channel
LV	Left ventricle
LVDP	Left ventricular developed pressure
LVEDP	Left ventricular end diastolic pressure
MAPK	Mitogen activated protein kinase
MAPKK	Mitogen activated protein kinase kinase
MAPKKK	Mitogen activated protein kinase kinase
MEF	Mouse embryonic fibroblast

mg	Milligram
MI	Myocardium infarction
mM	Millimolar
mmHg	Millimetres of mercury
mPTP	Mitochondrial permeability transition pore
mRNA	Messenger ribonucleic acid
NADH	Nicotinamide adenine dinucleotide
ng	Nanogram
nM	Nanomolar
NMR	Nuclear magnetic resonance
N-terminal	Amino terminal
PBS	Phosphate buffered saline
PCR	Polymerase chain reaction
PMSF	Phenylmethylsulfonyl fluoride
PVDF	Polyvinylidene difluoride
RNA	Ribonucleic acid
ROS	Reactive oxygen species
SAPK	Stress activated protein kinase
SDS	Sodium dodecyl sulphate
SDS-PAGE	Sodium dodecyl sulphate – polyacrylamide gel electrophoresis
SFM	Serum free media
SEM	Standard error of the mean
SI	Simulated ischaemia
SR	Sarcoplasmic reticulum
TAB1	Transforming growth factor -β –activated protein kinase 1 binding protein 1
TAE	Tris-acetate-EDTA
TAK1	Transforming growth factor -β –activated protein kinase 1
TAO1/2	Thousand and one amino acid protein kinase

TBS	Tris buffered saline
TBST	Tris buffered saline-Tween
TEV	Tobacco Etch Virus nuclear-inclusion-a endopeptidase
TEMED	Tetramethylethylenediamine
TGF	Transforming growth factor
Thr	Threonine
TNF-α	Tumour necrosis factor alpha
Tris	Tris (hydroxymethyl) methylamine
Tyr	Tyrosine
UV	Ultraviolet
WT	Wildtype
ZAP70	Zeta-chain-associated protein kinase 70

1 Introduction

1.1 Ischemic Heart Disease

Ischemic heart disease (IHD) is a pathological condition caused by an inadequate supply of blood to the myocardium. IHD also known as coronary artery disease (CAD) or coronary heart disease comprises a group of diseases which includes angina, myocardial infarction and sudden cardiac death. IHD along with heart failure, arrhythmias, cardiac arrest and stroke contributes to cardiovascular diseases (CVD). In 2010, more than 17 million deaths globally were caused by CVD; 7 million of which were caused by IHD (Lozano *et al*, 2012). 80,000 of the 7 million deaths were in the UK and together with 49,000 deaths from Stroke, it resulted in cardiovascular disease being the most common cause of death in the UK with almost 180,000 deaths in 2010 (BHF statistics, 2010). The morbidity and mortality from IHD is substantial and chronic CVD affects a significant portion of the population. It not only decreases quality of life but also causes an enormous pressure on an already limited NHS budget. In 2009 alone, it cost the UK's healthcare system £8.7 billion (BHF statistics, 2010).

The hallmark of ischaemic heart disease, as the name suggest, is ischaemia of the heart, i.e. lack of an adequate supply of blood. This prevents delivery of sufficient oxygen and nutrients to, and/or removal of the metabolites from, cells within the heart muscle. The cells cannot function or survive without oxygen that is required for aerobic respiration and metabolic imbalance triggers several biochemical reactions which can lead to myocyte death (Ferrari, 2000). There are many risk factors for IHD with the most common being smoking, hypertension, obesity, diabetes mellitus, high cholesterol and unhealthy lifestyle; consequently, 90% of IHD may be preventable (McGill *et al*, 2008). The current management for IHD is medication with Statins, which reduce cholesterol levels in the blood and anti-platelet therapy such as aspirin that prevents the risk of thrombus formation and Myocardial Infarction following erosion or rupture of an atherosclerotic plaque (Gutierrez *et al*, 2012; Wolff *et al*, 2009).

1.2 Atherosclerosis

Atherosclerosis, a vascular disease, is the main underlying cause of ischaemic heart disease (IHD). It is a chronic condition in which over time the artery wall thickens, stiffens and looses elasticity due to the build-up of atherosclerotic plaques. The atherosclerotic plaque is a fatty streak (cholesterol and lipids) that builds up along the inner lining of the arteries in the heart. According to the response-to-injury hypothesis, atherosclerosis begins with the dysfunction of endothelial cells which can be caused by several factors such as smoking, elevated level of LDL due to unhealthy lifestyle choices, hypertension, diabetes mellitus, viral infections, or genetic alterations (Ross *et al*, 1973). The insult of endothelial dysfunction then starts a chain of reactions, beginning with the accumulation of lipids and low-density lipoprotein beneath the endothelium (Hollander *et al,* 1979). This incites an inflammatory response with increased leukocyte, monocytes infiltration from the blood into the blood vessel. The LDL accumulation increases beneath the endothelium in the intima layer and free radicals and oxidizing enzymes, such as lipoxygenase, begin to oxidize the LDL (Yoshida *et al*, 2010). The oxidized LDL further enhances the inflammatory response as infiltrating monocytes differentiate into macrophages (Zhang *et al,* 2017). The macrophages engulf the oxidized LDL, via scavenger receptors, in an attempt to clear these particles. The intracellular LDL persists and in the process the macrophages turn into foam cells. The damage to the endothelial layer stimulates the proliferation and migration of the smooth muscle cells to form a fibrous cap. The process continues slowly and the vicious cycle of inflammatory response results in the growth of the foam cells leading to formation of fatty streaks in the blood vessel (Ross, 1999).

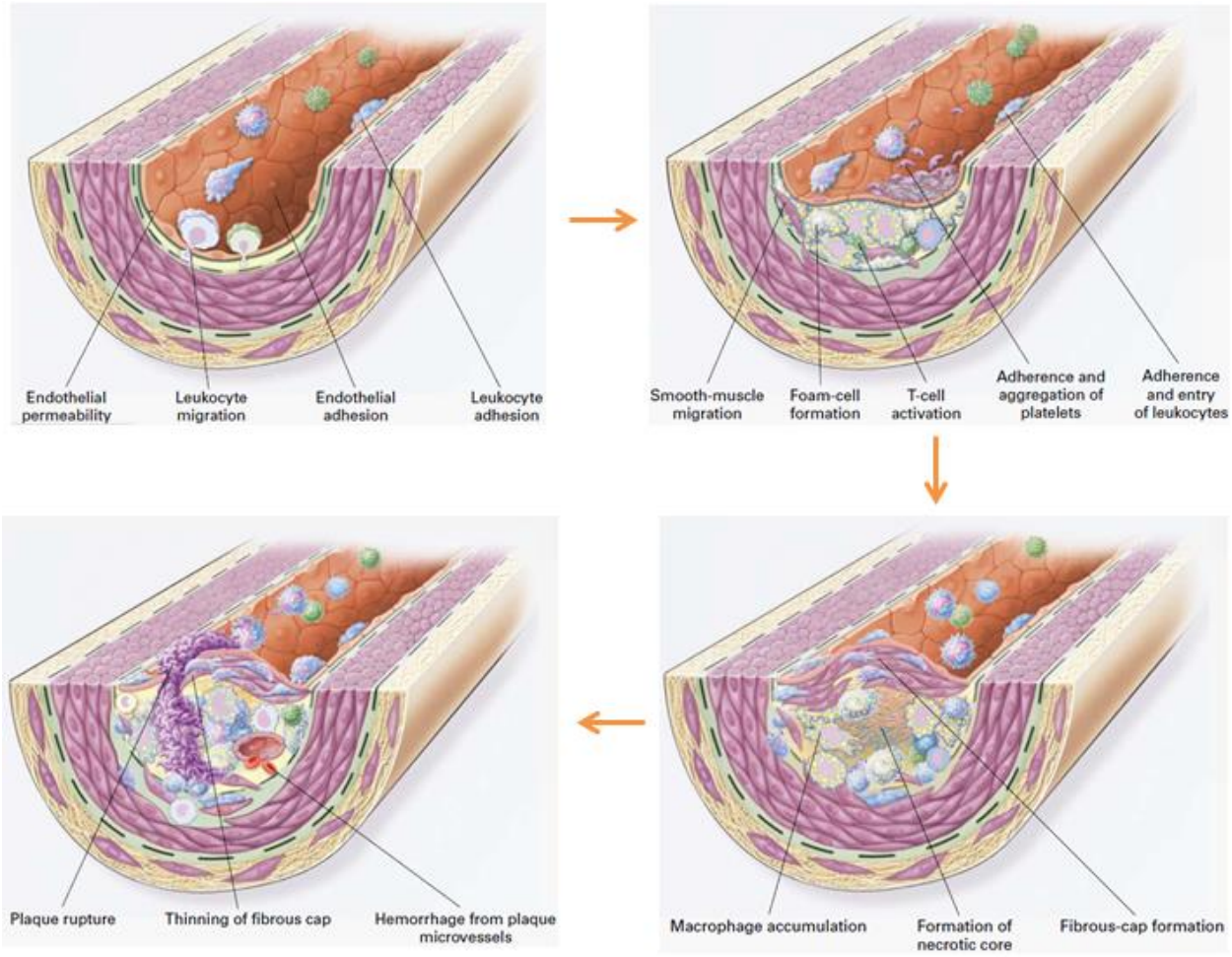

Figure 1.2 Progression of atherosclerosis: *The figure shows the mechanism of atherosclerosis as it progresses from one stage to another. The disease starts with endothelial dysfunction that causes an inflammatory response resulting in the formation of fatty streaks. A fibrous cap forms around the lesion and fatty streaks as a healing response but over time it can become unstable and rupture to cause thrombosis. The thrombus may occlude the artery which can result in Myocardial Infarction (Ross, 1999).*

Over time, the size of the atherosclerotic plaque increases, hardening the artery wall and obstructing the blood flow in the lumen of the artery. The lack of proper supply of the blood (oxygen and nutrients) leads to a condition known as angina pectoris – chest pain caused by cardiac ischemia. There are two types of angina; stable angina and unstable angina. Stable angina is a chest discomfort that is only felt during an activity such as walking, running or other physical or mental stress, but not during rest. In unstable angina however, chest pain symptoms occur during rest and are unpredictable. The difference between the two types of angina is determined by the pathophysiology of the atherosclerotic plaque within the coronary artery

(Chen *et al,* 2009). In stable angina, the atheromatous plaque restricts the full supply of the blood flow in the heart but the plaque itself is protected by a fibrous cap. The demand for blood by the heart is not high during rest; as a result myocardial ischaemia does not occur under resting conditions, so the patient is asymptomatic and angina-free. However, on exercise, the heart has to work harder to meet the body's demands and as a result its own oxygen demand increases. The increased demand cannot be met due to the atheromatous plaque obstructing the conduit epicardial artery, and preventing the increase in myocardial blood flow. As a consequence of the mismatch between myocardial demand for blood and coronary artery supply; ischaemia ensues which the person fells as chest discomfort. In unstable angina, the atheromatous plaque is unstable, causing variable obstruction/embolization which impedes flow to the heart muscle at rest. The processes contributing to instability include platelet aggregation and formation of blood clot/thrombus. The thrombus can occlude the residual lumen of the artery and block the vessel completely or it can travel down the artery and then block the smaller blood vessels within the myocardium. Unstable angina can therefore lead to Myocardial Infarction (Rajpurohit *et al, 2015)*. The likelihood of this progression is diminished by drugs and mechanical disruption of the plaque by balloon angioplasty and stent insertion (Clarkson *et al,* 1999).

1.3 Myocardial Infarction (MI)

Myocardial Infarction (MI) occurs when a thrombus blocks an epicardial coronary artery, or smaller distal blood vessels, to impede myocardial blood flow. Without blood, the oxygen and nutrients cannot be delivered to the region of the heart and metabolites cannot be washed out, as a consequence the effected area of myocardium cannot function normally.

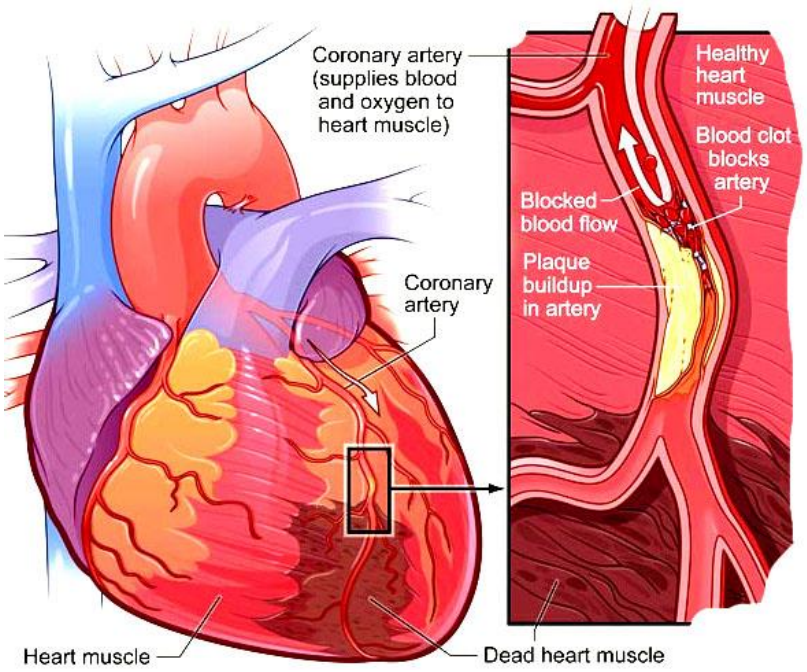

Figure 1.3 Myocardial infarction: *The diagram shows the damage to the heart caused by Myocardial Infarction. The atheromatous plaque and blood clot blocks the blood flow in the coronary artery which results in the necrosis of the distal region of myocardium supplied by the blocked coronary artery (National Institute of Health- https://www.nhlbi.nih.gov/health/health-topics/topics/heartattack).*

The immediate consequence of the thrombus is the creation of a hypoxic environment in the subtended myocardium. Without oxygen, the krebs cycle and oxidative phosphorylation ceases, which results in a dramatic fall of ATP production. In an attempt to maintain the ATP:ADP ratio, the cell switches to anaerobic respiration and glycogen breakdown and glucose uptake increase to stimulate glycolysis. The glycolysis converts a glucose molecule into 2 pyruvates and 2 ATPs. Due to the lack of oxygen, pyruvate cannot be oxidized to acetyl-coenzyme A (Acetyl-CoA) to feed into the Krebs cycle, making glycolysis the sole source of ATP. To increase the ATP production the cell speeds up glycolysis by converting pyruvate to lactate through lactate dehydrogenase, which in turn produces NAD^+ from NADH that is required for glycolysis (Guth *et al*, 1990; Marshall *et al*, 1981). Glycolysis however only produces around 5% of energy compared to aerobic respiration (2 ATP compared to 38 ATP per glucose) which is not enough to sustain proper cellular functions (Stanley, 2001). The cycle continues and lactate build-up overwhelms cell as it cannot be washed out due to lack of perfusion. The consequence is low

cellular pH which has two significant effects; first, it slows down glycolysis by inhibiting phosphofructokinase 1 (PFK), one of the enzymes in glycolytic pathway and second, it disrupts cellular haemostasis which triggers a host of downstream event that cause the cellular dysfunctions apparent in acute myocardial infarction (AMI) (Jennings, 1991).

The acidic environment caused by build-up of lactic acid activates the sodium-hydrogen exchanger, which in an attempt to normalise pH, causes intracellular sodium accumulation (Huber *et al, 2012)*. The increase in intracellular sodium in turn causes activation of the sodium-calcium exchanger, thereby causing the intracellular calcium concentration to rise. These abnormal biochemical changes can disrupt the heart's rhythm and chronotropic state (Murphy *et al, 2002)*. For example, the rise in intracellular calcium can overload the mitochondria, and sarcoplasmic reticulum (SR) which causes calcium leakage into the cytosol (calcium sparks). The calcium exits through the $3NA^{+}/2Ca^{+}$ exchanger that results in a net inward depolarizing current, which can trigger delayed after depolarisation. The low ATP caused by ischaemia affects the ion pumps such as sodium/potassium ATPase which causes imbalance in ionic gradient and results in increased extracellular potassium concentration (Fozzard et al, 1985). This in turn decreases the resting membrane potential of the cardiac cells and affects their excitation. The high extracellular potassium also causes reduction in duration of the action potential which makes its susceptible to re-excitation. The high potassium permeability can trigger early repolarisation and shorten refractory period which all may contribute to re-entry. Sodium channels responsible for the action potential exist in three forms; open, inactivated and closed. During ischaemic depolarization, the cell shifts the balance towards the inactivated state of these sodium channels which greatly reduces the number of channels available to be opened resulting in reduced excitation and conduction velocity (Fozzard et al, 1985). Additionally, the low pH increases the resistance of gap junctions and slows electrical conduction through the ischaemic myocardium (De Mello, 1982). All these ionic/electrophysiological perturbations in ischaemic myocardium predispose the heart to arrhythmias (Ruwald *et al, 2014)*.

Ischaemia also affects the ionotropic function of the heart. Under normal perfusion of the cells, 1/3 of ATP produced in the cell is used by ATPase pumps such as Na/K ATPase and the calcium pump (SERCA) in the sarcoplasmic reticulum, whereas 2/3 of ATP is used during contraction/relaxation by myosin ATPase to achieve crossbridge recycling (Stanley, 2001). So, the shortage of ATP during ischaemia means the ATPase channels cannot function properly which leads to the accumulation of sodium and calcium in cells which affects myocytes excitation, which in turn affects excitation -contraction coupling. The process of contraction is profoundly perturbed since the reduction in the concentration of ATP:ADP prevents myosin from detaching from actin at the end of the power stroke. This is exacerbated by the high intracellular calcium concentration which sensitises the myofilaments by binding to troponin C. The end result is rigor bond formation and a stiff non-contractile heart. This will affect excitation-contraction coupling and prevent the proper contraction of the heart.

With prolonged starvation of blood, cells in the heart will start to die by necrosis and apoptosis. Apoptosis is an event whereby cells under-go programmed cell death characterized by nuclear fragmentation and generation of apoptotic bodies (Arbustini *et al*, 2008). Necrosis on the other hand is a premature cell death caused by an external insult such as ischaemia that results in degradation of cell membranes and release of cellular products into the extracellular space which triggers an inflammatory reaction. During myocardial infarction, cardiac myocytes in the ischaemic region die by both apoptosis and necrosis, although it is unclear how much each pathway contributes to the infarction (James, 1998). Apoptosis is an energy-dependent event; as a result the energy depleted cells in the centre of the infarct are believed to die via necrosis, whereas the less energy-compromised cells in the border region of the infarct are believed to die via apoptosis (Webster, 2012). Early ischaemic stress may induce apoptosis but with prolonged ischaemia converts to necrosis as ATP concentration drops (Cruchten et al, 2002). With prolonged ischaemia, there is a significant rise in ADP, AMP and phosphate concentration in the cells. The increased AMP is converted into adenosine which is converted to inosine and xanthine through the purine degradation pathway. In the presence of residual oxygen, xanthine reductase

can be oxidized to xanthine oxidase which produces superoxide and other damaging reactive oxygen species (ROS) (Haelstrap et al, 2009). Additionally, nitric oxide synthase and NADPH oxidase also contribute towards the formation of harmful ROS and superoxides during ischaemia (Murphy, 2009). The rise in intracellular calcium resulting from low pH causes the mitochondria to take up calcium. The flooding of calcium in mitochondria, with increased phosphate and ROS triggers the opening of the mitochondrial permeability transition pore (mPTP) (Webster, 2012). The mPTP opening means the inner mitochondrial membrane no longer maintains a proton barrier which completely stops oxidative phosphorylation. Another major consequence of mPTP opening is the leakage of molecules smaller than 1.5kDa from the mitochondria (Seidlmayer *et al*, 2015). This not only imbalances the metabolic gradient between the mitochondria and cytosol but it also causes the swelling of mitochondria due to colloidal osmotic pressure caused by inflow of small osmolytes. Eventually, as the matrix expands the outer membrane cannot sustain the pressure leading to its rupture. This releases cytochrome c and other pro-apoptotic proteins to initiate apoptotic cell death (Halestrap *et al*, 2009). With prolonged ischaemia, the mPTP opening will drive necrosis and cause infarction of the myocardium. If an extensive area of the heart is affected its ability to pump blood is compromised and the consequence is maladaptive remodelling which eventually causes immediate or delayed heart failure. The mPTP opening is triggered by a combination of high intracellular calcium and ROS, and as ROS production is highest at the point of reperfusion due to the availability of oxygen, it may accelerate damage at the beginning of reperfusion, which is commonly known as ischaemia-reperfusion injury.

1.4 Cardiac hypertrophy

Cardiac hypertrophy is a physical change where the heart grows in size with thickening and/or lengthening of cardiac myocytes. There are two types of cardiac hypertrophy; physiological and pathological (Bernardo *et al*, 2010). Physiological cardiac hypertrophy is a uniform growth of ventricular wall and septum matched by an increase in chamber dimension (eccentric hypertrophy) that results in increased myocardial muscle mass and pumping ability. For example, during pregnancy or in trained athletes the myocardial wall and cavity enlarge as

myocytes increase in length which helps enable the necessary increase in cardiac output (Shimizu *et al*, 2015). Pathological hypertrophy however, is characterized by an uneven growth of cardiac myocytes with a net decrease in the ventricular chamber dimension (concentric hypertrophy) and wall thickening and is accompanied by an extensive fibrosis that does not result in an increased cardiac output (Heineke *et al*, 2006). Pathological hypertrophy is caused by hypertension, outlet valve stenosis, MI, or genetic mutations.

After the ischaemic insult of MI, the heart may undergo a compensatory change in an attempt to restore normal cardiac function (Zaino *et al*, 1963). For example, a prolonged duration of ischaemia can result in a large amount of necrosis and myocardial cell loss. This will affect the ability of the myocardium to pump blood properly and result in a reduced cardiac output for any given filling pressure. In order to compensate for the loss of cardiac output, the heart undergoes a process of pathological cardiac hypertrophy. Pathological cardiac hypertrophy results in further dysfunction of myocardium and with increased interstitial fibrosis the cardiac function progressively deteriorates and causes heart failure (Kerkela *et al*, 2006).

1.5 Heart Failure

Chronic heart failure, also known as congestive heart failure (CHF), is a condition where the heart is unable to pump and supply enough blood to meet the body's demand. It is characterized by shortness of breath, especially during exercise, and tiredness due to the lack of adequate perfusion of tissues with oxygen and nutrients from the blood. The most common cause of heart failure is coronary artery disease and previous myocardial infarction (CHF guideline). Hypertension, atrial fibrillation, and diabetes mellitus can also contribute to heart failure.

Patients that survive an episode of MI can go on to suffer from chronic heart failure if there is extensive damage to the myocardium. After MI, the heart undergoes remodelling to compensate for the damage caused by MI, in an attempt to maintain proper heart function. It is characterized by cardiomyocyte apoptosis, interstitial fibrosis, thinning of the ventricular wall and enlargement

of the ventricular chamber, and hypertrophy (Konstam *et al*, 2011). The immediate phase of remodelling can begin as quickly as a few hours after an infarct and involves the repair/clearance of necrotic tissue and replacement with fibrotic tissue that results in scar formation, elongation and the thinning of the infarct zone (Korup *et al*, 1997). This causes a significant increase in LV volume and in the short term is associated with improved cardiac output. However, if prolonged the latter phase of the remodelling is dominated by extensive fibrosis and pathological hypertrophic growth of the cardiac myocytes that results in a change in the shape of the left ventricular cavity from elliptical to spherical (Mitchell *et al*, 1992). Fibroblasts increase collagen synthesis and cause fibrosis in both infarcted and non-infarcted regions of the heart (Volders *et al*, 1993). Over time, with thin ventricular walls, the systolic and diastolic stress increases and results in further dilation with pathological cardiac hypertrophy. The end-systolic volume increases and the ejection fraction decreases progressively contributing to reduced cardiac output (Cohn *et al*, 2000). With ongoing interstitial fibrosis and pathological cardiac hypertrophy, the cardiac function deteriorates further and eventually causes heart failure.

CHF is a long, debilitating, multimechanistic, complex disease and there are multiple pathophysiological processes involved that lead from the fatty streak to the ruptured complex atherosclerotic plaque that causes myocardial infarction. Following this event are the immediate and delayed consequences of infarction that ultimately lead to heart failure. For the purposes of my research I will focus on the biochemical changes at the cellular level that follow the onset of myocardial ischemia with a particular focus on p38 mitogen-activated protein kinase (p38MAPK).

1.6 Mitogen-activated protein kinases (MAPKs)

MAPKs or mitogen activated protein kinases are a family of serine/threonine protein kinases responsible for relaying extracellular signals into cellular responses. They mediate their function by phosphorylating targets to regulate gene expression and protein function. MAPKs are activated by a wide range of stimuli such as mitogens, growth factors, inflammatory cytokines, pathogens, osmotic stress, heat shock, UV irradiation, ischaemia etc (Ono *et al*, 2000). As a result, MAPKs are involved in a host of cellular functions from gene expression and cell growth/division to survival and cell death. Their involvement in a plethora of signalling events has made MAPKs an attractive target for therapeutic intervention.

The MAPK family is made up of four members; Extracellular regulated kinases (ERK1/2), p38, c-Jun N-terminal kinase (JNK), and ERK5 (Fig 1.6). ERK1/2s' are mainly involved in cellular growth/division (mitosis/meiosis) whereas p38, JNK, and ERK5 are primarily involved in stress signalling pathways involving cytokines, heat shock proteins, ischaemia etc. MAPKs are activated via a 3-tier kinase cascade where the most upstream kinase (MAPKKK) activates an intermediate kinase (MAPKK), which then activates the MAPK. In the case of ERK, RAF proteins activate the intermediate kinase MEK1/2 which then activates ERK1/2. p38 is activated via intermediate kinases MEK3/6, which are activated via MAPKKKs such as TAK1 and ASK1. JNK is activated via intermediate kinases MEK4/7, which are activated via MAPKKKs such as MAPKKK1/2 and ZAK. MAPKs are activated when the dual-intermediate kinase phosphorylates its characteristic T-X-Y motif in the activation loop (T-E-Y in ERK, T-G-Y in p38, and T-P-Y in JNK). The phosphorylation of the T-X-Y motif causes structural rearrangement of the kinase that increases the catalytic activity and facilitates substrate binding, resulting in an increased kinetic activity of the kinase, thus an active kinase (Yurtsever *et al*, 2015).

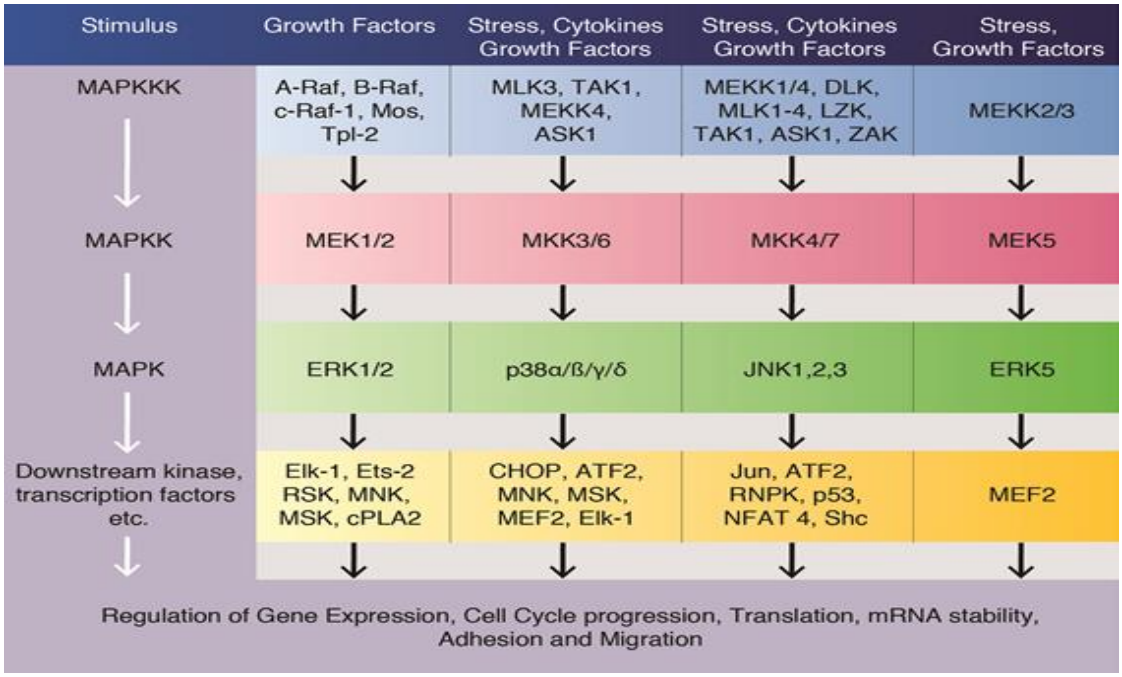

Figure 1.6 The classical MAPK activation pathway: *The diagram shows the classical 3-tier activation pathway of MAPKs with all 4 types of MAPKs; ERK1/2, p38, JNK and ERK5 (ThermoFisher Scientific).*

1.7 p38MAPK

p38MAPK is a 38kDa stress activated protein kinase that was discovered in monocytes that became tyrosine phosphorylated in response to lipopolysaccharide (LPS) (Han, 1994). p38 is made up of 2 main domains; the N-terminal domain (135 residues) mainly made up of β-sheets, and the C-terminal domain made up of α-helices (Fig1.7A). The p38MAPK family consists of four different isoforms; p38α, p38β, p38γ, and p38δ. These isoforms have a high degree of sequence homology, with 75% similarity between p38α (MAPK14) and p38β (MAPK11) isoforms, both of which are sensitive to inhibition by the pyridinyl imidazole molecule SB203580, the archetypal/model inhibitor. SB203580 belongs to the class of classical type I inhibitors which compete with ATP for p38's catalytic site and as a result causes reduced kinetic activity. p38γ (MAPK12) and p38δ (MAPK13) are 70% identical with each other but only 60% identical with p38α. The gatekeeper residue of Thr106 present in p38α/β that is crucial to the binding of these ATP-competitive drugs is replaced by a larger methionine in p38γ/δ, which

renders them resistant to type I inhibitors such as SB203580 (Risco *et al*, 2012). The p38α and p38β isoforms are expressed ubiquitously, p38γ expression is mainly in skeletal muscle and cardiac muscle, and p38δ is highly expressed in endocrine system such as kidney, pancreas, placenta, testis and lung (Cuadrado *et al*, 2010).

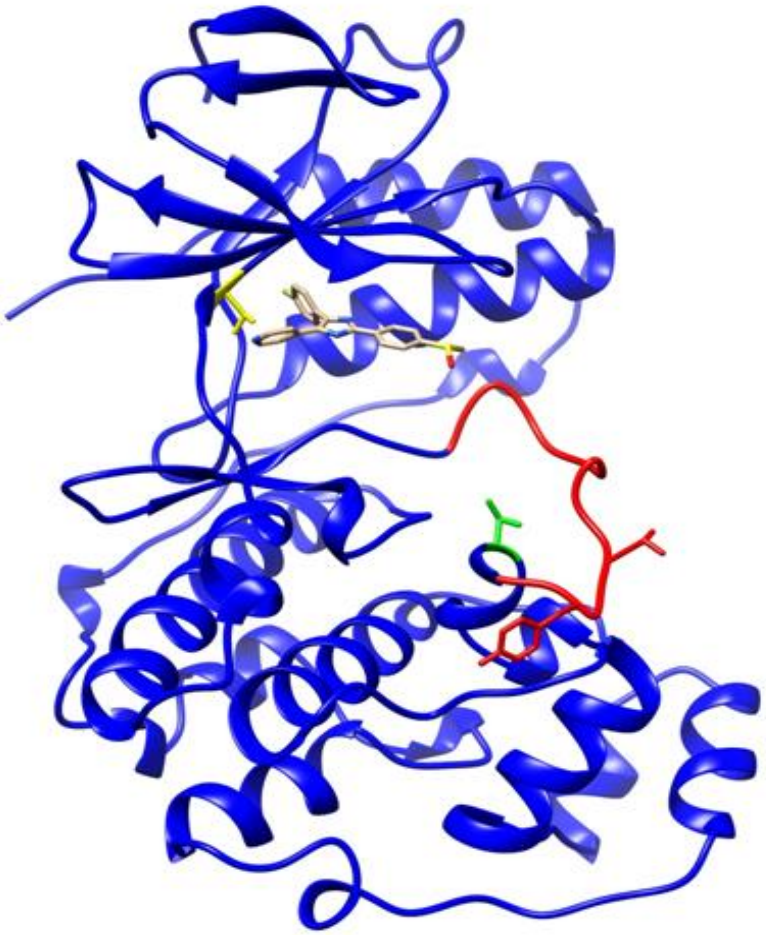

Figure 1.7A The crystal strucutre of p38α in a complex with SB203580: *The crystal structure of p38α (blue) with SB203580 occupying the ATP binding site. The Thr106 (yellow) is the gatekeeper residue and crucial in binding of SB203580 and other ATP-competitive inhibitors. The long activation loop illustrated in red contains the Thr180 and Tyr182 and phosphorylation of these residues makes the kinase active. Illustrated in green is Thr185, which we have hypothesized plays a role in the autoactivation mode of p38α caused by TAB1. The upper, N-terminal lobe, is comprised mainly of beta-pleated sheets (arrows) and the lower, C-terminal lobe, is comprised mainly of alpha helices (Honndorf VS, 2008; PDB:1A9U)*

MAPKs are activated by dual phosphorylation of a conserved Thr-X-Tyr motif on the activation loop by upstream kinases, as described earlier. In p38α, Thr180 and Tyr182 are phosphorylated by the dual specificity kinases, MKK3 and MKK6, and in some cases by MKK4. MKK3/6 in

turn are activated by upstream MAPKKKs such as -TAK1 and ASK1 completing the tri-kinase activation sequence. This describes the classical activation pathway of MAPKs. However in the case of p38, alternative activation mechanisms have been discovered (Fig 1.7B). In T-cells, p38 can become phosphorylated via ZAP70, a tyrosine kinase, on residue Tyr323 (Salvador, 2005). The phosphorylation of Tyr323 induces autophosphorylation of p38's T-G-Y motif, activating p38. Another mode of p38 activation is specific to p38α and it involves a scaffold protein, Transforming growth factor -β –activated protein kinase 1 binding protein 1 (TAB1). The interaction of p38α with TAB1 causes the auto-phosphorylation of T-G-Y motif in cis, thus activating p38α (Ge *et al*, 2002). The TAB1 mediated autoactivation of p38α has gained a lot of interest in the last decade and is the subject of my thesis.

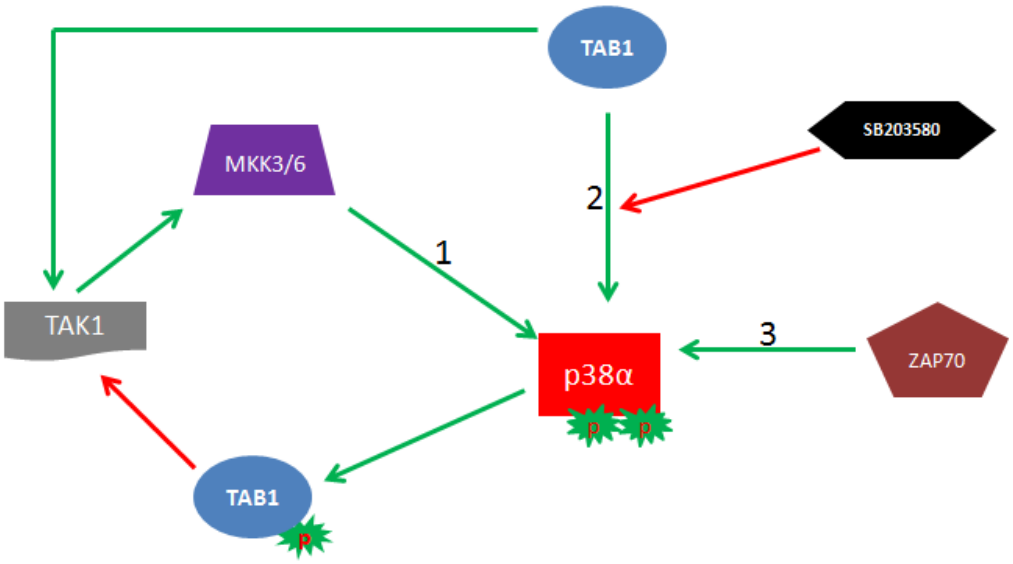

Figure 1.7B Activation mechanisms of p38α*: The schematic illustrates the 3 different activation mechanisms of p38.* ***1*** *is the classical activation pathway where MKK3/6 transphosphorylates p38.* ***2*** *is the TAB1- mediated autoactivation of p38α which is SB203580 sensitive.* ***3*** *shows the activation of p38 in T-cells where a tyrosine kinase ZAP70 causes phosphorylation of Tyr323 which in turn leads to autoactivation of p38. Once activated, p38 phosphorylates TAB1 which suppresses the ability of TAB1 to activate TAK1 and that in-turn reduces the activation of MKK3/6 and p38, which completes the feedback loop. Green line represents activation whereas the red lines represents inhibition.*

1.8 TAB1

Transforming growth factor -β –activated protein kinase 1 binding protein 1 (TAB1) is a scaffold protein and as the name suggest it binds and activates TAK1. The C-terminal region of TAB1 directly interacts with the N-terminal region of TAK1 to cause autophosphorylation of Thr184, Thr187 and Ser192 in the activation loop and induce TAK1's kinetic activity (Shibuya *et al*, 1996; Brown *et al*, 2005). In addition to regulating the TAK1 signalling pathway, TAB1 also plays a role in WNT-1, and interleukin 1 signalling pathways, as a result TAB1 is a vital protein in cellular signalling (Ninomiya *et al*, 1999). In fact its importance is attested by the fact that genetic deletion of TAB1 causes embryonic lethality in mice (Komatsu *et al*, 2002). In 2002, Ge and his group discovered that TAB1 also plays a role in p38α activation (Ge *et al*, 2002). They showed through a series of well-designed experiments that TAB1 binds to p38α and induces p38α autoactivation. The molecular mechanism behind this activation has been unknown for several years until our lab resolved the crystal structure of a p38α-TAB1 complex, and I will discuss this in further detail later in the thesis.

TAB1 is made up of 3 domains; PP2C-like pseudophosphatase domain, p38α binding domain and TAK1 binding domain (Fig1.8). The C-terminal region of TAB1 houses several phosphorylation sites which are important in its regulation; S423, T431, S438, S452, S453, S456, S457. The phosphorylation of S423 and T431 by p38α suppresses the ability of TAB1 to activate TAK1 (Shin *et al*, 2009). There are 4 members in the TAB family; TAB1, TAB2, TAB3, TAB4 (Takaesu *et al*, 2000; Cheung *et al*, 2004; Prickett *et al, 2008).* In this study we focus on TAB1 which is involved in p38α signalling. TAB1 has 2 different isoforms; TAB1α and TAB1β. The TAB1β isoform is approximately 10kDa smaller as it lacks the TAK1 binding domain, however it does have p38α binding domain, hence can induce p38α autoactivation.

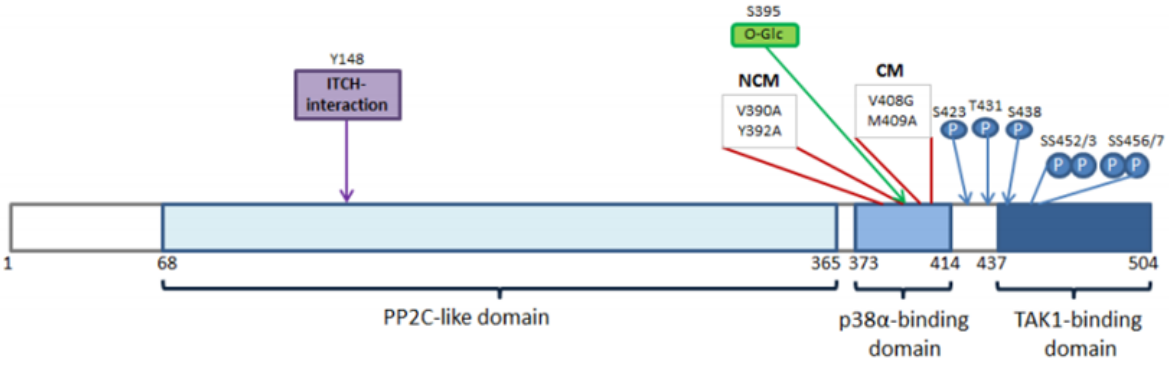

Figure 1.8 TAB1 domains: *The schematic shows TAB1 with its 3 main domains of PP2C-like domain, p38α-binding domain and TAK1-binding domain. TAB1β lacks the C-terminal TAK1 binding domain and as a result cannot activate TAK1. The C-terminus contains several phosphorylation sites which regulate TAB1 activity. CM and NCM regions are the sites responsible for interacting with p38α and induce p38α activation (Pelin Arabacilar).*

1.9 p38's cellular function

p38 is ubiquitously expressed and involved in a myriad of cellular signalling events. Its functional role starts as early as the embryonic developmental stage as the genomic deletion of p38α causes death (Adams *et al*, 2000). Belonging to the stress activated protein kinase family; p38 is primarily involved in the stress signal pathways such as inflammation, ischaemia, heat shock, osmotic stress, and apoptosis.

p38 causes the production of proinflammatory cytokines such as tumour necrosis factor alpha (TNF-α), interleukin 6 (IL-6), and interleukin -1 beta (IL-1β) (Zarubin *et al, 2005*). In fact, p38's role in inflammation was evident by the use of inhibitors which caused the reduction in the inflammatory markers in diseases such as rheumatoid arthritis, chronic obstructive pulmonary disease, coronary vascular disease etc (Westra *et al*, 2004; Armstrong *et al*, 2011; Medicherla *et al, 2008*). Additionally, p38 causes recruitment of adherent proteins such as VCAM-1 and plays a role in the regulation of immune cells (Pietersma *et al*, 1997; Aicher *et al*, 1999). It is widely accepted that p38 plays a role in apoptosis and promotes cell death however some studies have

shown that p38 promotes survival (Sarkar *et al*, 2002; Porras *et al*, 2004; Park *et al*, 2002). p38 has been shown to promote skeletal muscle differentiation, rescue neurons from cell death during neuronal differentiation, and arrest the cell cycle at G2/M under UV exposure (Bulavin *et al*, 2001; Zetser *et al*, 1999; Mao *et al*, 1999). p38 plays a role in proliferation and differentiation of lung epithelial cells as its inhibition was shown to affect lung homeostasis (Ventura *et al*, 2007). p38 has also been shown to play important role in early cardiogenesis during development via HSP25 pathway (Davidson, 2000).

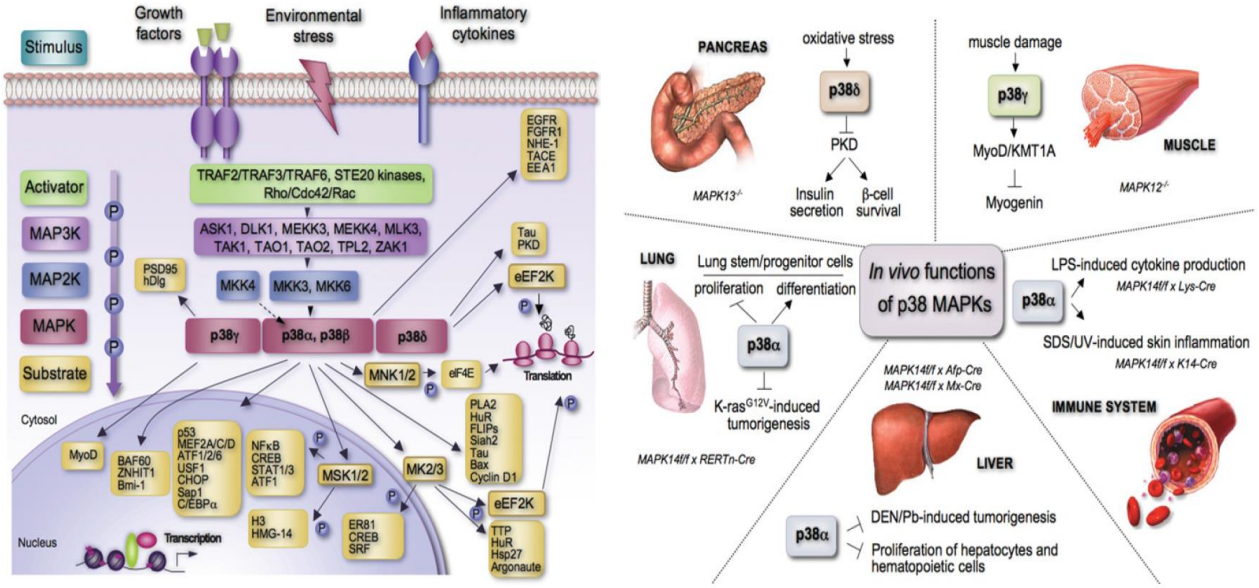

Figure 1.9 Physiological function of p38: *The schematic on the left shows the several signalling pathways p38 is involved in, and the schematic on the right shows the various physiological functions of p38 in different organ system (Caudrado et al, 2010).*

The evidence from the literature shows that p38 plays a role in a plethora of cellular signalling events and physiological functions (Fig 1.9). p38 interacts with a range of proteins that are kinases, phosphatases, scaffold proteins, structural proteins, membrane proteins, transcription factors etc to mediate its effect. For the purpose of my investigation, I will focus the discussion on the role of p38α in ischaemic heart disease (IHD).

1.10 p38 cellular localization

There is contrasting evidence in the literature on the subject of p38's cellular localization. Some have said that p38 translocates into the nucleus from cytoplasm once activated whereas others have said that p38 translocates into the cytosol once activated (Raingeaud *et al*, 1995: Ben-Levy *et al*, 1998). The discrepancy could arise from the fact that there are 4 different isoforms of p38 and they may interact differently with scaffold proteins depending upon stimulus which could determine its location in the cell. For example, in early phase of pressure overload hypertrophy, p38α and p38β were found in both cytoplasm and nucleus with no signs of p38γ and p38δ. However, in the late phase of hypertrophy the appearance of p38γ increased in the nucleus whereas the p38α's distribution remained unaffected (Dhanmendra *et al*, 2010).

One of the problems in determining the mechanism behind p38's cellular localization is the fact that unlike other MAPK's, p38 does not have a nuclear localization signal. For example in ERK2, during pathological cardiac hypertrophy ERK2 translocates into the nucleus after it autophosphorylates itself and unlocks the nuclear localization signal (Lorenz *et al*, 2008). In my study, I will investigate if p38α has a similar characteristic.

1.11 p38MAPK signalling in IHD

As mentioned earlier, ischemia in the heart causes several intricate biochemical changes within the cell that can lead to detrimental outcomes. This is where the p38 signalling comes into play, the p38**α** isoform to be more specific. MAPKs are well-known for their function in cell growth and division, with their associated pathological conditions of cancer and tumour formation. As a result, a huge amount of effort has been concentrated in studying MAPKs in the field of cancer biology. However with stress activated p38, MAPK's prominence in CVD is increasing rapidly, especially in ischemic heart disease. Studies in our lab and by several other groups have shown that there is an activation of p38α during myocardial ischemia and that this could be central to the damage caused under this circumstance. Ma *et al* showed that inhibiting p38 using SB203580 decreased apoptotic events and increased cardiac function in Langendorff perfused

rabbit hearts (Ma *et al*, 1999). Barancik and his group showed inhibition of p38α by SB203580 delayed ischaemic cell death in pig hearts (Barancik *et al*, 2000). Kaiser showed p38 works as a pro-death signalling molecule in both cultured myocytes and intact heart in rats (Kaiser *et al*, 2004). Gray's group showed p38α inhibitor SB239063 reduced apoptotic events and infarct size, and improved cardiac function (Gray *et al*, 2011). There are 100 additional publications from independent labs which collectively suggest that p38α aggravates the lethal injury to the heart. Therefore, appropriate controlled regulation of p38α might provide an opportunity to limit or inhibit the damage caused by p38α, and prevent the injury that occurs during and following MI. Such a therapy could limit myocardial infarction and its sequelae such as arrhythmia, pathological cardiac hypertrophy and heart failure.

p38α can be activated via three different routes as discussed earlier and interestingly, it is not the classical activation of p38α that occurs during myocardial ischemia. In a study carried out using a transgenic mouse model of wild-type MKK3 and knockout MKK3 -/- hearts, after 30 minutes of global ischemia, both WT MKK3 and MKK3 -/- hearts produced similar levels of p38 phosphorylation and infarction (Tanno *et al*, 2003). The study demonstrated activation of p38 despite the knockout of its activator MKK3, indicating p38 activation was not mediated via the canonical MAPKKK cascade. Instead, this unique activation of p38α was induced by interaction with the non-enzymatic scaffold protein TAB1. The interaction of p38α and TAB1 increases p38α's affinity for ATP, which results in increased catalytic activity and autophosphorylation of its Thr180 and Tyr182 residues, thus activating p38α (Ge *et al*, 2002). SB203580, an ATP-mimetic, inhibits this event by interacting with the gatekeeper residue Thr106 to occupy the ATP binding site which prevents ATP from binding, consequently inhibiting autophosphorylation of the T-G-Y motif (Eyers *et al*, 1999; Barancik *et al*, 2000). Recently, the molecular details of the interaction between p38α and TAB1 which leads to autophosphorylation of p38α were elucidated (De Nicola *et al*, 2013); it revealed that TAB1 makes a direct contact with p38α at two sites and confirmed that p38α autophosphorylates its activation loop in *cis*.

1.12 p38α and TAB1

The interaction between p38α and TAB1 that leads to p38α's autophosphorylation is a true enigma in the field of biology. Firstly, p38α is a serine/threonine kinase and yet it autophosphorylates itself on the Tyr182 residue of the activation loop. Secondly, for p38α to be activated, the T-G-Y motif needs to be phosphorylated by an upstream kinase which then induces the structural changes to increase ATP affinity and open the substrate binding cleft. However, in the case of TAB1-induced autophosphorylation, the ATP binding precedes the phosphorylation of the T-G-Y motif (De Nicola *et al*, 2013). This paradox has been likened to a "catch 22", and although being an unusual event this phenomenon has also been observed in other mammalian kinases (Lochhead *et al*, 2009; Shrestha *et al*, 2012). In 2013, our lab resolved the crystal structure of a p38α-TAB1 complex which answered the conundrum behind the catch 22 paradox. The crystal structure of p38α complexed with a chemically synthesized region of TAB1 peptide (384-412) responsible for the interaction revealed that the action of TAB1 binding mimics the effect of phosphorylation of the T-G-Y motif by MKK3/6, which causes an increased affinity of p38α towards ATP. The activation loop swings towards the catalytic site bringing the T-G-Y motif near ATP to facilitate autophosphorylation and make p38α kinetically active. The phosphorylation of Tyr182 residue however, still remains a mystery. The crystal structure and NMR data showed that TAB1 binds to p38α in a bipartite manner. The N-terminal region of TAB1 peptide binds to the lower hydrophobic pocket of p38α created by the αF and αH helices and the loop connecting helix α21.4 to helix αH (noncanonical lower site). The C-terminal region of the TAB1 peptide binds within the groove created by αD and αE helices and the reverse turn between β7 and β8 (canonical upper site or ED domain (Fig 1.12).

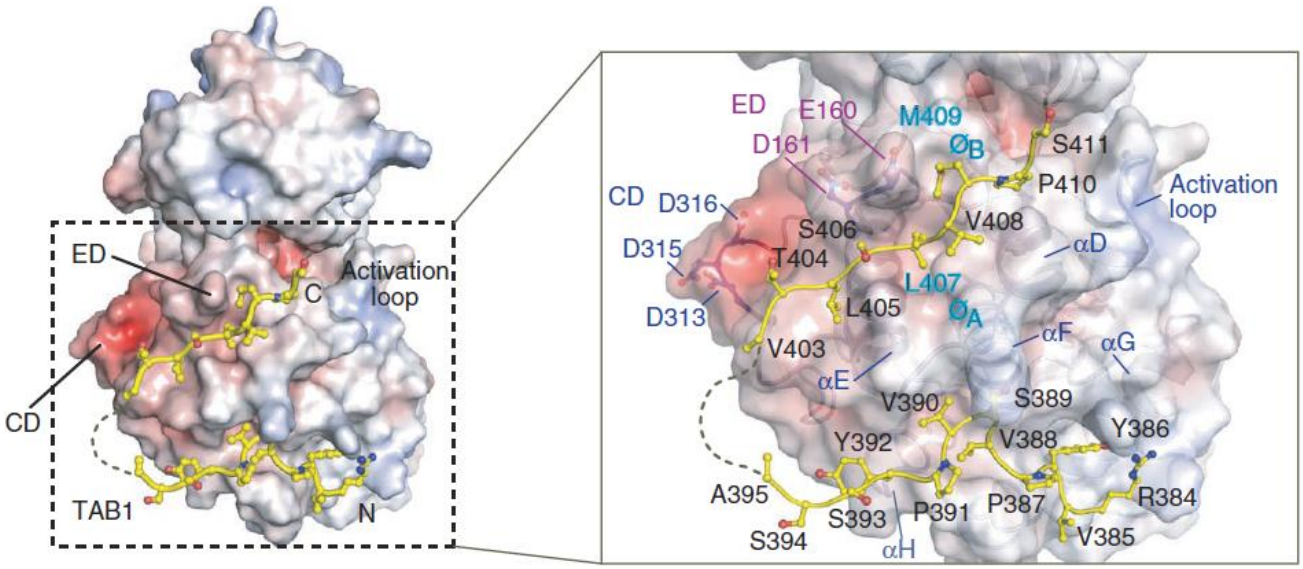

Fig1.12 Structural overview of p38α with TAB1 peptide (384-412): *The crystal structure revealed p38α binds to TAB1 in a bipartite manner as seen in this figure. The zoomed in section on right highlights the residues that are involved in the interactions (De Nicola et al, 2013)*

1.13 p38 inhibitors and clinical trials

One of the reasons why the studies on p38α took off over the last decade was due to the availability of several inhibitors especially those belonging to the Type I class, based on the pyridinyl imidazole backbone (Fig 1.12). These inhibitors compete with ATP for the catalytic site which results in reduced kinetic activity of the kinase and as a result inhibits the phosphorylation of its substrates. The crystal structure of the p38α-pyridinyl imidazole complex revealed that these inhibitors bind to an aryl-specificity pocket located behind the active site which is normally occupied by ATP's adenine ring. The 4-pyridinyl moiety of the drug interacts with the Thr106 (gatekeeper residue) in the hydrophobic pocket of p38α (Fig1.6A). In p38γ and p38δ the Thr106 is replaced by a bulkier methionine which prevents the drug accessing the catalytic site, and hence these p38 isoforms are resistant to these drugs (Eyers *et al*, 1998).

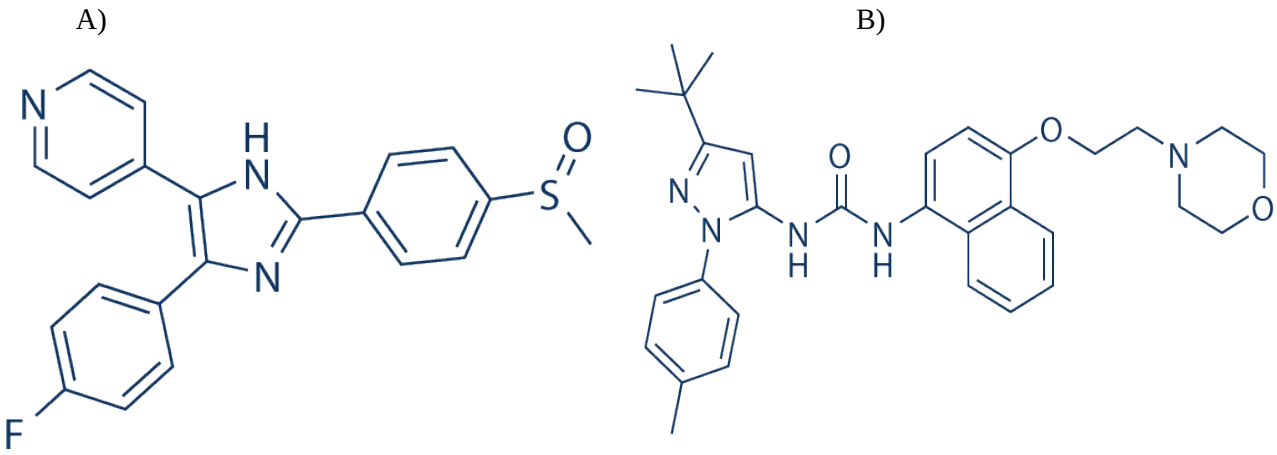

Figure 1.13: A) *The image shows the chemical structure of SB203580 (molecular weight: 377.43) which belongs to the Type I class of ATP competitive inhibitors.* ***B)*** *The image shows the chemical structure of BIRB796 (molecular weight: 527.66) which belongs to the Type II class of inhibitors.*

The majority of clinical trials of p38 inhibition were carried out for inflammatory diseases such as arthritis, chronic obstructive pulmonary diseases, psoriasis, and atherosclerosis. The initial success of these inhibitors in animal models had promised a positive outcome in clinical trials but it was not to be the case as almost all inhibitors failed. RWJ-67657, a p38α and p38β specific inhibitor, was one of the few inhibitors that promised positive results as several groups showed that it was good at lowering inflammatory biomarkers with minimal toxicity suggesting it could be useful in treating rheumatoid arthritis and sepsis (Fijen *et al*, 2001; Faas *et al*, 2002; Parasrampuria *et al*, 2003). It was in a phase I clinical trial for the treatment of arthritis and inflammatory bowel disease but it failed, and this turned out to be a trend that was followed by most inhibitors. VX-745 was shown to suppress the release of inflammatory mediators such as interleukin (IL)-1beta and tumour necrosis factor (TNF) alpha but it caused an elevation in liver transaminases (Haddad *et al*, 2001). Pamapimod, a selective inhibitor of p38α, was shown to have limited efficacy and cause adverse side effects like infection, skin disorders and dizziness (Cohen *et al*, 2009). VX702 was shown to reduce the inflammatory biomarkers but was associated with severe infections (Damjanov *et al*, 2009). A randomised study on the effect of BIRB-796 in Crohn disease found no efficacy and it caused liver toxicity (Schreiber *et al*, 2006). SCIO-469 had poor potency and patients suffered from rashes, dizziness, constipation, and

arthralgias, which were dose related (Genovese *et al*, 2008). More recently, the LATITUDE-TIMI 60 study was carried out after promising data from a phase 2 trial in non-ST elevation MI patients had indicated that Losmapimod attenuated inflammation and may improve outcome. But after the initial study in 3503 patients showed no difference in the reduction of major ischaemic cardiovascular events in 18 months, the second part of the trial involving approximately 22000 patients was then suspended (O'Donoghue *et al*, 2016).

At least 22 different p38 inhibitors have been investigated in PhaseI/II of clinical trials and the few that reached the phase III stage also failed (Hammaker *et al*, 2010). The lack of efficacy and selectivity, and the profound adverse side effects have significantly hampered the progression of p38α inhibitors in clinical trials. An alternative solution is therefore required to inhibit p38α, one of which could be not to target p38 directly but indirectly. Targeting other proteins involved in the p38 signalling pathway, and not p38α itself which is ubiquitously expressed and involved in a plethora of signalling events, could be the way forward.

1.14 Targeting the p38α-TAB1 interaction

The race to discover an effective inhibitor for p38α has been futile as discussed above and it is not surprising considering the nature of the target. Firstly, p38α belongs to the kinase family that comprises over 500 members, where the majority of them share some homology which makes achieving selectivity extremely difficult. Next, p38α is ubiquitously expressed and involved in several physiological events. Along with the detrimental role it plays in myocardium during MI and HF, it is also vital in maintaining physiological homeostasis and is involved in a plethora of cellular responses. Finally, there are 4 different isoforms of p38 in p38α, p38β, p38γ, and p38δ and all four isoforms are associated with variety of functions in different cell types. So selectively targeting p38α in the heart during MI is an inherently difficult task.

As a result the TAB1-mediated p38α autoactivation occurring in MI provides a new opportunity to target p38α therapeutically. The fact that p38α is activated via TAB1 during ischaemia means

we can selectively target this branch of p38α activation without affecting the classical activation pathway that is involved in very many other important signalling cascades. It allows us to achieve the circumstance-specific inhibition of p38α just in the event of MI. And as we are avoiding the blanket inhibition of p38α, it could potentially eradicate the toxicity problems seen with p38α inhibitors, which has been the Achilles heel in the clinical trials. The involvement of TAB1 in other important signalling pathways such as the TAK1 pathway also means that TAB1 cannot be targeted. Therefore, the best approach is to specifically target the interaction between p38α and TAB1. That could be achieved by either preventing the interaction between the two proteins or breaking the p38α-TAB1 complex once it forms.

In order to target the interaction between p38α and TAB1 a better understanding of the intricate structural details of the p38α-TAB1 complex is required at an atomic level. To address this, our lab recently published the crystal structure of p38α and the interacting region of TAB1 which revealed key residues involved in the binding between the two proteins (De Nicola *et al*, 2013). In this thesis, we examine the interaction between p38α and TAB1 in further detail and investigate the changes in the complex that are critical to the autoactivation process in a bid to develop small inhibitor molecules which can interfere with it.

1.15 Aim of the thesis

The ultimate aim of this thesis is to study the interaction between p38α and TAB1 in order to develop a small molecule to target it. However, specific aims are:

1. To confirm the TAB1 mediated p38 autoactivation.
2. To study the structural details of p38-TAB1 interaction
    a. Investigate the role of Thr185 in p38α's autoactivation mechanism
    b. Investigate the role of Thr185 in p38α's cellular localization signalling
3. To study the TAB1 KI mouse in the setting of myocardial ischaemia and determine p38α's signalling mechanism.

2 Material and Methods

In this chapter, I have described the principles and the general protocols for the common techniques used in my thesis. Full details of the protocols specific to individual experiments are described in the relevant result chapters.

All analytical-grade laboratory reagents were purchased from Sigma-Aldrich Chemical Company (Poole, UK) or ThermoFisher Biosciences (Hempstead, UK) unless stated otherwise.

2.1 Cell culture

Cell culture is a biological system in which cells are grown under a controlled environment. It is a laboratory technique for maintaining and growing cells (primary and immortalised) in a specific medium suitable for their survival. In my study, I have used 3 different cell lines and a primary cell line; Human Embryonic Kidney 293 (HEK293) cells, HELA cells, H9C2 cells, and Mouse Embryonic Fibroblasts (MEF), which were isolated from mouse embryos. All cell types were grown in a humid, 37^{o}C incubator in room air supplemented with 5% $CO_{2.}$

2.1.1 Human Embryonic Kidney cells

Human Embryonic Kidney 293, also known as HEK293, cells are a specific cell line derived from human embryonic kidney cells. HEK293 cells were transformed in 1977 by exposing them to sheared fragments of adenovirus type 5 DNA (Graham *et al*, 1977). Because of the transformed background, HEK293 cells are not an ideal model for normal or cancer cell studies. However, they are very easy to maintain in culture and straightforward to transfect with foreign DNA. Since they contain all the necessary machinery for gene expression and post-translational modifications, HEK293 cells have become an attractive tool in molecular biology.

In my studies, I used HEK293 cells extensively as an over-expression system. I cultured these cells in T75 flasks with full growth medium (Dulbecco's modified Eagle's medium containing 584mg/l L-glutamine, 10% v/v foetal bovine serum, 1% v/v penicillin/streptomycin) at 37^{o}C, in room air supplemented with 5% CO_2 in a water saturated incubator. The cell culture was maintained and upon reaching 80-90% confluency, they were transferred into new flasks with fresh full growth medium. For the purpose of the experiments, cells were split onto 6-well plates.

2.1.2 HELA cells

HELA cells are an immortal cell line derived from the cervical cancer cells of Henrietta Lacks. George Gey derived the cell in 1951 by expanding an isolated tumour cell, and named the cell line after Henrietta Lacks, HELA (Scherer, 1953). HELA cells are the first and the oldest immortal cell line grown in a lab. It is one of the most commonly used cell lines in biological and medical research. The vaccine for polio was developed by growing the virus in these cells (Brownlee, 1955).

Just like HEK293 cells, HELA cells are easy to transfect to express the protein of interest, and cells contain all the machinery required for post-translational modifications. HELA cells have a more abundant cytoplasm than HEK293 cells and as a result are more suited for immunofluorescence assays. HELA cells were grown in T75 flasks with full growth medium (Dulbecco's modified Eagle's medium containing 584mg/l L-glutamine, 10% v/v foetal bovine serum, 1% v/v/ penicillin/streptomycin) at 37^{o}C, in room air supplemented with 5% CO_2 in a water saturated incubator. Once they were reached 80% confluence, cells were either split into another T75 flask for culture or transferred to a 6-well plate for follow-on experiments.

2.1.3 H9C2 cells

H9C2 cells are a cardiac cell line derived from embryonic BDIX rat (strain used in cancer model) heart tissue (Kimes & Brandt, 1976). Although having a cardiac origin, these cells also exhibit features of skeletal muscle since they were immortalised through fusion with mononucleated myoblasts and consequently express nicotinic receptors and synthesize a muscle-specific creatine phosphokinase isoenzyme. As a result H9C2 cells are used in both cardiac and skeletal muscle studies. Although H9C2 cells lack morphological properties of adult cardiomyocytes, they still exhibit many cardiac-specific features such as electrical and hormonal signalling pathways and are shown to have morphological similarities to immature embryonic cardiomyocytes (Hescheler *et al*, 1991).

H9C2 cells were grown under the same conditions as HEK293 and HELA cells, as described above. The cells were cultured in T75 flasks with full growth medium (Dulbecco's modified Eagle's medium containing 584mg/l L-glutamine, 10% v/v foetal bovine serum, 1% v/v penicillin/streptomycin) at 37^{o}C, in room air supplemented with 5% CO_2 in a water saturated incubator. Upon reaching 80-90% confluency, the cells were transferred into new flask with fresh growth medium. For the purpose of experiments, they were split onto 6-well plates.

2.2 Transfection

Transfection is the process of introducing foreign genetic material into a cell. It is a common laboratory technique used to insert DNA into a cell so that encoded genes can be expressed to study the protein of interest. Transfection involves opening transient holes in the cell membrane to allow the uptake of DNA into the cell where it can undergo transcription/translation. There are several kinds of transfection such as viral, electroporation and chemical. The most commonly used method is the chemical based transfection that utilizes lipid polymers. Lipid based transfection uses lipid polymers to form a complex with DNA which is then taken up by cells. The DNA containing liposome complexes are positively charged on their surface which

fuses with the negatively charged plasma membrane to facilitate its transportation inside the cell via endocytosis. For my project, I used Turbofect^{TM} reagent, which is similar to lipid-based transfection, but is not a lipid polymer. Turbofect^{TM} is composed of a cationic polymer in sterile water. The polymer forms positively charged complexes with DNA which protects it from degradation and facilitates its delivery into the cells.

There are two types of transfection; transient and stable. In transient transfection, the persistence of the foreign DNA is limited by degradation and/or diluted through cell division. In stable transfection, the persistence of the foreign DNA is not limited since it integrates with the cell's genomic DNA (which is rare) or it confers an advantage to transfected cells by co-expressing a resistance gene (more common). The easiest method to achieve stable transfection is to use a vector containing a selective marker gene such as Geneticin or Blasticidin. When cells are grown in the medium containing the antibiotic, only the cells that have had successful transfection and taken up the foreign DNA containing the marker gene will survive. These cells can be cultured using the selective marker as long as needed.

2.3 *In vitro* kinase assay

An *in-vitro* kinase (IVK) assay is a method developed to test the ability of a protein kinase to phosphorylate its substrate. In a typical IVK reaction, a kinase and its substrate are mixed together in a tube with ATP and $MgCl_2$ at 37^oC to allow the kinase to phosphorylate the substrate. The phosphorylation status of the substrate can then be tested using phospho-specific antibodies with western blotting.

In our investigations, we carried out IVK reactions with p38α and TAB1 peptide, p38α and ATF2, and MKK6 and p38α. The recombinant p38α and MKK6 were produced in E.*coli*, whereas TAB1 peptide and ATF_2 fusion protein were bought from Activotec and Cell Signalling

Technology respectively. TAB1 (371-416) was a 46mer peptide that contained the residues (V390, Y392, V408, M409) responsible for binding to p38α.

TAB1 peptide:

NH_2- EMSQPTPTPAPGGRVYPVSVPYSSAQSTSKTSVTLSLVMPSQGQMV-COOH.

The concentration of proteins used in the IVK reactions are listed in the table below

Reagent	**Concentration (µM)**
p38α	3
MKK6	0.6
ATF2	0.86
TAB1 peptide	15

Table 2.3 IVK reagents: *The table lists the amount of each reagent used in a typical IVK reaction, unless stated otherwise (The reagent concentrations as used before in paper published in NSMB,* De Nicola *et al, 2013)*

The proteins were incubated in 1X kinase buffer (25mM Tris/HCl, pH7.5, 5mM β-glycerolphosphate, 2mM dithiothreitol, 0.1mM Na_3VO_4 and 1mM $MgCl_2$), with 550µM ATP for an appropriate amount of time at 37^{o}C. At the end of the reaction 2X SDS buffer was added to the mixture to terminate the reaction, and 5µl of the reaction mix was used to run on an SDS-gel for western blotting.

2.4 Western Blot

Western/immuno blotting is a widely used analytical technique that allows the detection of protein in a sample of cells/tissues. It is made up of 3 main steps; electrophoresis, transfer, and

detection. The electrophoresis involves separation of proteins in the sample based on their mass or their intrinsic charge and mass. The transfer involves the transfer of the separated protein from the gel onto a membrane, and the final detection phase involves detecting the protein of interest on the membrane using an antibody.

2.4.1 Sodium dodecyl sulphate polyacrylamide gel electrophoresis

Sodium dodecyl sulphate polyacrylamide gel electrophoresis or SDS-PAGE is an electrophoresis system which separates proteins based on their mass in a polyacrylamide gel once its denatured by sodium dodecyl sulphate, hence the name SDS-PAGE. SDS is an anionic detergent which breaks the non-covalent bonds in proteins that causes the protein to lose its native tertiary/quaternary structure. Additionally, SDS completely covers the protein with its strong anionic charge which is significantly stronger than the protein's native charge. The strong electrostatic repulsion of SDS forces the protein into a linear rod shape which allows for uniform movement of the protein through the gel during electrophoresis. The negative charge of the denatured protein moves towards the positively charged anode during electrophoresis. The smaller, lighter and shorter proteins will move faster through the gel than the bigger, heavier and longer proteins; as a result proteins are separated based on their mass. A known standard (molecular marker) is run alongside the samples as the reference.

For my projects, I used Mini Protean III one-dimensional gel electrophoresis system from Bio-rad to run SDS-PAGE gels. Almost all of the proteins I was investigating were between 25kDa and 70kDa, so I used 10% polyacrylamide gel unless stated otherwise (constituents in the table below). Polyacrylamide gels were poured into the 1mm space between the glass plates and left to set for 20 minutes. Also known as resolving gel, this part of the gel is responsible for the separation of the proteins. 2cm of stacking gel was layered above the resolving gel with a comb to form wells, where the samples are loaded and it ensures they migrate in a single compressed lane without any contamination from adjacent lanes.

Reagent	7.5% gel	10% gel	12.5% gel	15% gel	Stacking gel (4%)
MW range			10-100 kDa	5-70kDa	
DI H2O	9ml	5(7.5)ml	4(6)ml	3(4.5)ml	7ml
30% Acrylamide	4.5ml	4(6)ml	5(7.5)ml	6(9)ml	2ml
1.5M Tris-HCL (pH 8.8)	4.5ml	3(4.5)ml	3(4.5)ml	3(4.5)ml	-
0.5M Tris-HCL (pH6.8)	-	-	-	-	3ml
10% Ammonium persulphate	90µl	60(90) µl	50(75) µl	50(75) µl	100µl
TEMED	22.5µl	15(22.5) µ	15(22.5) µl	15(22.5) µl	10µl

Table 2.4.1: Composition of SDS-PAGE gels.

Once fully set, the gels were stacked into the electrophoresis tank and filled with running buffer (Tris-base, 0.025mol/L; glycine, 0.192mol/L; SDS, 0.1% w/v). The samples were loaded (5-15µl) into the wells and separated by electrophoresis with a voltage of 100V (Powerpac 300 Biorad, Herts, UK) for the first 15 minutes until the samples had migrated through the stacking gel into the resolving gel, after which the voltage was increased to 120V for the rest of the electrophoresis run. Upon completion of electrophoresis, gels were carefully disassembled from the glass plates and readied for the transfer.

2.4.2 Transfer

The transfer stage of western blotting involves transferring the separated proteins from the SDS gel onto a membrane. There are two types of membrane; nitrocellulose and polyvinylidene difluoride (PVDF) and I used the latter for my experiments. PVDF membranes are highly hydrophobic and ideal for detecting small amount of protein, as little as 10 pmoles (ThermoFisher Scientific). Because of their highly hydrophobic nature, they must be pre-soaked with methanol or ethanol prior to soaking them in the transfer buffer. Additionally, unlike the

nitrocellulose membrane, PVDF membrane can be stripped and re-probed several times. During transfer, the gel is placed on top of the membrane and sandwiched by blotting paper. The proteins are transferred by electrophoresis and the principle is the same as the one in SDS PAGE electrophoresis whereby an electric current is applied to move the negatively charged proteins towards the positively charged anode and in the process the proteins move from the gel onto the membrane.

I used a semi-dry transfer technique to transfer proteins from the gel onto a membrane. The PVDF membrane was pre-soaked in methanol for 1-2 minutes for activation before being soaked in transfer buffer (Tris-base, 25mmol/L; glycine, 150mmol/L; 20% (v/v) methanol) along with the SDS-polyacrylamide gel containing separated proteins. 12 pieces of 3M chromatography paper (Fisher Scientific, UK) were used as sandwich for transfer and soaked briefly in the transfer buffer. The gel was rested on the top of the PVDF membrane and sandwiched between the filter papers (6 on each side). Any air bubbles were removed and transfer was started by applying a constant voltage of 24V and current of 0.25Amp per membrane for 1 hour 15 minutes.

2.4.3 Detection

The final stage of western blotting is the detection phase where we detect the protein of interest using a specific antibody against the desired protein on the membrane. After completing the transfer of protein onto a membrane, the membrane is blocked with 4% milk +1% BSA in TBST for 1 hour to prevent any nonspecific binding of the antibody to the membrane. The membrane is designed to have a high affinity for proteins so antibody can also easily bind to the remaining binding surface that has not been occupied by the proteins in the sample during electrophoresis. This will give non-specific binding and a high background signal. So to prevent this, the membrane is incubated in milk or BSA (which is rich in protein) for 1 hour.

Following blocking, the membrane is incubated with primary antibody overnight at 4^{o}C. The antibody solution I used was prepared in 1% BSA-TBST and unless stated otherwise primary antibodies were prepared at a dilution of 1:1000 and secondary antibody at a dilution of 1:5000. The following day the membrane was washed 3 times in 15ml TBS-(Tween-0.01%) for 10 minutes to remove any unbound primary antibody. The secondary antibody which is linked to an enzyme horseradish peroxidase (HRP) was then incubated for 1 hour at room temperature. The membrane was washed again 3 times with 15ml of TBST for 10 minutes to remove any unbound secondary antibody.

Finally, the protein is detected using an enhanced chemiluminescence technique (Amersham, England). The membrane is blocked with an equal amount of stable peroxide solution and an enhanced luminol solution for two minutes. The HRP enzyme conjugated to the secondary antibody catalyses the reaction which produces light and the photons are detected by photographic film. The amount of specific protein on the membrane correlates with the amount of primary/secondary antibody bound to it and that correlates with the reaction catalysed by HRP which produces the band on the film, i.e. more protein in the sample means the band produced on the film will be darker and larger. The developed films were scanned using GS-800 scanner (Biorad) and the band densities were measured using Quality One program (Biorad).

2.5 Immunofluorescence

Immunofluorescence, also known as IF, is a light microscopy technique that uses fluorophore conjugated antibody to visualise the target antigen in a cell/tissue sample. The fluorophore allows visualization of the distribution of the target molecule within a sample using epifluorescence and confocal microscopes. There are two types of IF; Direct IF and Indirect IF. In direct IF, the primary antibody is directly conjugated to a fluorophore which allows visualization of target without the use of a secondary antibody. Indirect IF does not use a fluorophore-conjugated primary antibody, instead a secondary antibody conjugated with fluorophore is used for visualization. There are fewer steps in direct IF which saves time and

makes it the quicker protocol to complete. Additionally, the lack of the secondary antibody means there is no cross-reactivity and as a result it produces lower levels of non-specific background signal compared to the indirect IF. However, direct IF is less sensitive compared to indirect IF, as in indirect IF the signal is amplified as multiple secondary antibodies can bind to a primary antibody which significantly enhances the signal. As a result of this, less primary antibody is required with indirect IF making it the more affordable option. On the downside, indirect IF is more labour intensive and increases non-specific binding, but this can be controlled with optimization of the conditions.

2.6 Polymerase chain reaction

Polymerase chain reaction (PCR) is a technique used in molecular biology that allows the amplification of a single copy of DNA by several orders of magnitude. PCR, developed by Kary Mullis in 1983, uses thermal cycles of repeated heating and cooling to produce millions of copies of the DNA sequence from a single copy (Bartlett, 2003). This simple and cheap technique has revolutionised bio/medical research and is routinely used in DNA cloning, genetic fingerprinting, medical tests, phylogeny test etc. A PCR set-up requires four components; a DNA template that is to be amplified, forward and reverse primers complementary to the 5' and 3' end, heat stable DNA polymerase, and buffer containing deoxynucleoside triphosphates (dNTPs). A typical PCR reaction is run in a volume of 20-50µl with approximately 20-40 thermal cycle and consists of 3 main steps:

1. Initialization step: This initial step involves raising the temperature to 95^{o}C for couple of minutes to activate the DNA polymerase.
2. Thermal cycle step (20-40 cycles)
    - Denaturation: This step involves raising the temperature to 90-98^{o}C for 20-30 seconds to break the double stranded DNA into single strands by breaking the hydrogen bonds between the base pairs.

- Annealing: This step involves lowering the temperature to 50-65^{o}C for 20-30 seconds to allow the primers to stick to its complementary region on the single strands of DNA. The temperature and length of the annealing step depends on the individual primers.
- Extension: The final step of thermal cycle involves raising the temperature to 70-80^{o}C for optimum activity of polymerase so that it can start the synthesis of double stranded DNA using the dNTPs in the buffer. The length of this step depends on the length of the DNA extension and also on the type of polymerase as different polymerases have different activities.

3. Final extension: The final extension step involves raising the temperature to 70-80^{o}C for the final 5-10 minutes after the thermal cycle has completed to ensure that all remaining single stranded DNA is extended to form double strands.

After the final extension, the reaction can be kept on final hold where the temperature is set at 4-10^{o}C for short term storage of the reaction.

2.7 DNA agarose gel electrophoresis

Agarose gel electrophoresis is a gel electrophoresis technique that is used to separate DNA by its mass. Agarose gels range from 0.7%-2%, are easy to cast, and when an electric field is applied, the negatively charged DNA molecule moves toward the positively charged anode, resulting in separation of DNA by size. Agarose gel is a 3-dimensional matrix formed of helical agarose molecules in super-coiled bundles that forms channels/pores through which DNA can move.

The agarose gels were run in Tris-Acetate-EDTA buffer (40mM Tris, pH7.6, 20mM acetic acid, 1mM EDTA), supplemented with 0.01% (v/v) Gel Red^{TM} Stain (Biotium) for 1hour at 100V. The bands on the gel were viewed and photographed with a UV transilluminator (Syngene, GeneSnap).

2.8 Transformation for plasmid DNA amplification and protein production

Transformation is a technique where an exogenous genetic material is introduced into bacteria. For a successful transformation, bacteria must be competent i.e. they must be modified to have the ability to uptake foreign DNA. The commonly used technique is preparing the cells in a solution containing divalent cations (calcium chloride). The divalent cations assist in attaching the DNA to bacterial membranes at around 0^{o}C, and then a brief heat shock (37-42^{o}C) permeabilizes the membrane, subsequently the DNA is taken up inside the cell (Mandel & Higa, 1970). The bacteria is grown in a selective antibiotic medium so that only the transformed bacteria that have taken up the foreign DNA containing the antibiotic resistance gene can grow, allowing for selective growth.

In my experiments I used 100ng of DNA to transform 100µl of competent bacteria. For DNA production I used E.*coli* - DH5α cells, whereas for protein production I used E.*coli* – Rosetta^{TM} 2 cells. After adding the DNA, the cells were incubated on ice for 30 minutes. The cells were heat shocked at 42^{o}C for 30 seconds to allow the entry of the DNA into the cells. Then cells were immediately put back on ice and incubated for 5 minutes. 900µl of fresh LB (Luria-Bertani) media was added to the transformed cells and incubated at 37^{0}C in a shaker for 1 hour. 50µl of transformed cells were inoculated by streaking onto LB plates with appropriate antibiotics and incubated overnight at 37^{0}C. On the next day, a single isolated colony was picked to start a large scale growth either for DNA purification or protein purification.

Constituent	(g)
Bacto-tryptone	10
Bacto-yeast extract	5
NaCl	10
Add the constituents in a 950ml de-ionized water, adjust pH to 7 and top it up to make 1L of LB. Add 15g of Bacto-agar to make the LB-Agar. Sterilize by autoclaving and store at 4^{o}C.	

Table 2.8: Constituents of Luria Bertani medium

2.8.1 Mini Prep

A Mini prep kit (Macherey-Nagel) was used to purify the small amounts of DNA (nanogram) required for cloning, sequencing and transformation. All the reagents were provided in the kit and the isolation was done at room temperature. The transformed bacteria were grown in 1-5ml LB culture overnight at 37^{o}C. The next day the culture was centrifuged at 11,000g for 30 seconds to pellet the cells and supernatant was discarded. The pellet was re-suspended in 250µl of Buffer A1 (re-suspension buffer) by either pipetting up and down or using a vortex. Then 250µl of Buffer A2 (lysis buffer) was added and mixed gently by inverting the tube 5-6 times. The cells were incubated for 5 minutes and 300µl of Buffer A3 (neutralization buffer) was added. Then samples were mixed again by gently inverting the tube a couple of times. The cells were centrifuged at 11,000g for 5 minute and the supernatant was transferred to the NucleoSpin$^{(R)}$ Plasmid Columns. Columns were centrifuged at 11,000g for 1 minute and the supernatant was discarded as the DNA attaches to the silica membrane of the column. The DNA in the column was washed with 600µl of Buffer A4 (wash buffer) and centrifuged at 11,000g for 1 minute. The flowthrough was discarded and the column was centrifuged at 11,000g for 2 min to dry the membrane on the column. 50µl of nuclease free water was added to the column to elute the DNA by centrifuging it at 11,000g for 1 minute.

2.8.2 Maxi Prep

Maxi prep (QIAGEN HiSpeed$^{(R)}$) was carried out to purify large quantities of plasmid DNA (milligrams) required for transfection of mammalian cells. After growing the 5ml culture of transformed cells overnight it was transferred to a 150ml of LB media with appropriate antibiotic. The culture was grown overnight at 37^{o}C in an orbital incubator shaking at 200rpm. The bacterial culture was centrifuged at 6000g for 15 minutes at 4^{o}C. The supernatant was discarded and cells were re-suspended in 10ml of Buffer P1 and mixed thoroughly by pipetting up and down. 10ml of lysis buffer, Buffer P2 was added and mixed gently by inverting tubes couple of times. Cells were incubated for 5 minute and 10ml of neutralization buffer, Buffer P3 (pre-chilled) was added and mixed gently. The lysate solution was transferred into the barrel of a QIAfilter Cartridge and incubated for 10 minutes. During incubation, HiSpeed Maxi Tips were equilibrated with 10ml of Buffer QBT. After 10 minute incubation, the precipitated lysate was filtered with QIAfilter Cartridge into the equilibrated HiSpeed Maxi Tip by gravitational flow. The HiSpeed Maxi Tip was washed with 60ml of Buffer QC, and DNA was eluted with 15ml of Buffer QT into a 50ml falcon tube. DNA was precipitated by addition of 10.5ml of isopropanol and incubated for 5 minutes. The QIAprecipitator Maxi Module filter was attached onto the outlet nozzle of 30ml syringe and the precipitated DNA-isopropanol solution was filtered through it at a constant pressure. The filter was washed with 2ml of 70% ethanol and air dried by passing air through the filter using the empty syringe a couple of times. The QIAprecipitator was attached to the outlet nozzle of a 5ml syringe and DNA was eluted into a 1.5ml tube with 1ml of nuclease free water.

2.8.3 Agarose gel purification

PCR products after amplification are run on agarose gel to confirm identity by their mass and to separate and extract them for sequencing. The isolation/purification of PCR products from the agarose was carried out using the High Pure PCR Product Purification kit (Roche Diagnostics). After the agarose gel electrophoresis was completed, the desired DNA band from the agarose gel was excised using a scalpel. The excised gel was weighed and put in a 1.5ml eppendorf tube.

300µl of Binding Buffer per 100mg of agarose gel slice was added into the tube and incubated at 56^{o}C for 10-15 minutes with regular vortexing. Once the agarose gel was fully dissolved, 150µl of isopropanol per 100mg of agarose gel was added into the tube and vortexed thoroughly. The suspension was transferred into a High Pure Filter Tube and centrifuged for 30 seconds. The flowthrough was discarded and the tube was washed with 500µl of Wash Buffer and centrifuged at 16,000g for 1 minute. The flowthrough was discarded and washed again with 200µl of Wash buffer. The High Pure Filter Tube was inserted into a new eppendorf tube, and 50µl of nuclease free water was added and centrifuged at 16,000g for 1 minute to elute the DNA.

2.9 Recombinant protein expression in E.*coli*

Ever since the first human protein was expressed in E.*coli* in 1977, bacteria have been extensively used to express proteins in native and mutant forms (Itakura, 1977). The reasons behind E.*coli's* popularity are numerous. For example, E.*coli* can be transformed easily with different types of plasmids and exponential growth ensures a large protein yield in a short period of time. Additionally there are various strains of E.*coli* and this provides a range of options when trying to optimize the condition for better growth and yield.

In my project, I used Rosetta^{TM} BL21 (DE3) strain of E.*coli* to express p38α and its mutant. pETDuet plasmid, containing two multiple cloning sites (MCS), lac repressor gene (lac I), T7 promoter and ampicillin resistance gene, was used as a vector. p38α was cloned into the first multiple cloning site just downstream of the T7 promoter and lac operator; by Dr. Gian De Nicola. After successful transformation, the cells were grown in a 1.5L of LB media with appropriate antibiotic. Initially the cells were grown at 37^{o}C until the OD_{600} reached 0.5, after which the temperature was lowered to 21^{o}C and cells were induced with isopropyl-beta-d-thiogalactopyranoside (IPTG). IPTG is a galactose analogue that binds to the lac repressor and disrupts its ability to bind to the lac operator. This in turn induces the expression of T7 polymerase. T7 polymerase then activates the T7 promoter and starts the transcription of the

gene downstream of it. After induction, cells were grown at 21^{o}C for 5 hours, centrifuged to collect the cells and then stored at -20^{o}C until further use.

2.10 Protein purification

Protein purification is the process of collecting and purifying a specific protein from cells. The first part of purification involves separating the protein from non-protein complexes, and the second part involves isolating the desired protein from all other groups of proteins. The first part is fairly simple which involves breaking the cells apart and centrifuging to separate proteins from heavier molecules such as cellular organelles and debris. After growing the bacteria expressing the desired protein, cell pellets are lysed using a sonicator in a lysis buffer. A typical lysis buffer contains a detergent or an enzyme to break the cell membrane, and protease inhibitors to prevent endogenous proteases breaking down the protein of interest. After sonication, cells are centrifuged to separate the soluble fraction containing proteins, and non-soluble fraction containing the rest of the cellular debris. The non-soluble fraction is discarded and the soluble fraction is used to purify the desired protein.

The second stage of purification is more complicated and there are different types of purification techniques available. Each purification type utilizes different properties of the protein to achieve separation. In my project I have used three types of protein purification; affinity chromatography, ion-exchange chromatography, and size-exclusion chromatography. Affinity chromatography involves purifying the protein based on its high affinity for another protein, for example antibody to antigen, enzyme to substrate or ligand to receptor. In our case, we cloned p38α with a histidine tag which has a very high affinity for nickel. So, we have used nickel resin in a column to separate p38 from the rest of the cellular proteins. Ion-exchange chromatography involves separating proteins based on the ionic strength. Anion exchange resins have a negative charge so they are used to separate positively charged proteins, whereas cation exchange resins have a positive charge so they are used to separate the negatively charged proteins. Finally, the size-exclusion chromatography also known as gel filtration chromatography separates proteins

based on their size. The gel filtration column in made up of porous beads stacked in a column. The smaller proteins will enter these beads easily so will spend more time retained on the column. The larger proteins do not spend much time within the beads and as a result are eluted faster. This way the proteins are separated based on their size.

2.11 Isothermal titration calorimetry

ITC or isothermal titration calorimetry is a biophysical tool used to study the interaction between two biological molecules such as protein-protein, protein-DNA, and protein-inhibitor. ITC characterizes the thermodynamics of the interaction between two molecules to determine the binding affinity, enthalpy changes and stoichiometry of the interaction. It is a simple yet powerful technique that produces readout on how the two molecules interact with each other and how strong the interaction is. ITC is a very sensitive physical tool and the experiment is significantly dependent on the correct concentration of the two molecules, buffer, and the temperature of the environment.

An ITC machine can be either a single or dual injection variety (Duff *et al*, 1999). In a single injection instrument the titrant is added to the cell containing protein. In a separate control experiment the titrant is added to the buffer without the protein. In the dual injection instrument, the titrant is simultaneously added to the cell containing the protein and another cell containing the buffer. To run a typical ITC experiment, one protein is loaded into a cell and another into a syringe. Using a syringe, the protein is loaded and titrated into the calorimetric cell containing the other protein in a stepwise manner. This triggers the binding reaction and as the two proteins interact, the heat is either released or absorbed depending upon the type of reaction. The apparatus quickly changes the temperature of the cell to return it to the baseline after each injection; before the heat change from next injection is measured again, and the process continues until the end. With every injection, the amount of protein in the cell that is left to bind decreases and with it the heat release/absorbed also diminishes until only the background heat of dilution is observed. This change in the heat is detected and based on this change, the enthalpy

change, entropy, binding affinity, stoichiometry, and the binding constant; can be calculated. I carried out ITC experiments with the help of Dr Gian De Nicola and more details are provided in chapter 4.

2.12 Mass spectrometry

Mass spectrometry is an analytical tool that allows the identification of chemical constituents of a substance. It measures the mass-to-charge (*m/z*) ratio of ions to identify and quantify molecules in a sample. Mass spectrometry consists of 5 different stages

1. Vaporization
2. Ionization
3. Acceleration
4. Deflection
5. Detection

In a typical mass spectrometry procedure, a sample (solid/liquid/gas) is vaporized and ionized by bombarding it with electrons from an ion source. This causes the molecules in the samples to break into charged fragments. These ions are then accelerated through a magnetic field which causes them to deflect before they are detected by a detector. The amount of deviation depends on the mass-to-charge (*m/z*) ratio, i.e. the ions with same mass-to-charge ratio will undergo the same amount of deflection whereas ions of different mass-to-charge will deviate by different amounts. The computer software analyses the ion detector data and produces a graph in the form of spectra with the individual *m/z* ratio and relative abundance. The result is processed through a database to predict the identity of the molecule based on the *m/z.*

Protein mass spectrometry has revolutionized the field of proteomics and made significant contributions to the discovery of protein structure, function, modification and global protein

dynamics. The development of electrospray ionization (ESI) and matrix assisted laser desorption/ionization (MALDI) was the key to the advancement of mass spectrometry in proteomics (Domon *et al*, 2006). It allows the measurement of molecular masses of polypeptides and determination of additional structural features such as posttranslational modifications like phosphorylation. The mass spectrometry technique that allows the determination of posttranslational modifications is known as Tandem mass spectrometry, also known as MS/MS or MS2. It involves multiple mass spectrometry steps where the first stage (MS1), involves normal separation of the ions based on the mass-to-charge ratio. The second stage (MS2) involves selection of the precursor ions of the particular mass-to-charge ratio to create new fragment ions (product ions). These ions are separated again and the masses from these new fragment ions can be used to deduce any modification in the structural feature.

2.13 Simulated Ischaemia

Simulated ischaemia is an *in-vitro* technique developed to simulate the conditions that occur during tissue ischaemia, but in cultured cells. There are different versions of this technique and we have adapted ours based on the method developed by Kimio Esumi (Esumi et al, 1991). It is impossible to reproduce exactly the same conditions that cells are exposed to during myocardial infarction. However, our model of simulated ischaemia has many of the key features. One of the hallmarks of myocardial infarction is deprivation of oxygen or hypoxia and the ischaemic buffer simulates that with addition of an oxygen scavenger, sodium dithionite. However, it is important to note that sodium dithionate can cause causes oxidative stress, which should be considered whilst interpreting the results. The buffer also mimics the extracellular milieu of reversible myocardial ischaemia by modelling the hypoxic environment with addition of lactate, low glycolytic flux with 2-DOG, disruption of the membrane potential and electrical activity with high potassium, and acidic condition with low pH.

The ischaemic buffer (table C) and control buffer (table B) were made from the basic stock buffer shown in table A. For ischaemic buffer, all compounds were added except for sodium

dithionite, filter sterilized with 0.2µm filter, and warmed to 37^{o}C in water bath. At this stage pH of the buffer is approximately 6.8. After the buffer reaches 37^{o}C, sodium dithionite was added and it caused the pH of the buffer to drop further to approximately 6.3.The buffer is then immediately added onto the cells for an appropriate amount of time.

Basic stock buffer, pH7.4			
Reagent	Concentration (mM)	1X (g/L)	10X (g/0.2L)
NaCl	137	8	16
KCl	3.58	0.27	0.54
MgCl2.6H2O	0.49	0.10	0.2
CaCl2.2H2O	1.8	0.264	0.528
HEPES	4	0.953	1.906

Table 2.13A: Composition of basic stock buffer

Control buffer, pH7.4	
Reagent	Amount (Total 50ml)
10X basic stock buffer	5ml
Sterile ddH2O	45ml
20mM D-glucose	0.225g
1mM Na pyruvate	5.5

Table 2.13B: Composition of control buffer

Simulated Ischaemia/Reperfusion buffer, pH6.3	
Reagent	Amount (Total 50ml)
10X basic stock buffer	5ml
Sterile ddH2O	45ml
10mM 2-DOG	82.1mg
20mM Na lactate	172µl
1mM Na dithionite	8.7mg

Table 2.13C: Composition of ischaemia/reperfusion buffer

2.14 Langendorff perfusion of isolated mouse hearts

Langendorff retrograde perfusion of isolated hearts was pioneered by Oscar Langendorff in 1895 and since then it has been routinely used to study the patho/physiology of the heart (Bell, 2010). Langendorff perfusion is an ex-vivo technique which involves cutting out the heart from an animal and attaching it to a fixed cannula via the aorta through which the heart is perfused with a nutrient rich oxygenated buffer such as KREBs. The perfusate enters the heart via the aorta in a retrograde direction which causes the aortic valve to shut. This forces the perfusate to enter the left and right coronary arteries which supply blood to the heart muscle. This continuous delivery of oxygen and nutrients to the heart muscle enables the heart to beat continuously for several hours even outside an animal. The apparatus for Langendorff perfusion is water-jacketed, the circulation of warm water ensures the heart and buffer are maintained at 37^{o}C.

	Concentration (mM)	5L	2L	1L
NaCl	118.5	34.63	13.85	6.93
$NaHCO_3$	25	10.5	4.20	2.10
KCl	4.7	1.77	0.71	0.35
$MgSO_4.7H_2O$	1.2	1.47	0.59	0.29
KH_2PO_4	1.2	0.8	0.32	0.16
Glucose	11	9.9	3.96	1.98
Mix and bubble the solution with 95%O_2 + 5% CO_2 for 15 minutes before adding calcium chloride				
$CaCl_2.2H_2O$	1.4	1.04	0.42	0.21

Table 2.14: Composition of modified Krebs-Henseleit buffer

The Langendorff technique allows the measurement of different functions of the heart such as coronary flow, heart rate, contractile function etc. The other advantage of the technique is it allows pharmacological investigation by measuring the effect of drugs on the heart. The Langendorff technique can also be used to harvest the cardiac myocytes from the heart and culture them for studies. The contractile function of heart is measured by inserting a deflated intra-ventricular balloon. Once inside, the balloon is inflated to 5-10mm Hg to provide a pre-load stretch of myocytes to optimise systolic isovolumaemic pressure.

Langendorff perfusion requires practice and to ensure consistency the following inclusion criteria had to be met

1. Time from thoractomy to aortic cannulation must be less than 3 minutes.
2. Coronary flow must be between 1.5ml/min to 4ml/min
3. Unpaced heart greater than 300 beats/min

4. LVEDP less than 10mm Hg
5. LVDP must be greater than 60mm Hg with no persistent arrhythmia

More detailed protocols of experiments are described in chapter 6.

3 TAB1 induces p38α autoactivation

3.1 Introduction

The prototypical activation mechanism of a MAPK involves a 3-tier kinase cascade where the most upstream kinase (MAPKKK), activates an intermediate kinase (MAPKK); which then activates the MAPK. In the case of p38α, MAPKKKs such as TAK1 and ASK1 activate the dual-specificity intermediate kinases MEK3/6 and MEK4 which then activate p38α. In 2002 an alternative activation mechanism of p38α was discovered by Ge and co-workers when they showed TAB1, a scaffold protein, caused autoactivation of p38α (Ge *et al,* 2002). This study provided a new mechanism of p38α activation where they proposed the alternative activation pathway could operate in parallel with the canonical kinase cascade to regulate important signalling events. Subsequent studies in the last decade have shown that this mode of TAB1-mediated p38α activation could be harmful to the heart in ischaemic stress such as MI, and preventing its activation could be therapeutically beneficial (Barancik *et al*, 2000; Mackay et al, 1999, Ma et al, 1999; Saurin et al, 2001). The studies in our lab have revealed similar findings and with that we have focused our time and tools in studying the TAB1 induced mode of p38α activation with the aim of disrupting the p38α-TAB1 interaction. In this chapter, we look at the TAB1-mediated autoactivation of p38α. Using purified recombinant proteins in *in-vitro* kinase assays and endogenous proteins in mammalian cells, we study the mechanism of p38α autoactivation. Recently, we published the crystal structure of a p38α-TAB1 complex which revealed that TAB1 binds to p38α in a bipartite manner (De Nicola *et al,* 2013). Here, we explore that p38α-TAB1 crystal structure in detail and study the key residues involved in the interaction, and investigate the consequence of mutating these residues.

3.2 Specific Methods

3.2.1 cDNA constructs for mammalian cell over expression

pCDNA3 was used as a plasmid vector for expression in mammalian cells. The plasmid contains cytomegalovirus immediate early (CMV) promoter and SV40 polyadenylation sequence for high level expression in mammalian cells. It has an ampicillin resistance gene for selective cloning. WTp38α, WT TAB1, and mutant TAB1 (V390A/Y392A/V408G/M409A) were cloned into this plasmid.

cDNA	**Plasmid backbone**	**Resistance**	**Tag**	**Expected molecular weight (kDa)**	**Details & Source**
WT p38α	pCDNA3	Ampicillin	HA	40	Full length WTp38α (DR Y Wang, UCLA, USA)
WT TAB1	pCDNA3	Ampicillin	CFP	83	Full length WT TAB1 (Gian De Nicola)
TAB1 mutant (V390A, Y392A, V408G, M409A)	pCDNA3	Ampicillin	CFP	83	Full length mutant TAB1 (Gian De Nicola)

Table 3.2.1Plasmids used for mammalian cell transfection

3.2.2 Culture of HEK293 cells

HEK293 cells were used as the over-expression system to study TAB1 induced p38α activation. The cells were cultured in T75 flasks with full growth medium (Dulbecco's modified Eagle's medium, supplemented with 10% v/v foetal bovine serum, 1% v/v penicillin/streptomycin) at 37^{o}C in room air supplemented with 5% CO_2 in a water saturated incubator. Upon reaching 80-

90% confluency, the cells were transferred into new T75 flask with fresh full growth medium. For the purpose of experiments, they were split onto 6-well plates.

3.2.3 Transfection

HEK293 cells were seeded on 6-well plates in full growth medium at 37^{o}C and transfected upon reaching 60% confluency as described in chapter 2. The transfection was mediated using Turbofect reagent. Turbofect is a solution of cationic polymer in water, which binds with DNA to form a compact, stable, positively charged complex. This complex protects DNA from degradation and also facilitates its delivery into the cells by fusing with the negatively charged cell membrane.

The reagent mixture was prepared in eppendorf tubes. 100µl of Optimem solution was added into the tube followed by 1µg of DNA sample. 2µl of Turbofect reagent (2µl Turbofect per 1µg of DNA) was added to the tube, mixed gently and left for 30 minutes for complex formation. An appropriate volume of Optimem was added into the tube to make 1ml total volume. The tube was inverted gently for complete mixture of the transfection reagents which were then pipetted onto the cells in 6-well plates, in a drop-wise manner. The cells were incubated for 24hrs at 37^{o}C after which the transfection media was replaced with serum free media (SFM). In the experiments with inhibitors, drugs were incubated with SFM for the appropriate amount of time as needed. For western blot analysis the SFM was removed and the cells were washed with PBS. 200µl of 2X SDS-sample buffer (120mM Tris, pH 6.8, 6% w/v SDS, 20% v/v glycerol, 10% β-mercaptoethanol and 0.01% bromophenol blue) was added to each of the wells of the 6-well plate and cells were scraped into eppendorf tubes. The samples were heated to 95^{o}C for ten minutes before loading onto an SDS-PAGE gel for western blotting.

3.2.4 In vitro kinase assay

WTp38α, TAB1 (371-416) peptide, and double mutant TAB1 (371-416) peptide were used for IVK assays in the presence and absence of SB203580. The residues mutated on TAB1 peptide were: V390A Y393A (on the lower non-canonical site) and V408G M409A (on the upper canonical site). 3µM of p38α and 15µM of TAB1 peptide were incubated in 1X kinase buffer (25mM Tris/HCl, pH7.5, 5mM β-glycerolphosphate, 2mM dithiothreitol, 0.1mM Na_3VO_4 and 1mM $MgCl_2$). 5µl of 10mM ATP was added to the incubation mixture to start the reaction at 37^oC. 10 µM SB203580 was added in the reaction mixture to examine the sensitivity of the reaction to p38 inhibition. The samples were collected at four different time points of 30min, 1hr, 2hr, and 4hr. 2X sample buffer was added to the sample, heated to 95^oC for 10 minutes and used for western blot analysis.

3.2.5 Western Blot

Western/Immuno- blotting is a widely used technique that allows the detection of proteins on a membrane by an antibody after they are separated by electrophoresis. Samples were analysed by western blot as described in chapter 2. In brief, samples were lysed with 2X SDS sample buffer and boiled at 95^oC for 10 minutes. 10µl samples were run on 10% SDS polyacrylamide gel for 1hr 30 min and transferred to a PVDF membrane. The membrane was then blocked with phospho p38 antibody (Thr180/Tyr182) at a dilution of 1:1000 and total p38 antibody at a dilution of 1:1000 at 4^oC overnight. The membrane was washed three times with 15ml of TBST for 10 minutes each and blocked with rabbit secondary antibody conjugated with HRP (at 1:5000 dilution) for 1 hour at room temperature. The membrane was washed three times with 15ml TBST for 10 minutes each and developed by chemiluminescence technique.

3.2.6 Statistical analysis

Data sets were analysed by one way ANOVA (Analysis of Variance) and groups were compared using Tukey's test as a post-hoc. p value of less than 0.05 was considered significant.

3.3 Results

3.3.1 TAB1 induces p38α autoactivation

An *in-vitro* kinase assay was carried out using recombinant p38α and 29mer TAB1 peptide (384-412) at 37^{O}C in a kinase buffer with ATP for 2 hours as described in section 3.2.4. The western blot analysis of the IVK product showed that in the presence of TAB1, phospho-p38 signal at the T-G-Y motif increased, suggesting TAB1 promotes activation of p38α (Fig 3.3.1). The phospho-p38 signal was completely abolished in the presence of SB203580, an ATP-competitive inhibitor of p38 catalytic activity. Thus, the result indicates SB203580 is competing with ATP to block p38α's kinetic activity meaning TAB1 activates p38α via autoactivation.

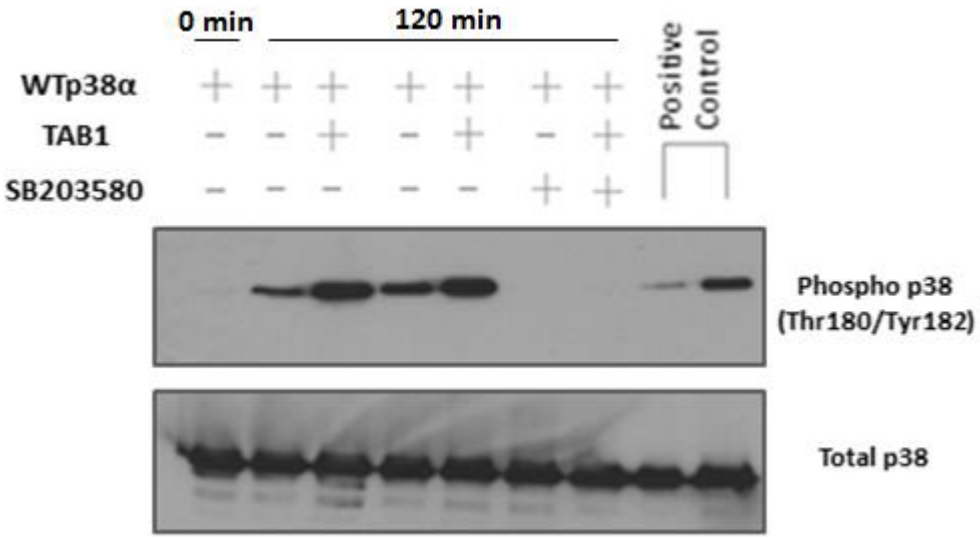

Figure 3.3.1 TAB1 causes p38α autoactivation: *Representative western blot figure of the IVK products probed with dual specificity phospho p38 (Thr180/Tyr182) antibody and total p38 antibody. The addition of TAB1 caused an increased phospho p38 signal which was inhibited 10μM SB203580, n=3.*

3.3.2 TAB1 induces p38α autoactivation in HEK293 cells

To complement our IVK experiment we used an over-expression system in mammalian cells where we transfected HEK293 cells with p38α and TAB1 as described in 3.2.3. Transfection of p38α caused a small increase in phospho-p38 signal (T-G-Y motif) compared to the control. Transfecting TAB1 had no effect on p38α activation. Co-transfection of p38α and TAB1 together however caused a marked increase in phospho p38 signal (T-G-Y motif), which was completely blocked by 10μM SB203580 treatment. The result suggests TAB1 causes autoactivation of p38α in HEK293 cells recapitulating the outcome from IVK assay in 3.3.1.

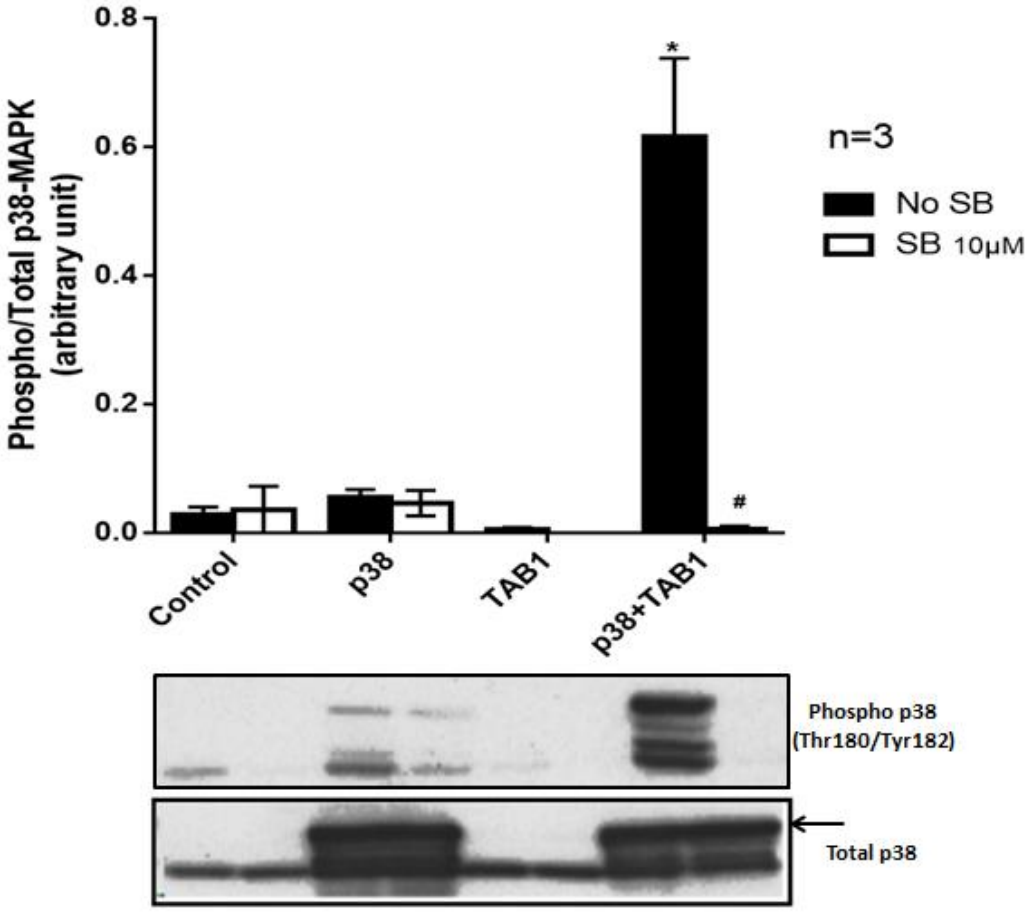

Figure 3.3.2 Co-transfection of p38α and TAB1 in HEK293 cells with SB203580 exposure: *The western blot figure shows a marked increase in phospho p38 signal at the T-G-Y motif in cells co-transfected with p38α and TAB1. 10μM SB203580 treatment completely abolished that signal. Arrow represents the ectopic band which runs higher than the endogenous band on an SDS-PAGE gel as it is heavier because of the hemagglutinin tag. The graphic representation above the western blot figure shows a significant difference in p38 activation when co-transfected with TAB1. Data represented as mean+/-SEM from 3 independent experiments (***** = P<0.05 vs control; # = P<0.05 vs p38+TAB1).*

3.3.3 TAB1 interacts with p38α in a bipartite manner

In 2013 our lab published the crystal structure of a p38α-TAB1 complex (De Nicola *et al*, 2013) which revealed TAB1 binds to p38α in a bipartite manner. NMR, X-ray crystallography and ITC data pointed out residues 385-394 and 404-412 on TAB1 to be the two regions involved in binding with p38α. To test this we mutated four of these key residues to produce a mutant TAB1 (V390A/Y392A/V408G/M409A). An *in-vitro* kinase assay was carried out with p38α, WT TAB1 and mutant TAB1 at 37^0C for 4 hours as described in section 3.2.4. The sample from the IVK reaction analysed by western blotting showed that WT TAB1 activated p38α at all four time points as evident by the phospho-p38 signal (T-G-Y motif) which got stronger with time (Fig 3.3.3). The mutant TAB1 was however, not similarly able to activate p38α with a faint phospho-p38 signal seen only at the 2 and 4hrs time point. In fact the signal with mutant TAB1 was even lower than the signal observed without TAB1. The result confirms that these residues are necessary for TAB1-p38α interaction as their mutation leads to an impaired p38α autoactivation.

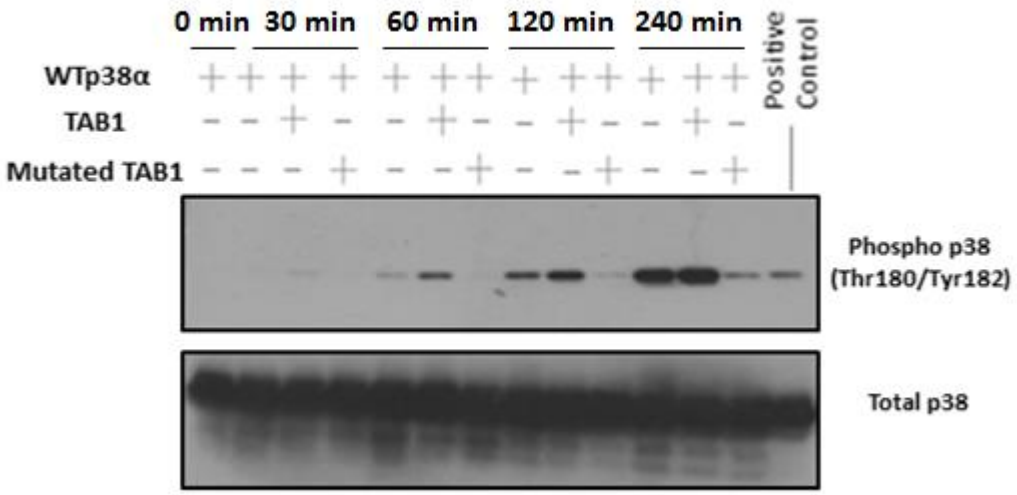

Figure 3.3.3 TAB1 binds to p38α in a bipartite manner: *Figure shows the western blot result of an IVK performed with p38α, WT TAB1 (371-416) peptide and mutant TAB1 (V390A/Y392A/V408G/M409A) peptide, as described in section 3.2. The western blot shows the IVK products at four different time points 30min, 1hr, 2hr and 4hr probed with dual phospho (Thr180/Tyr182) p38 antibody and total p38 antibody. WT TAB1 causes an increase in phospho-p38 signal at all 4 time-points; mutated TAB1 does not cause a similar magnitude of increase in phospho-p38.*

3.3.4 TAB1 interaction with p38α leads to p38α autoactivation in HEK293 cells

The IVK result showed that TAB1 binds to p38α in a bipartite manner and without the interaction, autoactivation does not happen. We sought to examine whether we could recapitulate this result in mammalian cells. We used an over-expression system in HEK293 cells and transfected p38α, WT TAB1 and mutant TAB1 (V390A/Y392A/V408G/M409A). 24hrs later, we saw an increased phospho p38 (T-G-Y) signal when p38α and WT TAB1 were co-transfected, as expected from the IVK with the corresponding peptide forms of TAB1. But co-transfection of p38α and mutant TAB1 did not lead to a similar increase in phospho p38 (T-G-Y) signal suggesting mutant TAB1 is unable to cause p38α autoactivation. The result supports the outcome from IVK assay and confirms a similar effect when the residues are mutated in full-length TAB1.

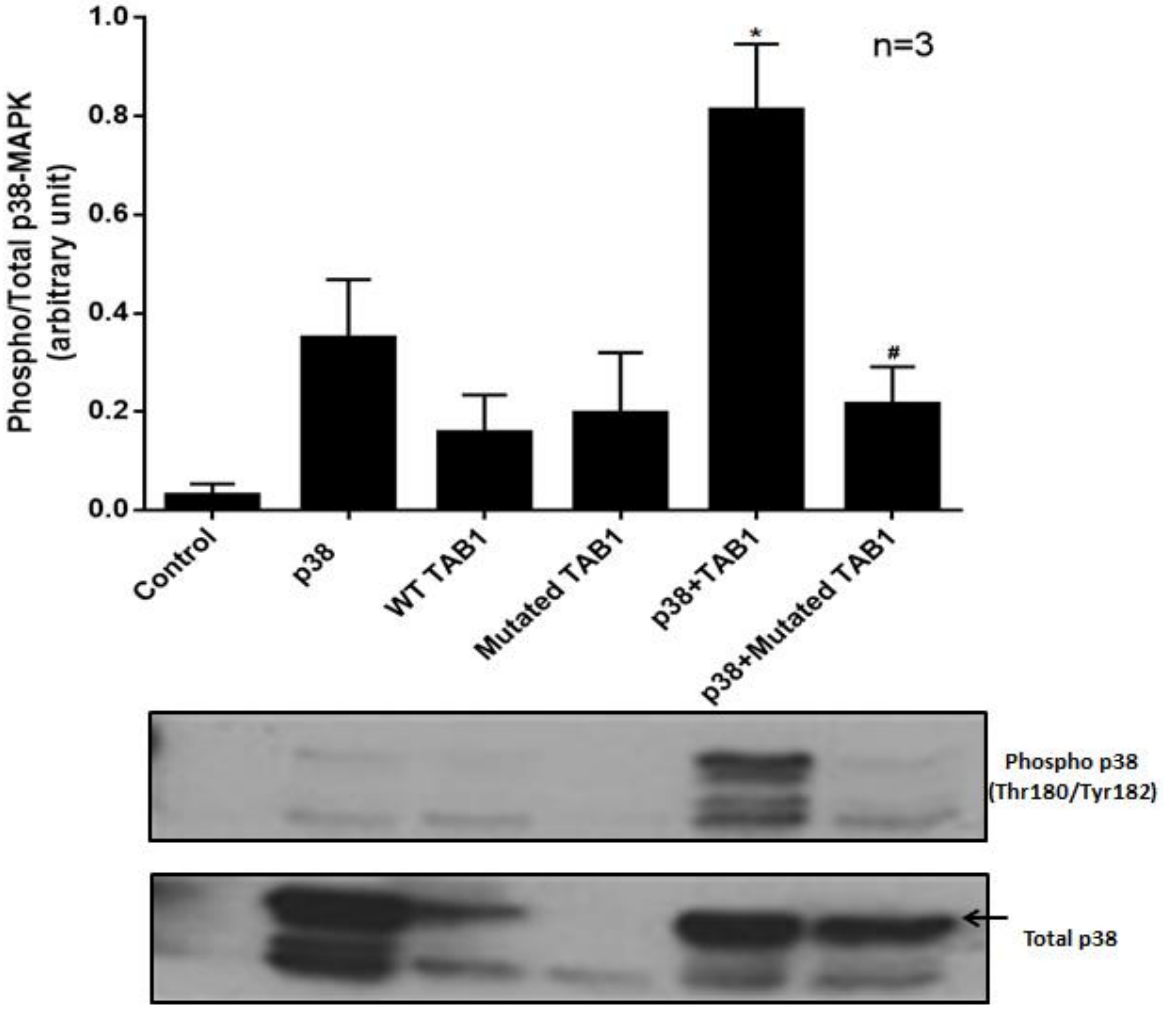

Figure 3.3.4 p38α-TAB1 interaction in HEK293 cells: *The western blot figure showed HEK293 cells transfected with p38α, WT TAB1 and mutated TAB1 as described in section 3.2. In samples transfected with p38+TAB1 there was a dramatic increase in phospho-p38 signal (T-G-Y), but not in cells transfected with p38+mutated TAB1. The graph above shows the quantification from western blot analysis which shows a significant difference in phospho-p38 signal between p38+TAB1 and p38+mutated TAB1. (Quantification from three separate experiments with data represented as mean+/-SEM.* ******* *= P<0.05 vs control; # = P<0.05 vs p38+TAB1). Arrow represents ectopic protein.*

3.4 Discussion

In this chapter, we investigated the TAB1 induced activation mechanism of p38α. Using an over expression system in mammalian HEK293 cells and recombinant proteins in *in-vitro* kinase assays, we showed that TAB1 interacts with p38α in a bipartite manner which causes p38α autoactivation.

3.4.1 TAB1 causes p38α autoactivation

The western blot analysis of IVK assay with recombinant p38α and 29mer TAB1 peptide (384-412) showed that phospho p38 signal increased markedly in the presence of TAB1 (Fig 3.3.1). This was completely abolished with 10μM SB203580, an ATP mimetic Type I inhibitor. SB203580, which belongs to a family of pyridylimidazole, competes with ATP for the ATP binding pocket of a kinase and diminishes its catalytic ability (Young *et al,* 1997). Thus, the IVK result of SB203580 inhibiting p38α activation suggests that TAB1 is causing p38α activation via an auto-activation mechanism. The result is in line with other studies in our lab where we have found that a kinase dead p38α that is unable to bind ATP cannot be activated via TAB1. The surprisingly high level of phospho p38 signal seen in the absence of TAB1 could be the result of incubating p38α in a tube with a high concentration of ATP at 37^{o}C for 2hours which causes it to auto-activate itself. The IVK result showed that TAB1 augments the p38α autoactivation. Next, we carried out a similar experiment in mammalian cells to see if we could replicate this result in a biological experimental model. We transfected HEK293 cells with p38α and TAB1 and looked at the activation profile of p38α. 24hrs after transfection, there was a significant increase in the phospho p38 signal in cells transfected with p38α and TAB1 compared to the cells transfected with just p38α or TAB1 alone (Fig 3.3.2). This signal was, as expected, completely blocked with a 2 hour treatment of 10μM SB203580. The result recapitulates the outcome produced from IVK assay in 3.3.1 confirming that TAB1 induces p38α autoactivation which is sensitive to SB203580, and supports the findings from the original study of Ge and co-workers (Ge *et al,* 2002).

3.4.2 TAB1 binds to p38α in bipartite manner to cause its activation

After confirming TAB1 mediates p38α autoactivation, we went on to investigate this activation mechanism in further details. The crystal structure of p38α and the interacting region of TAB1 in a complex was resolved by our lab recently which showed that TAB1 binds to p38α in a bipartite manner (De Nicola *et al*, 2013). The crystal structure showed that the C-terminal region of the TAB1 binds to the canonical region of p38α (where other p38α partners such as MKK3/6 and p38α substrates bind) while the N-terminal region binds to the non-canonical region. This interaction results in the structural re-arrangement of p38α that leads to p38α autoactivation. Originally, TAB1 (373-418) was believed to be the region interacting with p38α, however subsequent studies narrowed it down to a much shorter region of 29mer TAB1 (384-412) and suggested pro412 to be the key residue required for binding (De Nicola *et al*, 2013; Ge *et al*, 2002; Zhou *et al*, 2006). To confirm this, we ordered a 29mer WT TAB1 peptide and 29mer mutant TAB1 peptide with mutations in the four key residues that interact with the canonical and non-canonical region. We hypothesized that the WT TAB1 peptide will bind and auto-activate p38α but the mutant TAB1 peptide will not be able to bind to p38α and as a consequence cannot induce p38α autoactivation. The mutant TAB1 was created with 4 point mutations; V390A, Y392A (to disrupt the noncanonical site), V408G, M409A (to disrupt the canonical site).

We performed an IVK assay with recombinant p38α in the presence of WT TAB1 peptide (NH2- RVYPVSVPYSSAQSTSKTSVTLSLVMPSQ-COOH) and the mutated TAB1 peptide (NH2- RVYPVS**A**P**A**SSAQSTSKTSVTLSL**GA**PSQ-COOH). The western blot analysis of the IVK product showed that there was a marked increase in the phospho p38 signal in the presence of WT TAB1 but in the presence of the mutated TAB1, there was not. The phospho p38 signal was enhanced with longer incubation in the reaction mixture with WT TAB1 as expected, but not with the mutated TAB1. The result showed that even with a 4 hour long reaction time, mutated TAB1 was unable to activate p38α. A very faint phospho p38 signal is observed at the 4 hour time point. A high phospho p38 signal seen at 2 hour and 4 hour time points in the

absence of TAB1 was also not surprising due to the high ATP concentration at 37^{o}C which causes p38α to auto-activate itself, as seen previously in result 3.3.1. A lower p38 activation observed in the presence of mutated TAB1 than the one observed without TAB1 was unusual and may have arose due to mutated TAB1 protein interfering with the auto-activation of p38 that takes place in the presence of high ATP concentration without any other proteins to physically interfere. The IVK result suggests that our hypothesis is correct and the four mutated residues in TAB1 are necessary to bind to p38α which causes the structural re-arrangement within p38α that promotes p38α autoactivation. We also tested this in an over expression system in HEK293 cells and transfected p38α with WT TAB1 and mutated TAB1 where the same 4 residues are mutated. There was an increase in phospho p38 signal in all transfected cells compared to the untransfected cells (Fig 3.3.4). More importantly, there was a significant increase in phospho p38 signal when cells were co-transfected with p38α and WT TAB1 but not when cells were co-transfected with p38α and mutated TAB1. In fact the phospho p38 signal observed in cells co-transfected with p38α and mutated TAB1 was similar to the ones observed in cells transfected with p38 or TAB1 alone. The result showed that the mutated TAB1 is unable to augment p38α activation suggesting it cannot bind to p38α, unlike WT TAB1. The results from IVK assay and transfection experiment in HEK293 cells confirm that 29mer TAB1 peptide is the region of TAB1 that is responsible for interacting with canonical and noncanonical region of p38α; thus supporting our hypothesis that TAB1 binds to p38α in a bipartite manner.

The results from this chapter offer insights into the interaction between p38α and TAB1, which could impact on developing an inhibitor to prevent the interaction between p38α and TAB1. The canonical region of p38α is shared by upstream kinases of traditional activation pathway and designing a small molecule to target this region could lead to a blanket inhibition of p38α. This will cause the disastrous side effects we have seen in the clinical trials (Marber, 2011). However, to our knowledge there are no known molecules that bind to the noncanonical region of p38α, which makes it an ideal target for a small molecule. An inhibitor that blocks only the noncanonical region of p38α could potentially result in a selective inhibition of p38α caused by

TAB1, without affecting the MKK pathway or other p38α binding partners. It could achieve the much yearned selective inhibition of p38α that is so highly desirable in p38α therapeutics. Hence, the finding of TAB1 binding to p38α in a bipartite manner could be crucial in p38α therapeutics.

4 Thr185 plays a key role in the auto-activation process of p38α

4.1 Introduction

In the third chapter we discussed the activation of p38α mediated via TAB1. Using an over-expression system in HEK293 cells and recombinant proteins in *in-vitro* kinase assays, we showed that TAB1 robustly induced the dual phosphorylation of p38α at the T-G-Y motif. The phosphorylation was sensitive to an ATP-mimetic, SB203580 which led us to confirm that TAB1 is causing autoactivation of p38α. We and various other groups have shown that this mode of p38α activation during myocardial infarction (MI) is harmful to the heart and as a result preventing TAB1 mediated p38α autoactivation would be therapeutically beneficial. To date the studies of p38 inhibition in the setting of MI have used ATP-competitive inhibitors. Unfortunately, these inhibitors have repeatedly failed in clinical trials despite the availability of different scaffolds and mechanisms of binding to p38. In large part this failure is attributable to toxicity (Marber *et al*, 2011) which is common between inhibitors suggesting it is an "on-target" effect. Such toxicity is not entirely surprising considering the ubiquitous nature of p38α and its involvement in a plethora of cellular responses. In cardiomyocytes for example, p38 plays a protective role during ischaemic preconditioning but is lethal in myocardial infarction (Clark et al, 2007; Sicard e al, 2010). Targeting TAB1 would be an alternative strategy but its knockout results in embryonic lethality and it plays an important role in the TAK1 signalling pathway (Komatsu et al, 2002). Therefore, ischaemia selective TAB1 dependent auto-activation of p38α provides a better opportunity for circumstance-selective inhibition of p38α which could potentially reduce the toxicity seen in clinical trials, making it a very attractive therapeutic target to pursue.

To target TAB1 induced auto-activation of p38α, a greater depth of understanding of the molecular interaction between these two proteins is required. To address this, we recently published the crystal structure of p38α and the interacting region of TAB1 which revealed key

residues involved in the binding between the two proteins (De Nicola *et al*, 2013). The crystal structure showed that TAB1 binds to p38α in a bipartite manner which causes structural changes that result in an increased affinity for ATP. The N-terminus and the C-terminus lobes of p38α move towards each other, this movement swings the activation loop (Leu171-Val183) containing the T-G-Y motif towards the catalytic site which facilitates its auto-phosphorylation, rendering the kinase active. Closer inspection of the crystal structure revealed the formation of a hydrogen bond between the side chains of Thr185 on the activation loop and Asp150 of the HRD domain (Figure 1). This hydrogen bond appeared to orientate the activation loop into a position that enabled the T-G-Y motif to access the catalytic site thereby promoting auto-phosphorylation. Therefore, we hypothesised that the inability to form this hydrogen bond would deprive p38α of the free-energy required to reorientate the activation loop and thereby disable the autophosphorylation mechanism. We tested this by mutating Thr185.

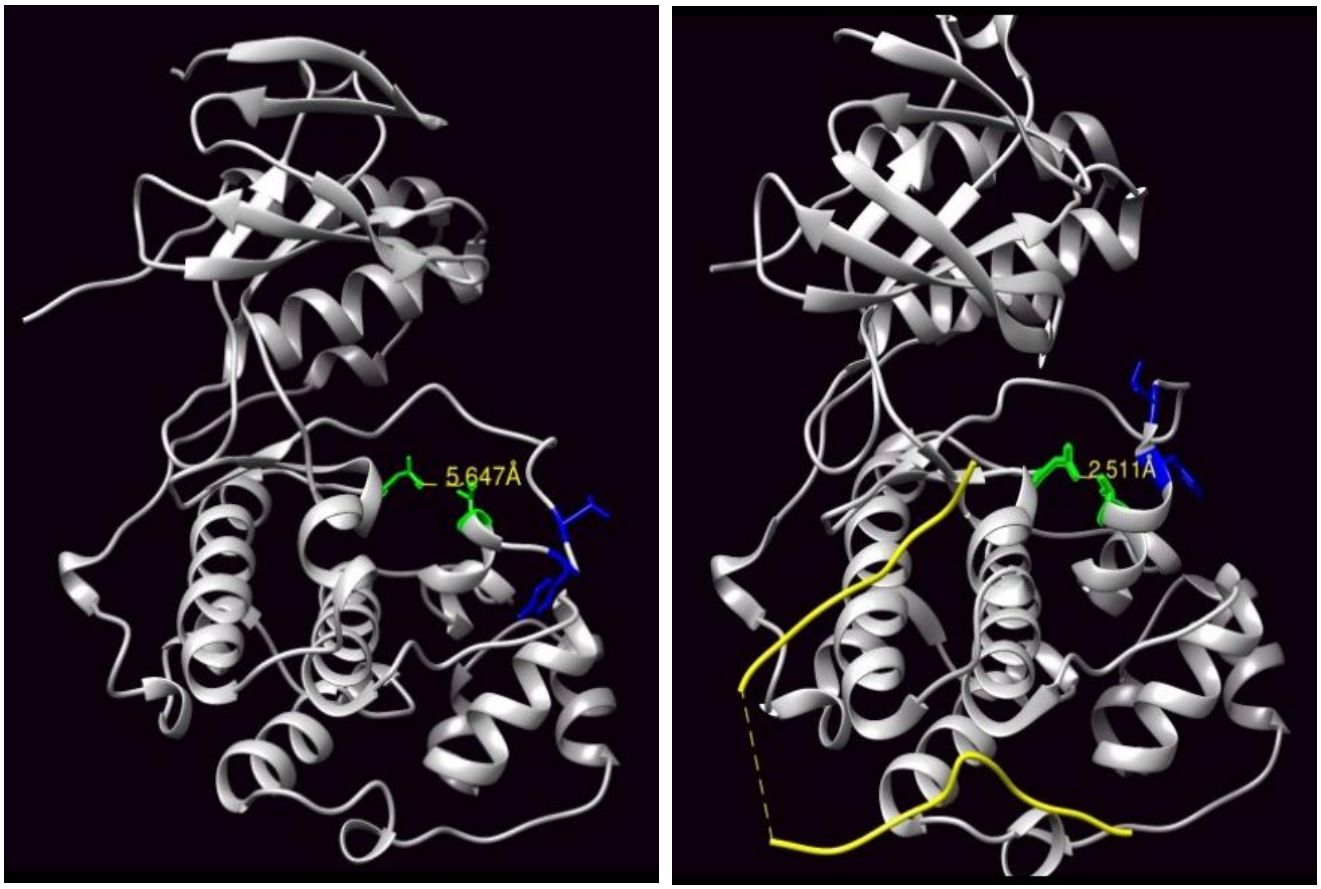

Figure4.1: The crystal structure of WTp38α on the left, and the WTp38α- TAB1 peptide (yellow) on the right. *In the WTp38α, the Thr185 and Asp150 (green) are 5.647Å apart which prevents the formation of hydrogen bond and the T-G-Y motif (blue) is facing away from the catalytic groove preventing autophosphorylation. When the TAB1 is bound, the Tyr182-Thr185 forms an alpha helical segment which is stabilized by the hydrogen bond formation between Thr185 and Asp150 and in the process the activation loop swings towards the catalytic site bringing the T-G-Y motif to the proximity required for autophosphorylation.*

4.2 Specific methods –

4.2.1 cDNA constructs

4.2.1.1 cDNA constructs for bacterial over expression

pETDuet was chosen as a bacterial expression vector to clone the insert of mutant p38αT185G. p38αT185G was cloned in the first multiple-cloning site. The C-terminus and the N-terminus fragments of p38αT185G were produced by two separate PCRs with complementary internal primers containing the required mutations. The PCR products from these reactions were then combined to form a template for the second PCR reaction with external primers to form the complete cDNA of p38αT185G harbouring the desired mutation.

cDNA	Plasmid backbone	Resistance	Details
WT p38α	pETDuet	Ampicillin	Full length WT p38 α-MAPK
p38αT185G	pETDuet	Ampicillin	Full length mutant T185G p38α-MAPK

Table 4.2.1.1 Plasmids used for transformation

4.2.1.2 cDNA constructs for mammalian cell over expression

pCDNA3 was used as the plasmid for expression in mammalian cells. The plasmid contains cytomegalovirus immediate early (CMV) promoter and SV40 polyadenylation sequence for high level expression in mammalian cells. It has an ampicillin resistance gene for selective cloning. Both WTp38α and p38αT185G mutant were cloned into this plasmid.

cDNA	Plasmid backbone	Resistance	Details
WT p38α	pCDNA3	Ampicillin	Full length WT p38 α-MAPK
p38αT185G	pCDNA3	Ampicillin	Full length mutant T185G p38α-MAPK

Table 4.2.1.2 Plasmids used for mammalian cell transfection

4.2.2 Bacterial transformation and growth

4.2.2.1 Transformation and plasmid DNA growth

100ng of plasmid DNA encoding the mutant p38αT185G containing the ampicillin resistance gene was added to 50µl of E. *coli* strain Rosetta™ 2 cells and incubated on ice for 30 minutes (The Rosetta™ 2 are specifically designed to enhance the expression of eukaryotic proteins). The cells were heat shocked at 42^0C for 30 seconds to facilitate the entry of the DNA. The cells were immediately put back on the ice and incubated for 5 minutes. 950µl of fresh LB (Luria-Bertani) media was added to the transformed cells and incubated at 37^0C in a shaker for 1 hour. Following 1 hour, 30µl of LB culture was spread onto LB plates (ampicillin) and incubated overnight at 37^0C. A single colony was picked and used to make a starting culture (15ml) overnight at 37^0C incubator.

4.2.2.2 Protein production in bacteria

The starting culture containing the transformed cells was added to 800ml LB containing ampicillin (100µg/ml) and grown in a 37^0C incubator until the absorbance measured at OD_{600} was 0.6. The culture was cooled down to room temperature and induced with IPTG (Isopropyl β-D-1thiogalactopyranoside) at 1mM final concentration for induction of protein expression. The culture was left to grow in a shaker for 5 hours at 25^0C. The culture was spun using a JLA-

8.1000 rotor (Avanti series, Beckman Toulter) at 6238 RCF (5000 RPM) for 30 minutes at 4^0C to pellet the cells.

4.2.3 Protein Purification

The bacterial pellet was re-suspended in 25ml of cold lysis buffer (Buffer A made up of 500mM NaCl, 50mM Tris, 20mM Imidazole, supplemented with 0.1g of lysozyme, 160µl of 100mM PMSF, 2mM DTT and a tablet of cOmplete™ protease inhibitor cocktail (Roche). The lysate was sonicated at 33% amplitude with a Vibra-cell™ sonicator (Sonics) for a pulse sequence of 4 seconds on, 25 seconds off on ice until the entire pellet broke down and lysate was clear. The lysate was then centrifuged using a JA20 rotor (Avanti™ series, Beckman Coulter) at 35000 RCF for 45 minutes at 4^0C. The soluble fraction of the lysate which contains the protein of interest was transferred into a new tube and passed through a 0.45µM filter and kept on ice ready for purification.

4.2.3.1 Nickel column affinity purification

A nickel-affinity column was used as the first purification step as our protein is expressed with a polyhistidine tag. Prior to its use, the nickel column was washed with 2 column volumes (CV) of deionised water to remove the ethanol in which it is stored. The column was washed with 2 CVs of Buffer B (500mM NaCl, 50mM Tris, 150mM Imidazole –pH7.5) to remove residual contaminants. The column was washed with 2 CVs of Buffer A (500mM NaCl, 50mM Tris, 20mM Imidazole –pH7.5) to equilibrate it before the addition of the soluble fraction. As the soluble fraction passes through the column, our protein with the histidine tag binds to the nickel resin while the unbound debris and other proteins passes through and is collected as the flow through. The column was washed with 5 CVs of Buffer A (with 2mM DTT) to remove any residual impurities that were bound to the column. Buffer B (with 2mM DTT) was added to elute our protein from the nickel column as the high concentration of Imidazole in buffer B acts to displace and elute the bound protein off the column. The eluted protein was dialysed in a 6000-8000 MWCO dialysis tube overnight in 2 litres of dialysis buffer (100mM NaCl, 20mM

Tris, 2mM DTT –pH7.5) in order to remove the high concentration of imidazole in which the protein was eluted.

4.2.3.2 Ion exchange chromatography

Ion exchange chromatography was used as the second purification step. Ionic exchange chromatography separates protein based on their charge at a given pH and takes advantage of the affinity of molecules to the given ion exchanger. We used a Mono Q 5/50 GL column (GE Healthcare Life Sciences), a strong anion exchange column within the ÄKTA purification system. Before starting the purification, the column was washed with 2CVs of deionised water, 2CVs of Buffer B (1M NaCl, 50mM Tris, 2mM DTT –pH7.5, filtered/degassed) to remove contaminants and 2CVs of Buffer A (50mM Tris, 2mM DTT –pH7.5, filtered/degassed) to equilibrate the column. The dialysed protein from the Nickel column purification was filtered using a 0.45µM filter and automatically loaded onto the Mono Q column using a 50ml superloop. Initially, roughly 10 CVs of Buffer A was applied to the column to remove bound contaminants then a gradient of 0-60% of elution buffer (Buffer B) was applied, totalling 40 CVs to elute the protein with flow collected at 0.5ml per fraction. The sample (protein) concentration was measured as it was eluted into fractions by a UV detector (280nm), and a chromatograph (relevant peak), representing the fractions with the greatest protein concentration (Unicorn software), was produced by the program. The fractions containing the eluted protein, represented by the peak, were collected in a falcon tube and the protein concentration was measured using a nanodrop at an absorbance of 280nm. 20µl of sample was also taken to run on an SDS-PAGE gel and coomassie stained to confirm the protein identity by its molecular weight. The rest of the protein sample was kept on ice and used either for the activation of the protein or dialysed overnight in 2 litres of Dialysis buffer (100mM NaCl, 20mM Tris, 10mM DTT –pH7.5) to get rid of the excess salt and ready it for the final purification step of size-exclusion chromatography.

4.2.3.3 Size Exclusion Chromatography

The final step of purification was carried out using a gel filtration column in the ÄKTA purification system. The gel filtration column separates molecules based on their size with high purity yield and is often used as the final purification step (polishing step). The dialysed protein from the previous purification step was filtered using 0.45µM filter and concentrated to 10mg/ml using a 10,000 MWCO centricon. The reason for concentrating the sample was to reduce the total volume of protein as the maximum capacity of the column (HiLoad 26/60 Superdex 75- Ge Healthcare Life Sciences) is limited to 12 ml. The column was washed with 1 CV of deionised water and equilibrated with 1CV of buffer (100mM NaCl, 20mM Tris, 10mM DTT –pH7.5, filtered/degassed). Once the sample was loaded into the column using a 50ml superloop, the column was pumped with 1.5 CV of buffer and 0.5 ml of sample per fraction was collected. The samples from different fractions were pooled as represented by the peak given by a UV detector (280nm) and their constituent protein concentration was measured using a nanodrop at 280nm absorbance. The samples were divided into aliquots, flash frozen using liquid nitrogen and stored at -80^{0}C for future use.

4.2.4 Isothermal titration calorimetry (ITC)

ITC was carried out in an ITC200 microcalorimeter from Microcal (GE Healthcare Life Sciences). 70µl of 180µM p38α was loaded into a syringe and 320µl of 20µM TAB1 peptide was loaded into the cell. Prior to loading, both syringe and cell were rinsed extensively with de-ionized water. After loading the samples, the temperature for the reaction was set at 25^{0}C, the number of injections was set at 13 with 3µl sample per injection with spacing of 400 seconds between each injection to enable the system to reach equilibrium. The reaction was started and the first addition was done after achieving the baseline stability. After completion of the experiment, Microcal Origin 7.0 data software was used to analyse the result. Integrated heat data obtained for the titrations corrected for heats of dilution were fitted with a nonlinear least-squares minimization algorithm to a theoretical titration curve. The heat of the first injection was discarded from the analysis to avoid artefacts due to diffusion through the injection port

that occur during the long equilibrium period which affects the local protein concentration near the syringe. The data fitting gave us the values for binding stoichiometry (n), binding affinity (K), molar enthalpy change (ΔH). The molar entropy (ΔS) was calculated using ΔS = ΔH- ΔG, where ΔG= -RT x lnK (R=1.987 cal mol^{-1} K^{-1}, T=298K).

4.2.5 Crystallization and structure determination

The p38αT185G-TAB1 complex at 12mg/ml was preincubated with 1mM SB203580 and crystallized by sitting-drop vapour diffusion at 4^{o}C. The complex crystals grew in two different conditions yielding two different forms; 1, p38α-TAB1 tetragonal, 20%w/v PEG3350, 0.2M Na/K tartrate, 0.1M bis-Tris propane, pH6.5. 10% ethylene glycol, and 2, p38α-TAB1-S04 tetragonal, 25% w/v medium-molecular-weight PEG smears, 0.2M ammonium sulphate, 0.01M $CdCl_2$, 0.1M HEPES, pH7.5. The crystals were cryoprotected with mother liquor supplemented with 20% ethylene glycol. The diffraction data were collected using beamline I03 and I04 at Diamond Light Source and processed and scaled with MOSFLM and SCALA. The structure was solved by molecular replacement with a p38α monomer and PHASER[45] as a search model.

4.2.6 *In-vitro* Kinase assay

An *in-vitro* kinase assay was performed to activate p38α by MKK6, and ATF2 by p38α. 1mg of p38α was activated with 0.2mg of MKK6*dd*. The reaction was supplemented with 3.3ml of EGTA at 1mM, 3.3ml of $MgCl_2$ at 100mM and 360µl of ATP at 20mM. The final reaction volume of 33ml was made up using buffer (100mM NaCl, 20mM Tris, 2mM DTT –pH7.5). The samples were mixed gently and the reaction tube was incubated at 37^{0}C for 2 hours. After 2 hours, 300µl of amylose resin was added to the reaction tube to remove MKK6 (MKK6 was tagged with Maltose binding protein which has high affinity for amylose). The sample was centrifuged for 5 minutes to pellet the amylose resin bound with MKK6 and rest of the sample was separated and filtered through a 0.45µM filter. The sample was passed through the Mono Q column for another step of purification to remove the impurities from the activation process of *in-vitro* kinase assay. Once purified, the sample was dialysed overnight in the dialysis buffer

(100mM NaCl, 20mM Tris, 10mM DTT –pH7.5) to get the end product of active p38α. The IVK for ATF2 was carried out for 30 minutes using 0.86μM ATF2, 0.2μM p38α and 550μM ATP in a kinase buffer.

To carry out the TAB1 mediated activation of mutant p38αT185G; 3μM of p38α was used with 15μM of TAB1 peptide (384-412) and incubated in 1X kinase buffer (25mM Tris/HCl -pH7.5, 5mM β-glycerolphosphate, 2mM DTT, 0.1mM Na_3VO_4 and 1mM $MgCl_2$). 5μl of 10mM ATP was added to the incubation mixture to start the reaction at 37^{o}C. The samples were collected at four different time points of 30min, 1hr, 2hr, and 4hr. 2X sample buffer (20% glycerol, 6% SDS in 0.12M Tris –pH6.8, 10% 2-mercaptoethanol and 0.4% Bromophenol Blue) was added to the sample, heated to 95^{o}C for 10 minutes and used for western blot analysis as described previously in the second chapter (2.1.4). The samples were run on a 10% SDS-PAGE gel, transferred onto a membrane and probed with dual monoclonal phospho p38 (Thr180/Tyr182) antibody (Sigma), total p38 antibody (Cell Signalling), phospho ATF2 antibody (Cell signalling).

4.2.7 Ischaemic buffer

The recipe for Ischaemic buffer has been adapted from Esumi et al, 1991 which is described in Punn et al, 2000. 50ml of Ischaemic buffer (127mM NaCl, 3.58mM KCl, 0.49mM $MgCl_2.6H_2O$, 1.8mM $CaCl_2.2H_2O$, 4mM HEPES, pH7.4) was made up using 5ml of 10X basic stock solution and 45ml of sterile deionised H_2O. 10mM 2-DOG and 20mM Na lactate was added to the 50ml solution and filter sterilised using a 0.2μm syringe, warmed to 37^{O}C. pH of the solution at this point is 6.8. Once the solution was warmed up, 1mM Na dithionite was added to the solution (pH drops to 6.3) and mixed before quickly adding it onto the cells for 10mins. Cells were washed with PBS prior to the addition of ischaemic buffer. After 10mins, cells were collected using 150 μl of 2X SDS buffer and analysed by western blotting.

4.2.8 Western Blot

Western blotting was done as described earlier in chapter 2. Briefly, samples were lysed with 2X SDS sample buffer and boiled at 95^{o}C for 10 minutes. 5µl of IVK samples and 10µl of cell samples were run on 10% SDS polyacrylamide gel for 1hr 30 min and transferred to a PVDF membrane. The membrane was then blocked with 4% milk and 1% BSA in TBST for 1 hour at room temperature. The membrane was then probed with appropriate antibody (see table below) overnight at 4^{o}C. The membrane was washed three times with 15ml of TBST for 10 minutes each and blocked with rabbit secondary antibody conjugated with HRP for 1 hour at room temperature. The membrane was washed three times with 15ml TBST for 10 minutes each and developed by chemiluminescence technique.

	Cell samples	**IVK samples**
Phospho p38 antibody (T180/Y182)	1/1000	1/5000
Total p38 antibody	1/2000	1/10000
Phospho TAB1 (Ser423)	1/1000	N/A
Total TAB1	1/2000	N/A
Phospho MKK3/6	1/1000	1/5000
Phospho ATF2	N/A	1/2000
Total ATF2	N/A	1/10000
Secondary antibody	1/5000	1/8000

Table 4.2.8 Antibodies used for western blot

4.2.9 Statistical analysis

Data sets were analysed by one way ANOVA (Analysis of Variance) and groups were compared using Tukey's test as a post-hoc. p value of less than 0.05 was considered significant.

4.3 Results

4.3.1 First purification step: Nickel column affinity purification of p38αT185G

After carrying out the large scale growth of transformed bacteria (Rosetta^{TM} 2) expressing the protein of interest, several purification techniques were employed. Bacteria were lysed as described in section 4.2 and the soluble fraction containing protein was used for purification. Since the protein was cloned with a polyhistidine tag at the C-terminal end, a nickel column was used for the first purification. At each step of the nickel column purification, 20µl of samples were collected to run on 10% SDS-PAGE gel and stained with Coomassie Brilliant Blue to provide a visual estimate of purity. As evident from the image of the gel in figure 4.3.1, the protein purity increases at each step of Nickel column purification with a single band seen on the elution fraction around 38kDa molecular weight. The total fraction represents the soluble fraction of the lysate; Flow-through fraction represents the flow through collected after passing the soluble fraction through the nickel column where the protein binds to the column and remaining contaminants pass through the column; wash represents washing of the column with buffer A (low salt); and finally the elution fraction represents our protein p38αT185G which is eluted with high salt buffer B.

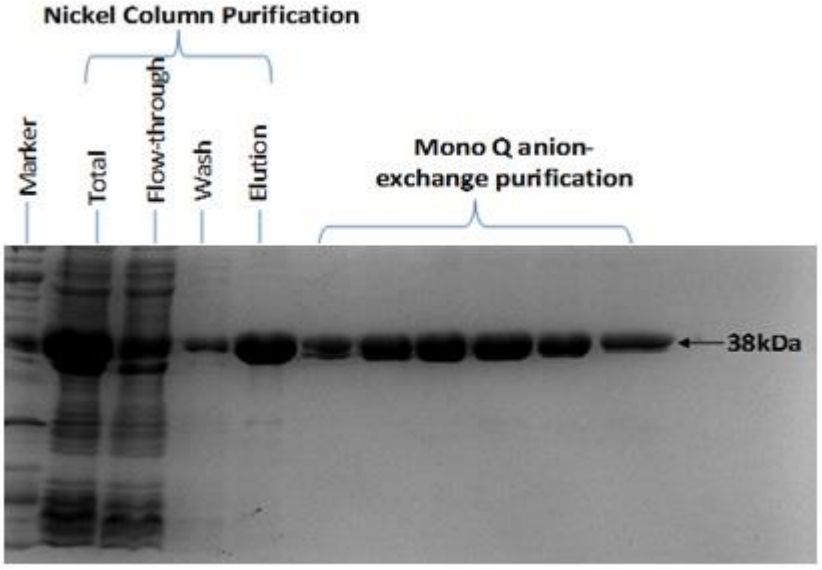

Figure 4.3.1 Coomassie Brilliant Blue staining of SDS-PAGE gel: *The image shows the SDS-PAGE gel following coomassie staining of samples from each step of Nickel column purification and the samples collected from different fractions of the subsequent MonoQ anion exchange purification. As highlighted, the relevant band is seen around molecular weight of 38kDa, which is the molecular weight of the protein p38 (although the protein runs a little higher on the gel (~40kDa) due to polyhistidine tag). As seen, the p38α band gets cleaner after each stage of Nickel column purification and a clean single band is seen on the fractions collected from the anionic exchange chromatography column.*

4.3.2 Second purification step: Ionic-exchange chromatography of p38αT185G

After the Nickel affinity column purification, the elution fraction was purified further using ion exchange chromatography to improve the purity level. We used an anionic exchanger Mono Q 5/50 GL column (GE Healthcare Life Sciences). With pI value of 5.4, p38αT185G is negatively charged at pH7.5 and will initially bind to the column. But as the gradient of high salt buffer B increases during purification, p38αT185G's affinity is diminished by the increasing concentration of negatively charged chloride ions which results in the displacement of p38α. Thus p38αT185G gets eluted off the column with higher purity, separating it from other contaminating proteins and residues. As seen in figure 4.3.1, the fractions collected under the main peak of chromatogram (Fig 4.3.2) contain a single band representing our protein

p38αT185G. This step removed the faint bands that were seen on the elution fraction of the previous Nickel column purification, further improving the purity of our protein.

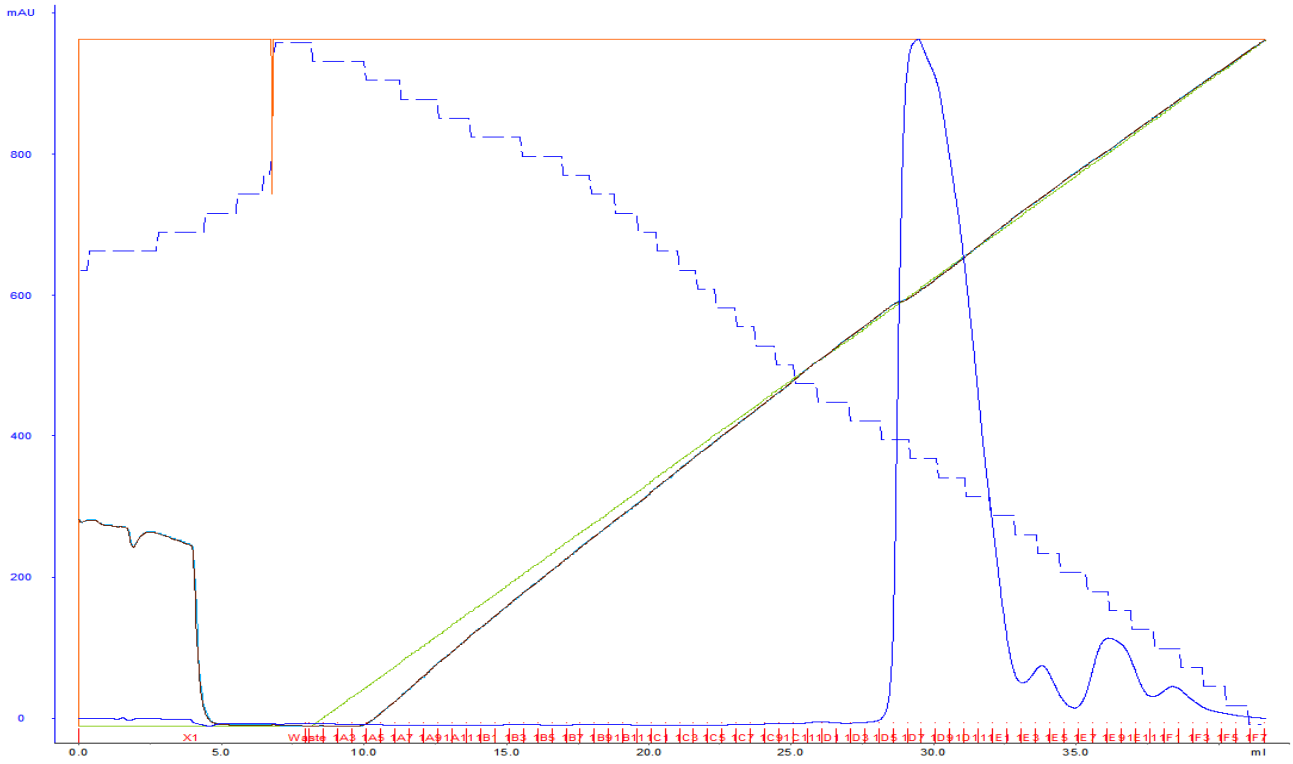

Figure 4.3.2 Mono Q anionic exchange purification: *The chromatograph shows the absorbance at 280nm (blue peak) which represents the elution of protein from the column. The dominant peak around 1000mAU represents p38αT185G and corresponding fractions under this peak were collected and ran on the SDS gel shown in figure 4.3.1. The subsequent small peaks represent the elution of trace proteins with different phosphorylation states, as the column separates protein based on ionic strengths which varies according to the phosphorylation state (negative charge), and were discarded.*

4.3.3 Third purification step: Size exclusion chromatography of p38αT185G

Finally, a gel filtration column was used as the last step of protein purification; this polishing step increased the purity close to 100%. The samples collected after this step were either immediately used for our experiments or stored at -80^{0}C for future use. The purity of samples can be seen in figure 4.3.3A which shows the elution fraction from the size-exclusion

chromatography purification. It is also reflected in the chromatograph in figure 4.3.4B with a single peak of UV absorbance at 280nm (blue trace).

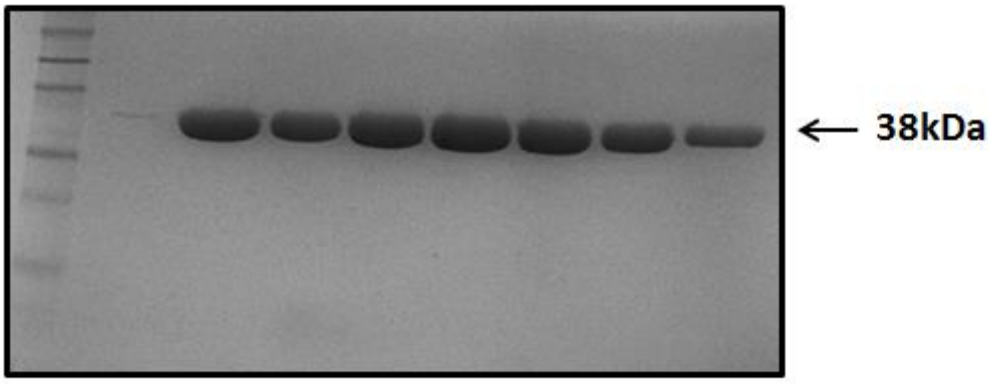

Figure 4.3.3A Coomassie Brilliant Blue staining of the SDS gel: *The SDS gel after coomassie staining of the fractions eluted from the gel filtration column. The samples were taken from the fractions under the peak on the chromatograph as seen in figure 4.3.4B. A single clean band is seen around 38kDa molecular weight without any impurities.*

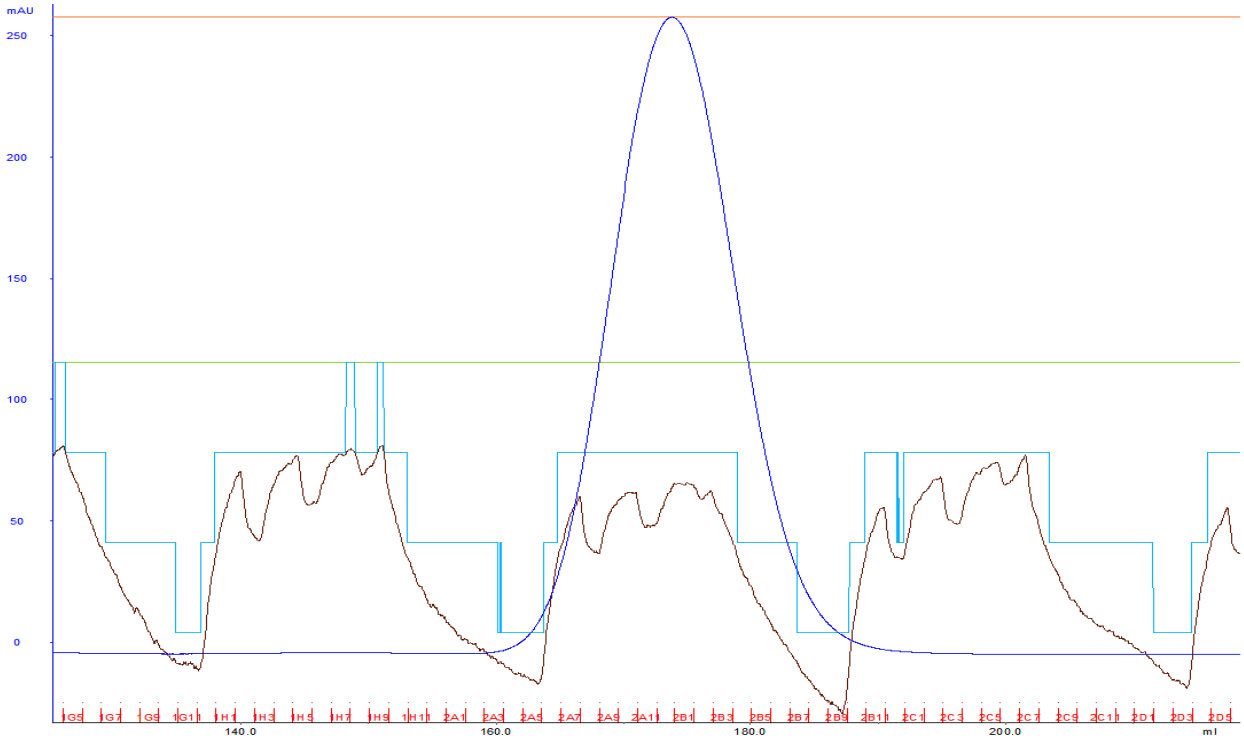

Figure 4.3.3B Chromatograph of gel filtration column: *The chromatograph shows a single blue peak at 280nm absorbance, representing a single pure protein being eluted from the column. The other coloured line represents different parameters of purification; brown line represents the conductivity, light blue represents percentage of buffers and the green line represents the pressure in the column.*

4.3.4 Isothermal titration calorimetry

p38α autoactivation is the consequent result of TAB1 interacting with p38α, i.e. without the p38α-TAB1 interaction, the auto-phosphorylation of p38α's T-G-Y motif cannot happen. So before testing our hypothesis that the p38αT185G mutation impairs TAB1-induced p38 auto-activation, we needed to confirm that the p38αT185G mutant kinase is able to bind TAB1. ITC was performed with recombinant p38αT185G and 29mer TAB1 peptide (384-412) as described in section 4.2.4. The results showed that p38αT185G was able to bind to TAB1 and the mutation did not affect its ability to interact with TAB1 (Fig 4.3.4). Data analysis confirmed that the mutant protein p38αT185G was interacting strongly with TAB1 similar to WTp38α with a binding affinity of 9.76 X $10^{\wedge 5}$/mol.

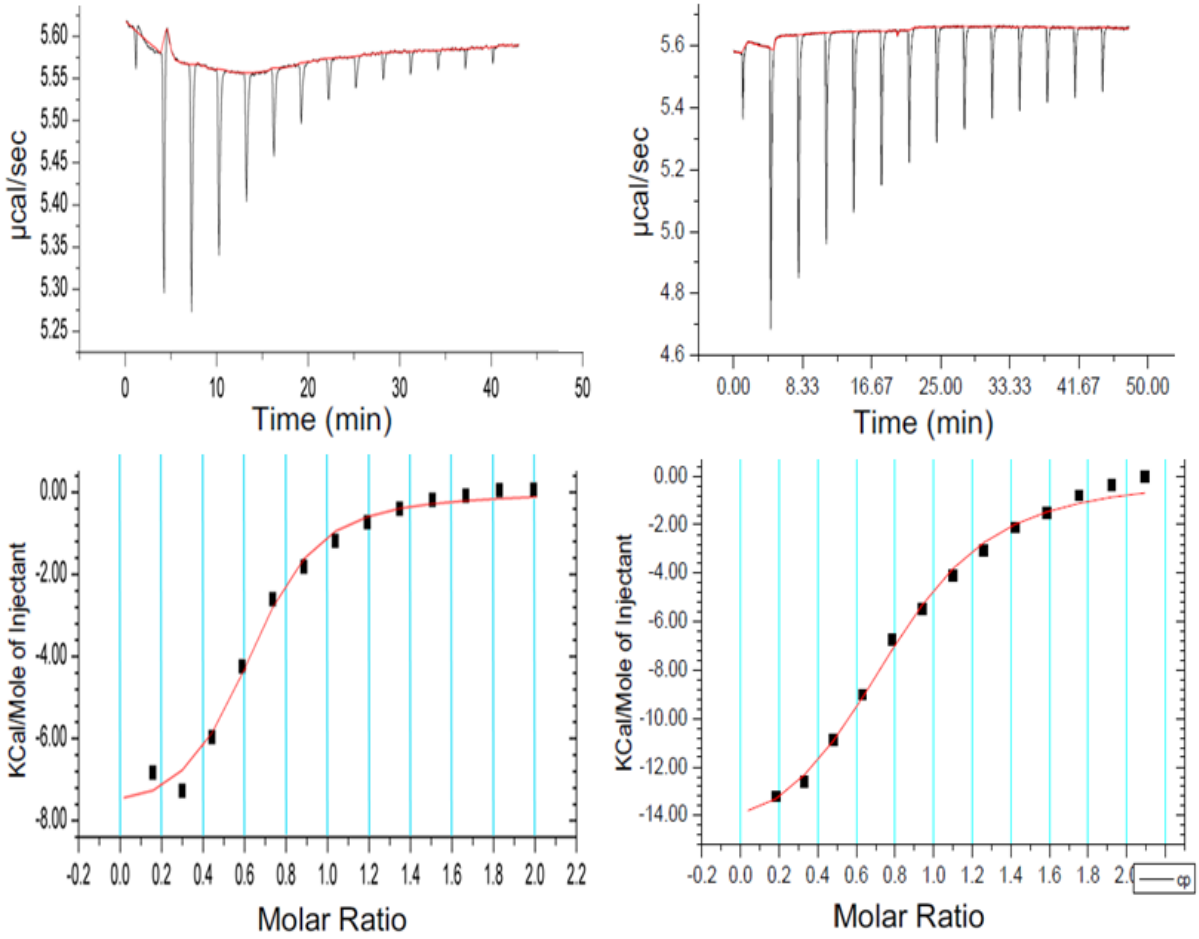

	N	Kd (M^{-1})	ΔH (cal/mol)	ΔS(cal/mol/deg)
p38αT185G-TAB1 (384-412)	0.60567	9.76E5 (+/-59275)	-8540 (+/-789)	-1.23 (+/-2.7)
WTp38α-TAB1 (384-412)	0.782	4.35E5 (+/-72000)	-15930 (+/-710.3)	-27.6

Figure 4.3.4 ITC titration profile of p38αT185G on the left and WT p38α on the right with TAB1 peptide (384-412) and a table summarizing the thermodynamic parameters of the interaction: *The top figures shows the raw data traces of differential power recorded (µcal/sec) over time generated by formation of a complex between p38αT185G and TAB1 peptide (384-412) (left) and WTp38α and TAB1 peptide (384-412) (right), with sequential injections of p38αT185G into TAB1 peptide. The plot of the heat evolved per injection over molar ratio calculated from integration of the data, corrected for the dilution. The bottom figure represents the thermodynamic parameters of the interaction which is summarized in the table below it, from 3 independent experiments with standard deviation.*

4.3.5 Crystal structure of p38αT185G and TAB1 peptide (384-412)

Following the confirmation of interaction between p38αT185G and TAB1 with ITC, we crystallized the p38αT185G-TAB1 complex in order to see its structure and compare it with the WTp38α-TAB1 *(This was carried out by Dr Gian De Nicola and Dr Charles Nichols).* The crystal structure revealed many shared features between these complexes with the notable exception of the activation loop confirmation. The crystal structure showed that without the hydrogen bond between Thr185 and Asp150, the activation loop (Leu171-Val183) of p38αT185G is not able to adopt the orientation observed in WTp38α. The helical extension of the c-terminal portion (Tyr182-Thr185) of the activation loop of WTp38α that orientates T180 towards the catalytic cleft, is absent in p38αT185G. This crystal structure indicates that our hypothesis could be correct and without the hydrogen bond between Thr185 and Asp150, the activation loop cannot orientate towards the catalytic site, which would be predicted to impair the auto-phosphorylation of T-G-Y motif. With this encouraging finding, we proceeded to test our hypothesis.

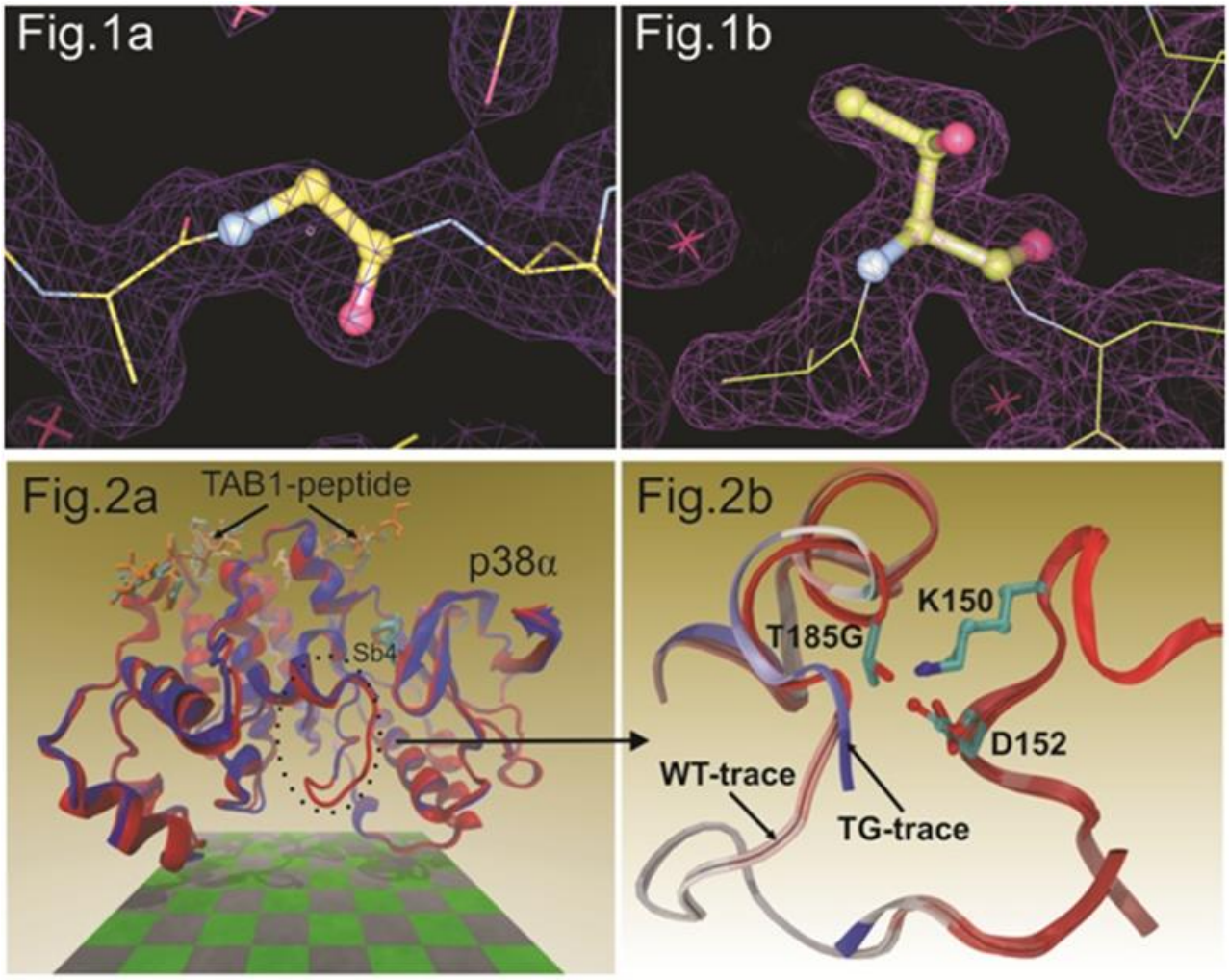

Figure 4.3.5 Crystal of p38αT185G-TAB1 peptide (384-412) complex. *1) Representative p38α 2fo-fc electron density maps at 1.0σ, residue 185 highlighted in CPK format (1a shows p38αT185G, 1b shows WTp38α). 2a) Cartoon format illustrates the structural comparison of wild-type (WT) in red and T185G (TG) in blue p38α co-crystallised with TAB1 peptide and ATP-analogue SB. 2b) Close-up of loop containing residue Thr185 and its H-bonds with Asp150 in the WT. The Thr185 residue in T185G trace is not shown but its relaxation can be seen compared to the WT (blue trace compared to red). The relaxation of the C-terminal end of activation loop in T185G trace caused high B factor (100 compared to 40 in WT) indicating a very mobile activation loop, which as a result could not be resolved in the crystal structure. Side-chain atoms of residue D150, K152 and T/G185 are shown in liquorice (WT) or CPK (TG) formats. Lattice constraints prevent complete loss of helical structure, but the B-factor analysis clearly shows a dramatic destabilisation of the 185-helix and connected N-terminal loop region.*

4.3.6 p38αT185G's autoactivation is impaired

To test our hypothesis of impaired autoactivation of the p38αT185G mutant, we carried out an *in-vitro* kinase assay (IVK) with recombinant p38αT185G and 29mer TAB1 peptide (384-412). The IVK assay was carried out in an eppendorf tube with p38αT185G (3µM), TAB1 peptide (15µM) and ATP (550µM) in 1X kinase buffer for 4 hours at 37^{o}C. The product of the reaction was collected at four different time points for analysis by western blot. The western blot result shows TAB1 caused autoactivation of WTp38α at 4 different time points but was not able to cause autoactivation of the p38αT185G mutant as seen by the lack of phosphorylation at T-G-Y motif (Fig 4.3.6). This result suggests that the hydrogen bond that forms between Thr185 and Asp150 is essential in the process of p38α autoactivation caused by TAB1.

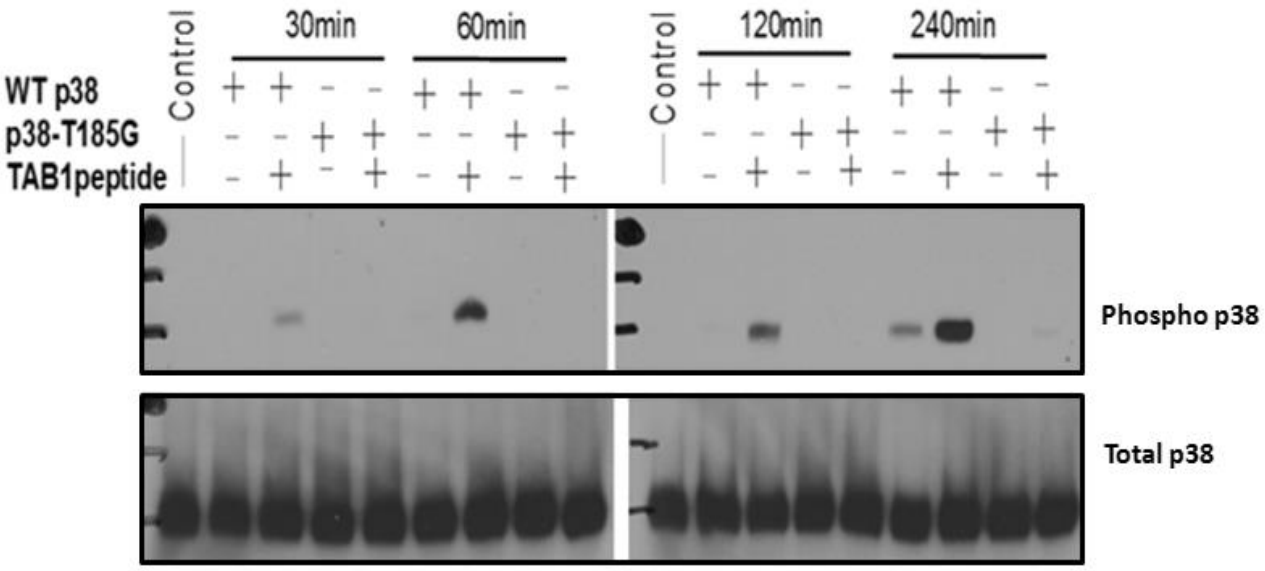

Figure 4.3.6 In-vitro kinase assay with WTp38α, p38αT185G and TAB1. *The western blot analysis of kinase assay performed with WTp38α and p38αT185G mutant in the absence and presence of TAB1 peptide (384-412) at 4 different time points. Phospho p38 signal can be seen in the sample with WTp38α and TAB1 which becomes stronger with time. The phospho p38 signal in sample with p38αT185G and TAB1 remains undetectable with a very faint signal barely visible only at the 4hrs time point.*

4.3.7 p38αT185G autoactivation is impaired in HEK293 cells

The IVK result suggested that the hydrogen bond that forms between Thr185 and Asp150 is essential in TAB1 induced p38α autoactivation which supports our hypothesis. To further examine this mechanism, we used an over-expression system in mammalian HEK293 cells and ectopically expressed p38αT185G in HEK293 cells together with TAB1. 24hrs after transfection there was a significant increase in phospho-p38 (T-G-Y) signal in cells transfected with WTp38α and TAB1, however no such increment was observed in cells transfected with the p38αT185G mutant and TAB1 (Fig 4.3.7). The result mirrors the outcome from IVK and provides another strand of evidence to support our hypothesis that the hydrogen bond formation between Thr185 and Asp150 is a prerequisite step for TAB1 induced p38α autoactivation and without it the process is significantly compromised.

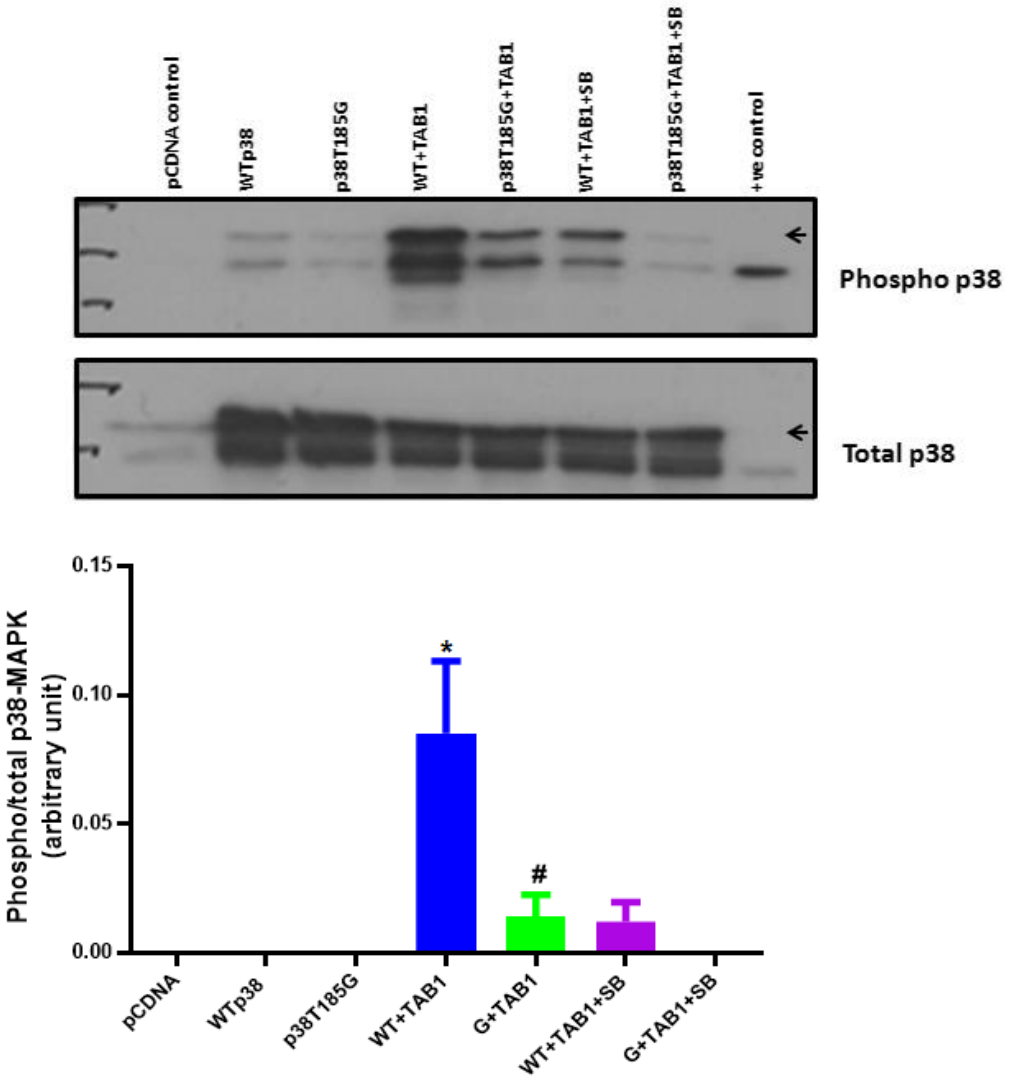

4.3.7 Western blot analysis of HEK293 cells transfected with WTp38α, p38αT185G and TAB1. *Western blot result of HEK293 cells co-transfected with WTp38α or p38αT185G and TAB1 treated with SB203580 (10μM). There was a significant difference between the wtp38α and p38αT185G activation when co-transfected with TAB1. The phospho-p38 signal was reduced by SB203580 treatment indicating the mode of activation to be autoactivation. The result clearly illustrates the impaired autoactivation in p38αT185G compared to WTp38α. The arrow represents the ectopic p38 which runs higher than the endogenous p38 as it is heavier because of the polyhistidine tag. At the bottom is the graphic representation of the quantification of 3 independent experiments which shows a significant difference between WTp38α and WTp38α+TAB1 (*), and WTp38α+TAB1 and p38αT185G+TAB1 (#). Data represented as mean+/- SEM, $p<0.05$.*

4.3.8 Simulated Ischaemia does not cause autoactivation of p38αT185G

In order to provide a more physiologically relevant stimulus to test our hypothesis of TAB1-induced p38α autoactivation, we decided to use ischaemic stress. We transfected HEK293 cells with either WTp38α or p38αT185G, and subjected cells to simulated ischaemia using simulated ischaemia buffer (relying on endogenous TAB1 to cause p38α autoactivation). After 10 minute incubation in ischaemic buffer, we saw increased phospho p38 (T-G-Y) signal in cells transfected with WTp38α compared to the control baseline (Fig 4.3.8), which was SB203580 sensitive confirming the mode of p38 activation to be autoactivation. In cells transfected with the p38αT185G mutant, we did not see an increased phospho-p38 signal compared to the control baseline with ischaemia indicating impaired autoactivation. The result recapitulates the outcome from previous experiments of IVK and over-expression with TAB1 in HEK293 cells.

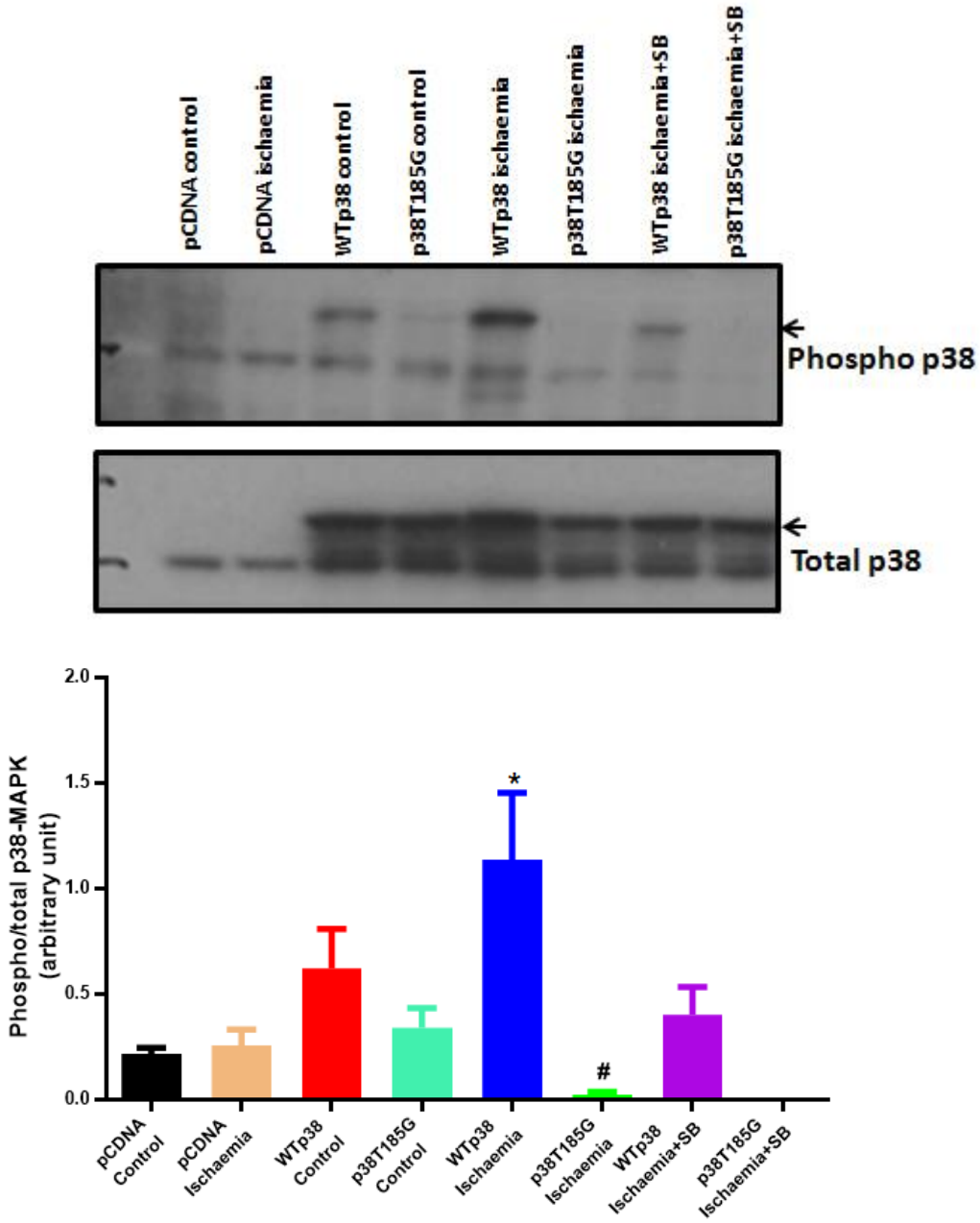

4.3.8 Western blot analysis of HEK293 cells subjected to simulated ischaemia. *Western blot result of HEK293 cells transfected with WTp38α or p38αT185G exposed to ischaemia buffer for 10 minutes in the presence of SB203580. There was a significant increase in phospho-p38 signal compared to control baseline when treated with ischaemic buffer in cells transfected with WTp38α. This was inhibited was SB203580 at 10μM. In cells transfected with p38αT185G, no increment in phospho-p38 signal was observed with ischaemic buffer compared to the control. The arrow represents the ectopic p38α. Below the blot is the graphic representation of the quantification of 3 independent experiments which shows a significant difference between wtp38α and p38αT185G autoactivation caused by ischaemic buffer. Data represented as mean+/- SEM, n=3, p<0.05, * = against control, # = against WTp38 ischaemia.*

4.3.9 p38αT185G and WTp38α are similarly activated by upstream kinases

Having obtained results to support our hypothesis that the hydrogen bond between Thr185 and Asp150 plays an important role in p38α's autoactivation process, we asked ourselves whether it had a similar role in p38α's classical activation pathway. To investigate this we carried out an *in-vitro* kinase assay with p38α and the dual specificity kinase MKK6, an upstream activator of p38. The IVK assay was carried out as described earlier with p38α, the constitutively active MKK6dd and ATP at 37^{O}C in a kinase buffer. After 2 hours of IVK reaction, the constitutively active MKK6 was able to activate the p38αT185G mutant in a similar way to WTp38α (Fig 4.3.9). The result suggested that hydrogen bond between Thr185 and Asp150, unlike in p38α's autoactivation mechanism, has no impact on p38α's trans-activation mechanism involved in the canonical pathway of p38α activation.

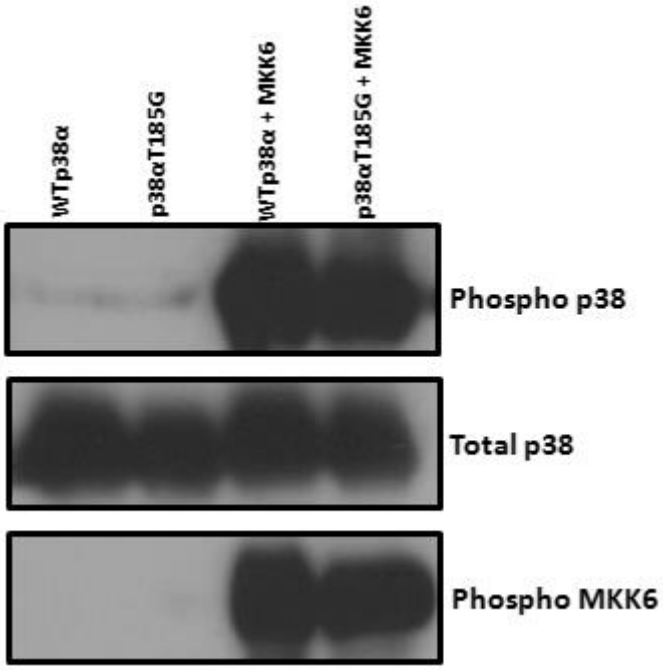

Figure 4.3.9 Activation of p38αT185G and WTp38α by upstream kinase MKK6. *Western blot of the product of the IVK reaction between WTp38α/p38αT185G and MKK6dd. MKK6dd was able to equally phosphorylate both WTp38α and p38αT185G as seen by the similar phospho-p38 signal.*

4.3.10 p38αT185G and WTp38α are similarly activated by upstream kinase in HEK293 cells

Following the IVK result, we next examined whether these differential effects could be recapitulated in mammalian cells. We used an over-expression system to transfect HEK293 cells with WTp38α or p38αT185G, TAB1 and MKK3, another upstream activator of p38α. 24hrs following transfection, we saw an increased phospho-p38 signal in cells transfected with WTp38α and TAB1 compared to control but not in cells transfected with p38αT185G and TAB1. In cells transfected with WTp38α and MKK3, we saw a significant increase in phospho-p38 signal which was expected but we also saw similar level of increased phospho-p38 signal in cells transfected with p38αT185G and MKK3. The result suggests there is no difference between WTp38α and p38αT185G transphosphorylation by upstream kinases, paralleling the result from IVK.

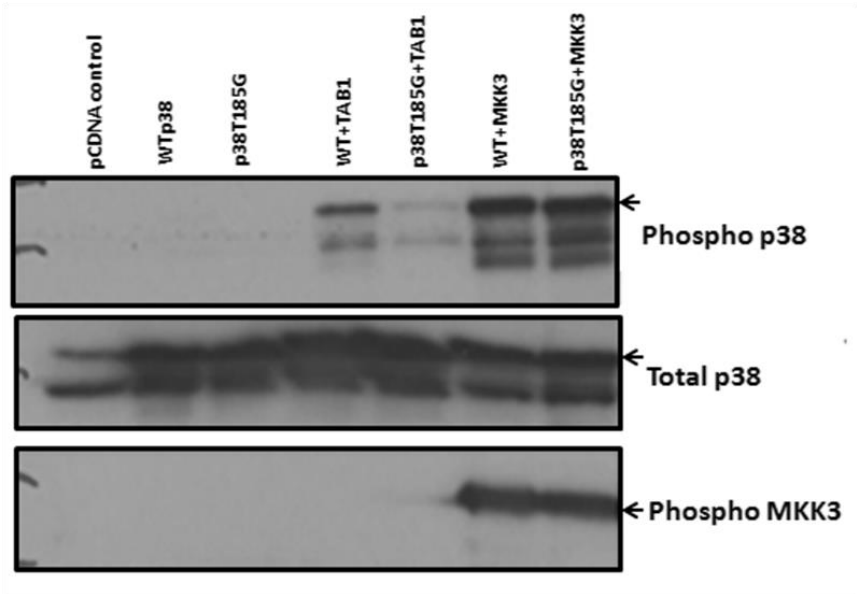

Figure 4.3.10 Activation of p38αT185G and WTp38α by TAB1 and MKK3. *Western blot figure shows the result of HEK293 cells transfected with WTp38α/p38αT185G, TAB1 and MKK3. There was increased phospho-p38 signal in cells transfected with WTp38 and TAB1 compared to control but not in cells transfected with p38αT185G and TAB1. There was a marked increase in the phospho p38 signal in cells transfected with both WTp38 and TAB1, but not p38αT185G and TAB1. Phospho-MKK3 signal can be seen in cells transfected with MKK3 indicating active MKK3. Arrow heads represents ectopic band which run higher than endogenous due to their tags.*

4.3.11 p38αT185G and WTp38α are similarly able to phosphorylate downstream substrates.

The results so far suggest that the hydrogen bond between Thr185 and Asp150 plays an important role in p38α's auto-activation by TAB1 but not in p38α's ability to be trans-activated by MKK3/6. Next we wanted to investigate whether the hydrogen bond would have an impact on p38's ability to phosphorylate its downstream targets. We carried out an *in-vitro* kinase assay with WTp38α, p38αT185G and activating transcription factor -2 (ATF2) which is a well known substrate of p38 as described in 4.2.5. The IVK result showed that both WTp38α and p38αT185G mutant were able to phosphorylate ATF2 similarly (Fig 4.3.11). The result suggests that p38α's catalytic ability is not affected by the mutation in p38αT185G.

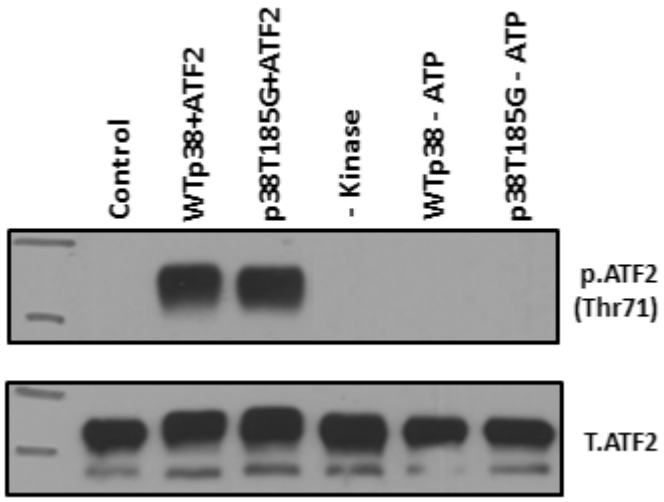

Figure 4.3.11 Activation of ATF2 by WTp38α and p38αT185G: *Western blot of the product of the IVK reaction between recombinant WTp38α/p38αT185G and ATF2. A clear phospho ATF2 signal was observed in sample with WTp38 and ATF2, and p38αT185G and ATF2.*

4.3.12 Activation of TAB1 by WTp38α and p38αT185G in HEK293 cells

To further confirm the previous IVK result which suggested no difference in p38αT185G's ability to phosphorylate its substrate compared to WT, we carried out an over-expression experiment in HEK293 cells to look at another of p38's prominent substrates, TAB1. WTp38α, p38αT185G and TAB1 were transfected in HEK293 cells and 24hrs later analysed by western blotting. The result showed that the cells transfected with p38αT185G had a similar level of phospho-TAB1 signal compared to the cells transfected with WTp38α (Fig 4.3.12). Although the result recapitulates the IVK outcome carried out with ATF2, this result is surprising. In the IVK assay, the active p38αT185G had been pre-activated with MKK6 so there was an equal amount active WTp38α and p38αT185G. However, in this case the active p38αT185G is lower than the WTp38α as seen by the phospho p38 signal.

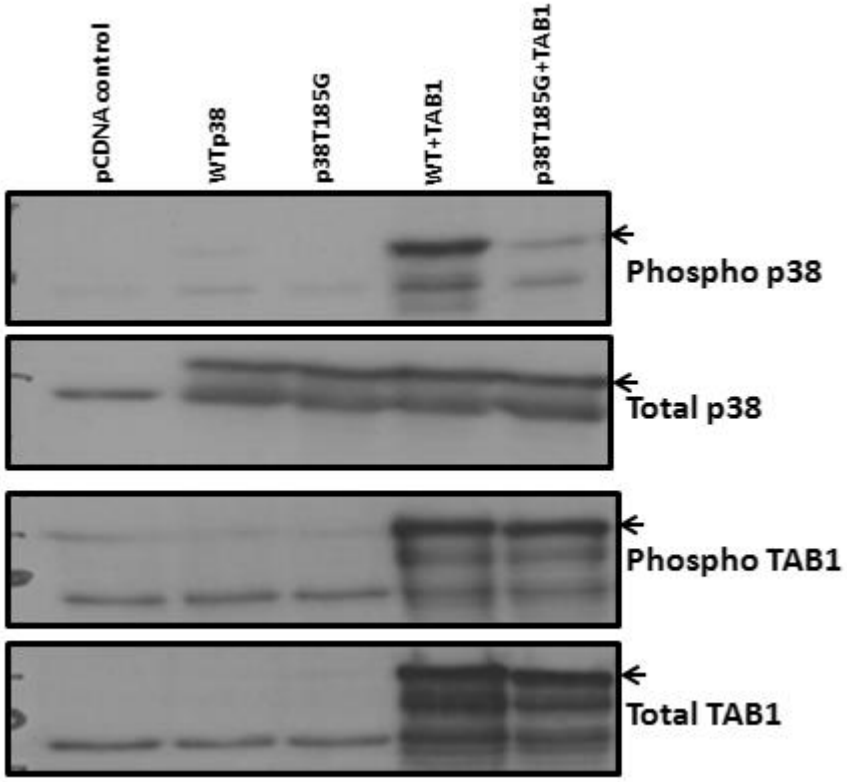

Figure 4.3.12 Activation of TAB1 by p38αT185G and WTp38α. *Western blot of the HEK293 cells transfected with WTp38α, p38αT185G, and TAB1. There was increased phospho-p38 signal in cells transfected with WTp38 and TAB1 compared to control but not in cells transfected with p38αT185G and TAB1. There was a similar level of increment in phospho TAB1 signal in both WTp38 and p38αT185G transfected cells indicating both WTp38α and p38αT185G are able to activate TAB1 equally. Arrows indicate ectopic band.*

4.3.13 The T185G mutation makes a difference at lower enzyme concentrations.

From our results in 4.3.9 we concluded that the hydrogen bond between Thr185 and Asp150 does not have an impact on p38α's phosphorylation by MKK3/6. The same conclusion was made on p38α's catalytic ability based on the ATF2 (Fig 4.3.11) and TAB1 (Fig 4.3.12) data. However, the IVK experiments carried out were performed using high enzyme concentration which is not ideal. The high enzyme concentration not only makes the reaction conditions unphysiological, but it also leads to artefactual stoichiometry which can give rise to misleading results when trying to interpret enzymatic activity. Therefore in order to address this deficiency, we carried out a kinetic assay where we lowered the concentration of enzyme to the low nanomolar range. The IVK was carried out at a constant p38α concentration and varying concentrations of MKK6 for 20 minutes. There was no difference between WTp38α and p38αT185G mutant transphosphorylation by MKK6 above 0.02μM (20nM) concentration of MKK6. Below 6.6nM concentration, MKK6 was able to activate WTp38α much more efficiently than the p38αT185G mutant (Fig 4.3.13 A). Similarly in the IVK assay with p38α and ATF2, there was no significant difference in p38αT185G mutant's ability to activate ATF2 compared to WTp38α until 0.006μM (60nM) concentration of p38α (Fig 4.3.13 B). From 20nM concentration and onwards, p38αT185G's ability to phosphorylate ATF2 was significantly reduced compared to WTp38α.

A)

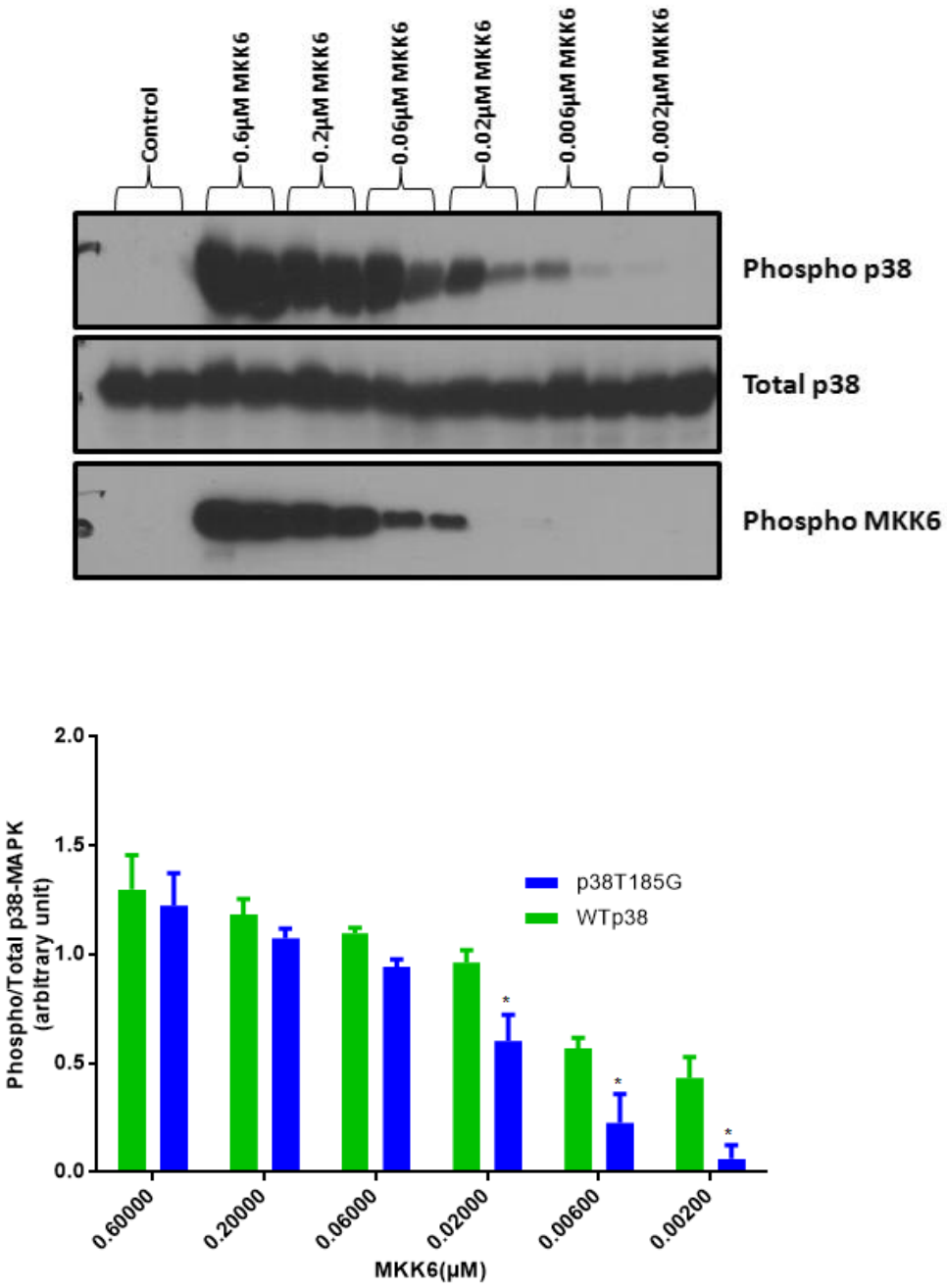

Figure 4.3.13A Kinetics of WTp38α and p38αT185G activation by MKK6. *Western blot of the product of the IVK reaction between WTp38α/p38αT185G and different concentrations of MKK6dd. There was a significant difference in phosphorylation of WTp38α and p38αT185G phosphorylation by MKK6 below 0.02µM MKK6dd. The graph below represents the quantification from 3 independent experiments, data represented as mean +/-SEM, p<0.05. (* = significant against the WTp38α at that concentration).*

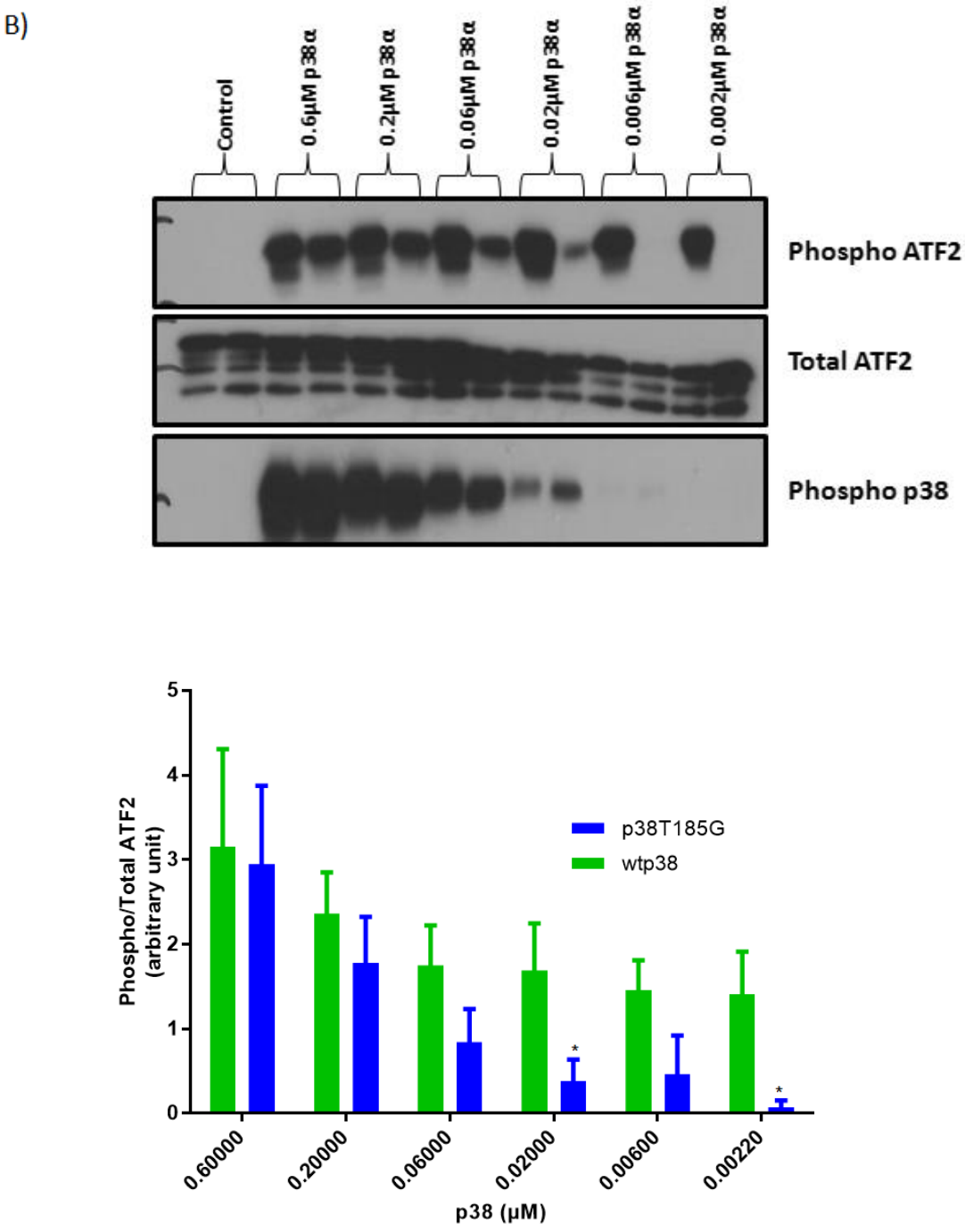

Figure 4.3.13B Kinetics of activation of downstream substrate ATF2 by WTp38α and p38αT185G.*Western blot of the product of the IVK reaction between ATF2 and different concentrations of WTp38α and p38αT185G. There was a significant difference in phosphorylation of ATF2 by WTp38α and p38αT185G below 0.02μM. The graph below represents the quantification from 3 independent experiments, data represented as mean +/-SEM, p<0.05. (* = significant against the WTp38α at that concentration).*

4.4 Discussion

In this chapter we investigated the potential role played by Thr185 in the TAB1 induced p38α autoactivation mechanism. We hypothesized that the hydrogen bond that forms between the side chains of Thr185 and Asp150 provides energy to hold the activation loop in its new orientation that facilitates the T-G-Y autophosphorylation. To test our hypothesis we created a mutant p38αT185G which cannot form a hydrogen bond between Thr185 and Asp150.

4.4.1 p38αT185G binds to TAB1

Before we tested our hypothesis, it was necessary to confirm that the mutant p38αT185G was able to bind to TAB1. The autoactivation of p38α is the consequence of TAB1 binding to p38α, so to test the effect of T185G mutation on the autoactivation mechanism, we needed to make sure that p38αT185G can also bind to TAB1. To investigate this, we carried out an isothermal titration calorimetry experiment with recombinant p38αT185G and 29mer TAB1 peptide (384-412). The ITC data showed that p38αT185G was indeed able to bind to TAB1, similar to WTp38α as seen in figure 4.3.3. Both the WTp38α and the mutant p38αT185G were interacting with TAB1 in a strong manner with a binding affinity of 4.35 X 10^5 /mol and 9.76 X 10^5 /mol respectively. The result indicates that the hydrogen bond between Thr185 and Asp150 does not impact p38α's ability to interact with TAB1. The result is expected as the crystal structure of WTp38α-TAB1 complex clearly illustrates the residue Thr185 structurally far away from the two interacting regions (De Nicola *et al*, 2013). The raw data analysis showed the stoichiometry (n) of the WTp38α and the mutant p38αT185G with TAB1 to be 0.78 and 0.61 respectively, however this was due to the underestimation of the TAB1 peptide concentration made after dissolving the peptide in the buffer. ITC is an extremely sensitive biophysical tool where the concentrations of the proteins have to be exact, which otherwise will produce a wrong result. TAB1 peptide lack enough of the tyrosine/tryptophan residues, which nanodrop relies on when measuring the protein concentration. As a result, the protein concentration we entered into the

program to calculate the stoichiometry was undervalue to the actual concentration of protein used in the experiment and this resulted in the lower n number. We concluded both the WTp38α and the mutant p38αT185G was binding to TAB1 in a 1:1 manner with stoichiometry (n) of 1, and the crystal structure clearly confirms that. The ITC data confirmed that the T185G mutation did not hamper the p38αT185G's ability to interact with TAB1.

After confirming the interaction between mutant p38αT185G and TAB1, we resolved the crystal structure of the p38αT185G-TAB1 complex. The crystal structure confirmed the lack of threonine at 185 residue, which was replaced by glycine as seen in figure 5.3.5.1a/b. When TAB1 binds to the WTp38α, the Tyr182-Thr185 extends to form an alpha-helical segment that swings the activation loop towards the catalytic site. The formation of the extended helical segment is stabilized by the hydrogen bond formation between the Thr185 and the Asp150. In the crystal structure of p38αT185G and TAB1, the Gly185 and Asp150 were unable to form a hydrogen bond as expected and the Gly185 appeared to be further away from Asp150 (Fig 5.3.2b). As a result of this, the Tyr182-Thr185 appeared more relaxed and did not extend to form a helical segment. The lack of the extended helical segment should prevent the swing of the activation loop towards the catalytic site and prevent the T-G-Y autophosphorylation. However, due to the high B-factor, the T-G-Y part of the activation loop could not be resolved in the crystal structure, which means the activation loop was too mobile for it to be crystallized. This supports the first part of our hypothesis that the lack of the hydrogen bond between the Thr185 and Asp150 means there was not enough energy required to hold the activation loop near the catalytic site, which otherwise would have been resolved in the crystal structure. The activation loop did not relax completely either as in the monomeric WTp38α form due to the lattice constraint from the adjacent p38αT185G monomer. The crystal structure confirms that p38αT185G mutant cannot form hydrogen bond between the side chains of Thr185 and Asp150, which prevents the swing of the activation loop towards the catalytic site.

The ITC data showed that the mutant p38αT185G was able to bind to TAB1 similar to the WTp38α, and the crystal structure of the p38αT185G with TAB1 confirmed this. The crystal structure also illustrated that the lack of hydrogen bond between Asp150 and Thr185 destabilized the activation loop and with these encouraging initial findings, we next investigated whether this would reflect in a lack of T-G-Y autophosphorylation.

4.4.2 Thr185 plays a crucial role in the TAB1 induced p38α's auto-activation mechanism

To test our hypothesis, we carried out an *in-vitro* kinase assay with p38αT185G and TAB1 peptide (384-412) and analysed its activation status at 4 different time points. The western blot in 4.3.6 shows that in the presence of TAB1 peptide, the WTp38α was phosphorylated at the T-G-Y motif at all 4 time points, whereas the mutant p38αT185G was not. Only a weak phospho p38α signal was seen at the 4 hour time point with p38αT185G in the presence of TAB1. The result suggests that the p38αT185G cannot be activated by TAB1, which supports our hypothesis. To gather further evidence, we decided to test our hypothesis in a living system with a mammalian cell line HEK293 cells. We transfected the HEK293 cells with WTp38α and the mutant p38αT185G in the presence of TAB1. 24 hours later, we analysed the cells with western blotting and probed with phospho p38 antibody. The co-transfection of WTp38α and TAB1 significantly increased the phospho p38 signal (Fig 4.3.7) which supports the original study that TAB1 causes p38α activation (Ge *et al*, 2002). This increment was inhibited by 10μM SB203580 treatment which confirms the mode of TAB1-induced activation to be auto-activation. The co-transfection of p38αT185G and TAB1 did not cause a similar increase in the phospho p38 signal and was significantly lower than the phospho p38α signal seen with the WTp38α. The lower phospho p38 signal on the endogenous band in p38αT185G sample was however a surprise, a result which was consistent throughout the project and rest of the projects in the lab. It's an anomaly we cannot explain at this time and requires further investigation. This signal was also completely abolished by SB203580 treatment. The result suggests that TAB1 is unable to cause autoactivation of p38αT185G similar to the WTp38α. Next, we decided to test

our hypothesis using a more physiologically relevant stimulus of ischaemia which is a well-known stimulus that induces TAB1-mediated p38α activation (Li *et al*, 2005; Tanno et al, 2006). We transfected the HEK293 cells with WTp38α or p38αT185G, then subjected them with simulated ischaemia using an ischaemia buffer for 10 minutes. 10 minute incubation time was chosen as previous experiments in the lab had indicated it to be the time-point at which phospho p38 signal was the highest. 24hours after transfection, the cells were treated with ischaemia buffer for 10 minutes and analysed by western blotting. The western blot showed that the simulated ischaemia caused a significant increase in phospho p38 signal in cells transfected with WTp38α compared to the baseline control, but not in the cells transfected with p38αT185G (Fig4 .3.8). The signal was completely inhibited by the 10μM SB203580 treatment. One of the main components of ischaemia buffer is sodium dithionite, which causes oxidative stress that also activate p38, however, it has been shown to be via ASK1-MKK3/6 pathway (Nagai *et al*, 2007). Additionally, inhibition by SB203580 suggests that ischaemia buffer is causing autoactivation not transactivation. The result suggests that the TAB1 induced autoactivation is impaired in the mutant p38αT185G recapitulating the results from previous IVK and TAB1 transfection experiments. The 3 independent experiments have given the same outcome which suggests that the p38αT185G's autoactivation mechanism is impaired, i.e. the hydrogen bond between the Thr185 and Asp150 is crucial in mediating autoactivation of p38α caused by TAB1.

4.4.3 Thr185 does not play a role in MKK3/6 mediated p38α trans-activation mechanism.

The data collected so far suggests that the hydrogen bond formation between Thr185 and Asp150 is a key step for a successful p38α autoactivation. We wanted to find out whether it had a similar role in p38α's alternative activation mode of transphosphorylation caused by upstream kinases. We carried out an *in-vitro* kinase assay with p38αT185G and constitutively active MKK6*dd* for 2 hours. The IVK result showed that MKK6 caused a huge phospho p38α signal in both WTp38α and the mutant p38αT185G as seen in figure 4.3.9. The result indicated that the transactivation mode of p38α is not impaired in the mutant p38αT185G suggesting the hydrogen

bond between Thr185 and Asp150 is not important in the transphosphorylation of p38α. We also tested this in HEK293 cells by transfecting WTp38α or p38αT185G with MKK3. 24 hours after transfection, the co-transfection of WTp38α and MKK3 caused a huge phospho p38α signal, as expected. Similarly, the co-transfection of p38αT185G and MKK3 also caused a similar level of phospho p38 signal (Fig 4.3.10) suggesting that the p38αT185G is able to be activated by MKK3 similar to the WTp38α. The result supports the outcome from the IVK assay, suggesting that the trans-activation mode of p38α caused by MKK3/6 is not affected by Thr185. The result is not a surprise as MKK3/6 docks to p38α's canonical binding domain to phosphorylate the T-G-Y motif and Thr185 is not thought to play any part. In the autoactivation mechanism, TAB1 binding leads to structural changes that increases ATP affinity and promotes autophosphorylation. The hydrogen bond formation is the part of that structural change which makes it crucial for autoactivation process. However, when MKK3/6 binds to p38α, the significant structural changes takes place after MKK3/6 phosphorylates the T-G-Y motif on the activation loop. The phosphorylation of the T-G-Y motif is the significant change that alters p38α's structure, which relieves steric blocking, increases ATP affinity, and facilitates substrate binding, which makes p38α kinetically active.

4.4.4 Thr185 does not impact p38α's catalytic activity

We also carried out tests to investigate if Thr185 was important in p38α's catalytic activity. p38α is a serine/threonine kinase that catalyses its targets by transferring the γ-phosphate from the bound ATP onto substrates. We ran an *in-vitro* kinase assay with active WTp38α or active p38αT185G and activating transcription factor -2 (ATF2), a well-known substrate of p38α. After 30 minutes of IVK reaction, ATF2 was equally activated by both the WTp38α and the mutant p38αT185G as seen by the phospho ATF2 signal in figure 4.3.11. The result suggests that the Thr185 does not impact p38α's kinetic activity. We also carried out this experiment in the HEK293 cells by co-transfecting the cells with WTp38α or p38αT185G and TAB1, which is another downstream substrate of p38α. 24 hours later, the co-transfection of WTp38α and TAB1 increased the phospho TAB1 signal as expected (Fig 4.3.12). Similarly, the co-transfection of

the mutant p38αT185G and TAB1 also produced a similar phospho TAB1 signal suggesting that p38αT185G's ability to phosphorylate its target has not been impaired.

In the *in-vitro* kinase reaction carried out in 4.3.11, there was an equal amount of active WTp38α and mutant p38αT185G, however in the HEK293 cells, there was less active p38αT185G in the cells compared to the active WTp38α as seen in western blot figure 4.3.12. The lower amount of active p38αT185G was due to its impaired autoactivation mechanism caused by TAB1 we discussed earlier, and with that we expected more TAB1 activation in the cells transfected with WTp38α compared to the cells transfected with the mutant p38αT185G. There are a couple of explanations for this; one being although we transfected the mutant p38αT185G in the cells, there is still the presence of endogenous WTp38α that can phosphorylate TAB1, another explanation is that there are other kinases in the cells phosphorylating TAB1 such as TAK1, ERK1, and JNK (Mendoza *et al*, 2008; Wolf *et al*, 2011). The IVK and transfection data seem to suggest that the mutation of Thr185 does not affect p38α's kinetic activity.

4.4.5 The T185G mutation makes a difference at lower enzyme concentrations.

From the discussion in 4.4.3 and 4.4.4, we concluded that Thr185 neither plays a role in its activation by upstream kinases nor its kinetic activity to phosphorylate substrates. However, the IVK assays were carried out with high enzyme concentration which not only makes it very different from the physiological environment of the cells but it can also give rise to artefactual stoichiometry that may give misleading results when trying to compare the enzymatic activity. To address this, we repeated our IVK assays by titrating the enzyme concentration down from 0.6μM to 2nM. The IVK result confirmed that there was no difference in MKK6's ability to phosphorylate mutant p38αT185G compared to the WTp38α at high nanomolar concentrations. However, from the 20nM range MKK6 was unable to phosphorylate p38αT185G as well as it was able to phosphorylate WTp38α and the difference became more marked with lower enzyme concentration. Similarly, we repeated this experiment with p38αT185G and ATF2 by titrating

active p38αT185G with the same concentrations as MKK6. Again at high nanomolar concentration there was no difference between WTp38α and p38αT185G in their abilities to activate ATF2. However, from 60nM concentration, p38αT185G was unable to phosphorylate ATF2 as well as the WTp38α. Just like with the MKK6, the difference between the WTp38α and the mutant p38αT185G was more marked at the lower concentrations and from 6nM concentrations p38αT185G was almost unable to activate ATF2. The result suggests that the mutation has indeed affected the p38αT185G's functionality at lower nanomolar concentration. Exactly how the T185G mutation has caused this effect, and how it would translate physiologically is however, difficult to explain at this point and requires further investigation with in-vivo models.

The result gathered in this chapter suggests that Thr185 plays a significant role in the TAB1 induced autoactivation of p38α. Thr185 does not seem to play a role in the classical activation pathway nor does it seem to affect its kinetic activity, however at very low nanomolar concentrations it does seem to have an impact on both signalling pathways.

5 Could Thr185 play a role in p38α's cellular location?

5.1 Introduction

In the last chapter we studied the role of Thr185 in TAB1-mediated p38α autoactivation and concluded that Thr185 plays a significant role in the process. The findings suggest that there could be an alternative method, beside the use of small molecules, to target the TAB1-p38α complex. In this chapter we shift our attention to the potential role of Thr185 in determining p38α's cellular localization.

In 2008, Kristina Lorenz and her group published a paper in Nature Medicine to show that the autophosphorylation of Thr188 in ERK1/2 directs ERK into the nucleus to phosphorylate its target in cardiac hypertrophy (Lorenz *et al*, 2008). They suggested a signalling cascade involving the following components the Raf-MEK-ERK kinase cassette, phosphorylation of the ERK's TEY motif, dimerization of ERK1/2, followed by binding of the β/γ subunit from G_q protein which finally leads to the autophosphorylation of Thr188 that triggers ERK's translocation into the nucleus. From the last chapter we know that Thr185 of p38α plays a role in p38α autoactivation; based on the ERK paradigm we pondered if Thr185 could play a similar role in p38α's cellular localization too. The underlying rationale is that p38 is a close relative of ERK in the MAPK family and the corresponding residue of Thr188 in ERK is Thr185 in p38α. Belonging to the same kinase family, ERK and p38 share a very similar tertiary structure, as seen in figure 5.1A, which suggests complementary function. Furthermore, the interaction of ERK with β/γ subunit from G_q protein is similar to the interaction of p38α with TAB1. And finally, the signalling event in ERK occurs during cardiac hypertrophy and TAB1-p38α signalling occurs during the pathological stress of myocardial ischaemia. These compelling similarities between ERK and p38 in regards to the signalling role played by Thr188 and Thr185 respectively, warrant further investigation.

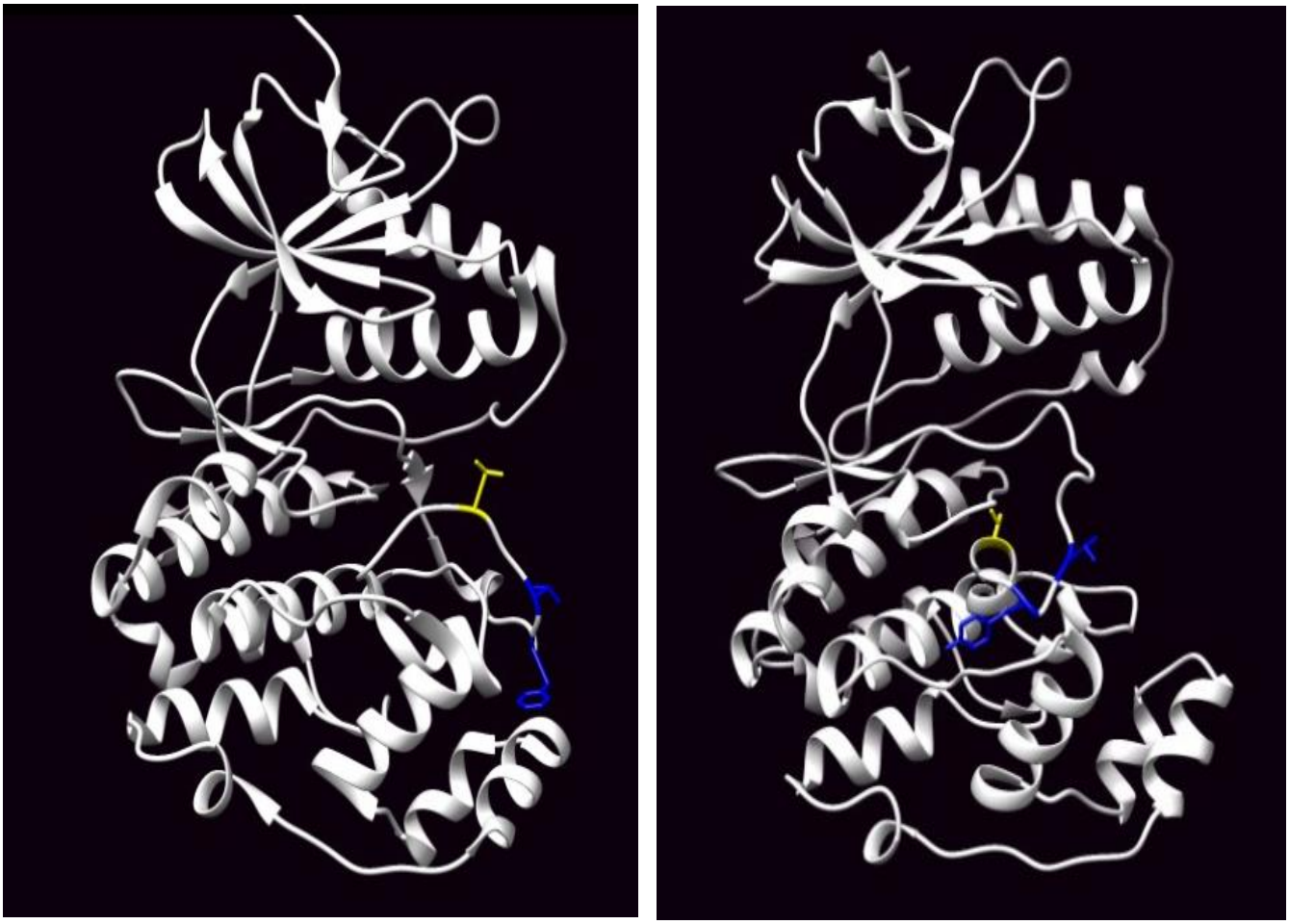

ERK2 **p38α**

```
ERK 181 FLTEYVATRWYRAPEIMLNSKGYTKSIDIWSVG 213
p38 178 EMTGYVATRWYRAPEIMLNWMHYNQTVDIWSVG 210
          * ***************   *    ******
```

Figure 5.1A The Crystal structure of ERK2 and p38α: *The crystal structure highlights the similarity between the two MAPKs' family member ERK (left) and p38α (right). Both have two main lobes of N-terminus and C-terminus with an interposed, long activation loop. Below the crystal structure is the alignment of the ERK2 and p38α sequence which highlights Thr188 in ERK2 and Thr185 in p38 (yellow), two residues C-terminal of their TEY and TGY activation motifs (blue) respectively.*

We hypothesise that p38α's interaction with TAB1 leads to the autophosphorylation of Thr185 residue and that causes the localization of p38α into the nucleus where it phosphorylates its nuclear targets (Fig 5.1b)

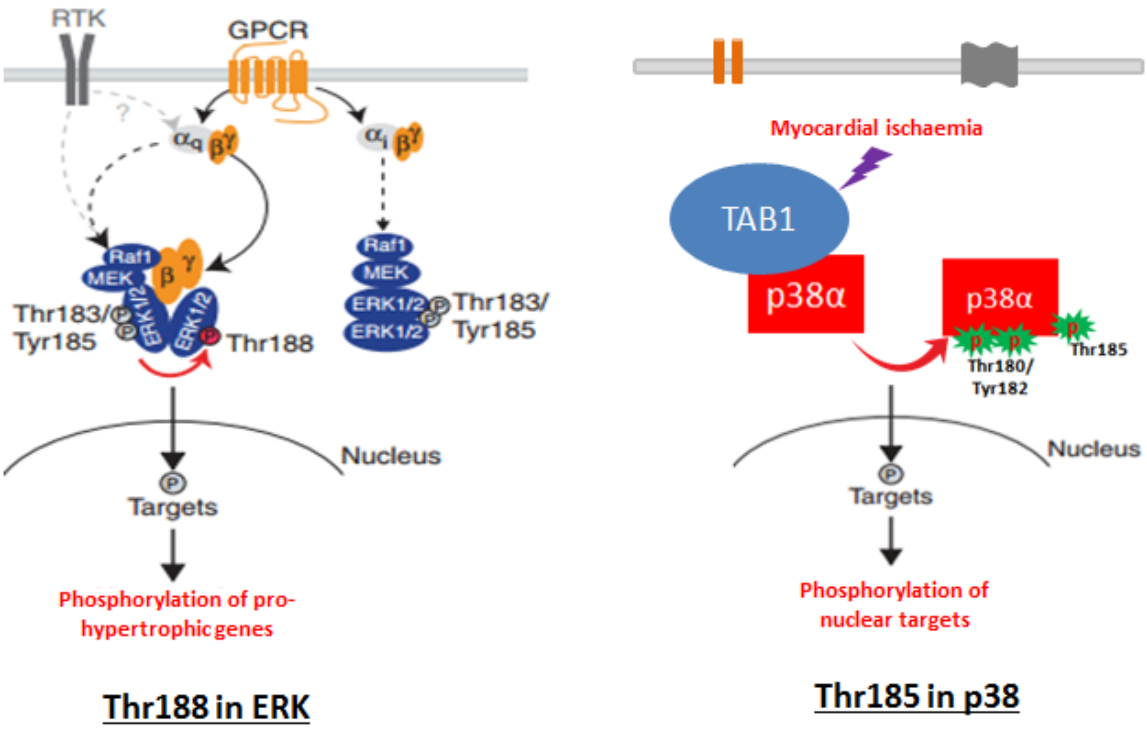

Figure 5.1 B The signalling role of Thr188 in ERK2 and Thr185 in p38α: *The schematic diagram illustrates the signalling role played by Thr188 in ERK (left) and Thr185 in p38α (right). The schematic cartoon of ERK signalling is taken directly from the Kristina Lorenz's paper published in Nature Medicine in 2008. The schematic cartoon of p38α on the right is the working model we have proposed.*

5.2 Specific Methods

5.2.1 pCDNA constructs for mammalian cell over expression

pCDNA3 was used as the plasmid vector for expression in mammalian cells. The plasmid contains cytomegalovirus immediate early (CMV) promoter and SV40 polyadenylation sequence for high level expression in mammalian cells. It has an ampicillin resistance gene for selective cloning. WTp38α, p38αT185G, p38αT185D and WT TAB1 were cloned into this plasmid.

p38αT185G and p38αT185D were cloned in two stages. The overlapping C-terminus and N-terminus halves of p38α were produced in separate PCR reactions using an external primer and complementing internal primer containing the desired mutation. The PCR products from these reactions were then combined to form the template for a second PCR reaction with external primers to produce the full length p38α mutants.

External Primers for p38α

p38α Forward Length: 5’ ATGGATCCAG AAAACCTGTA CTTCCAAGGA ATGTCGCAGG AGAGGCCCAC GTTC 3’

p38α Reverse Length: 5’ CGGTCATGCT GCAGTTATCA GGACTCCATT TCTTCTTGGT CAAGGGGTGG TG 3’

Internal Primers with desired mutations

p38αT185G Forward: 5’ CTA CGT GGC CGG TAG GTG GTA CAG 3’

p38αT185G Reverse: 5’ CCT GTC ATT TCA TCA TCT G 3’

p38αT185D Forward: 5’ CTA CGT GGC CGA TAG GTG GTA CAG 3’

p38αT185D Reverse: 5’ CCT GTC ATT TCA TCA TCT G 3’

cDNA	Plasmid backbone	Resistance	Tag	Expected molecular weight (kDa)	Details & Source
WT p38α	pCDNA3	Ampicillin	HA	40	Full length WTp38α (DR Y Wang, UCLA, USA)
p38αT185G	pCDNA3	Ampicillin	HA	40	Full length mutant p38 (Cloned from WTp38α)
p38αT185D	pCDNA3	Ampicillin	HA	40	Full length mutant p38 (Cloned from WTp38α)
WT TAB1	pCDNA3	Ampicillin	CFP	83	Full length WT TAB1 (Gian De Nicola)

Table 5.2.1Plasmids used for mammalian cell transfection

5.2.2 HELA cells

HELA cells are an immortal cell line derived from the cervical cancer cells of Henrietta Lacks. They were derived by isolating one tumour cell and expanding it to generate the cell line. George Gey who derived the cell in 1951 named the cell line after **He**nrietta **La**cks, HELA (Scherer, 1953). HELA cells are the oldest and one of the most commonly used cell lines in biological and medical research. The vaccine for polio was developed by growing polio virus in these cells (Brownlee, 1955).

Just like HEK293 cells, HELA cells are easy to transfect to express the protein of interest and they contain all the machinery required for post-translational modifications. HELA cells were grown in T75 flask with full growth medium (Dulbecco's modified Eagle's medium, supplemented with 10% v/v foetal bovine serium, 1% v/v/ penicillin/streptomycin) at 37^{O}C and

5% CO_2 in a water saturated incubator. The cells were split onto another T75 flask for culture and 6-well plate for the experiments once they were 80% confluent.

5.2.3 Cellular fractionation

The cellular fractionation of HEK293 cells was carried out using a kit from Thermo-Fisher Scientific (78833). The fractionation was carried out 24 hours after transfection. The cells were washed with PBS and harvested with 200µl of trypsin-EDTA. The cells were centrifuged at 320g for 5 minutes and supernatant was carefully removed leaving the pellet as dry as possible. 200µl of CER I reagent (with protease inhibitor) from the kit (78833) was used to resuspend the cells by vortexing on the highest setting for 15 minutes and incubated on ice for 10 minutes. 11µl of CER II was added into the tube and vortexed for 5 seconds. The cells were incubated for 1 minute and vortexed again for 5 seconds before being centrifuged for 5 minutes at 16000g. The supernatant (which contains the cytoplasmic fraction) was transferred immediately into a pre-chilled tube on ice. The pellet was re-suspended with 100µl of ice cold NER reagent (with protease inhibitor) and vortexed for 15 seconds every 10 minutes for a total of 40 minutes. The tube was centrifuged at 16000g for 10 minutes and the supernatant (which contains the nuclear fraction) was transferred into a pre-chilled tube. The cytoplasmic and nuclear extracts were stored at -80^{o}C for analysis by western blotting.

5.2.4 Western blot

The cytoplasmic and nuclear extracts were run on SDS PAGE and transferred onto PVDF membrane as described previously in chapter 2 and probed with total p38α antibody (1/1000) and GAPDH antibody (1/1000). GAPDH antibody was used as a marker for the efficiency of fractionation between the cytoplasmic and nuclear extracts. Rabbit secondary antibody conjugated to HRP (1/5000) was used to develop the blots for visualisation as described before.

5.2.5 Immunocytochemistry

For immunocytochemistry, HELA cells were seeded in a 6-well plate with sterile coverslips and transfected once they were 70% confluent. 24hrs later, the transfection media was aspirated off and cells were washed with cold PBS. The cells were fixed with 4% paraformaldehyde in PBS for 10 minutes followed by two 5 minutes wash with PBS. 1ml of 0.2% v/v Triton X-100 in PBS was used to permeabilise the cells for 20 minutes at room temperature. The cells were washed 2 times with PBS for 5 minutes each. They were then blocked with 0.2% Triton X-100, 2% w/v BSA in PBS for 2 hour at room temperature. After blocking, the cells were probed with anti-HA-mouse (CST) antibody at 1/200 dilution in 2% w/v BSA-PBS overnight at 4^{o}C. Anti-HA antibody was used because both WTp38α and p38αT185G were cloned with a hemagglutinin tag.

The following day, the cells were washed with cold PBS three times for 5 minutes each. The cells were incubated with anti-mouse CY3 conjugated secondary antibody at 1/200 dilution for 2 hours. The plates were protected from light with aluminium foil from this stage onwards. After 2hrs incubation, the cells were washed with cold PBS for three 5 minute washes. The cover slips were taken out and air-dried for 30 minutes. 3 drops of Vectashield (DAPI) solution was placed on the coverslip and mounted on the microscope slide. The coverslip was fixed onto the slide with nail varnish, left to dry and stored at 4^{O}C in the dark before being analysed by confocal microscopy.

5.2.6 Ischaemic Buffer

The ischaemic buffer was made up as described in Chapter 2. 24hrs after transfection, cells were washed with warm PBS and 2ml of warm ischaemia buffer was added onto the cells. For cells exposed to pharmacological inhibitors, 10μM of SB203580 was added onto the cells 30 minutes prior to the addition of ischaemia buffer. After 10 minutes of exposure to ischaemia buffer, cells

were quickly washed with PBS and collected with 150µl of 2X SDS buffer and analysed by western blotting.

5.2.7 In-vitro kinase

An *in-vitro* kinase assay was performed as described previously in chapter 2. In brief, WTp38α at 3 µM, TAB1 (371-416) peptide at 15µM, and 0.855µg of MKK6 were used in an IVK reaction for 2 hours at 37^{o}C in 1X kinase buffer (25mM Tris/HCl, pH7.5, 5mM β-glycerolphosphate, 2mM dithiothreitol, 0.1mM Na_3VO_4 and 1mM $MgCl_2$). 5µl of 10mM ATP was added to the incubation mixture to start the reaction at 37^{o}C. 2X sample buffer was added to the sample to terminate the reaction, heated to 95^{o}C for 10 minutes and 5µl was used to run on SDS-gel for western blot analysis.

5.2.8 Mass spectrometry

5µl of IVK product were run on 10% SDS gel for 1 hour 30 minutes and stained with coomassie for 1 hour at room temperature to visualise the protein bands. The band of interest was excised by cutting close to the edge of the band, chopped into 2mm^2 pieces and transferred into an eppendorf tube. The gel pieces were washed with 100mM Ambic buffer for 5 minutes. The gel pieces were washed with acetonitrile two times and dried in a speed vacuum for 5 minutes. The gels were rehydrated with 10mM DTT and heated at 56^{o}C for 30 minutes. The DTT was discarded and gels were washed with acetonitrile again two times and dried in a speed vacuum for 5 minutes. 55mM Iodoacetamide (IAA) was added and incubated for 20 minutes in the dark at ambient temperature. The supernatant was discarded and washed with 100mM of Ambic buffer two times for 5 minutes. The supernatant was discarded and gels dehydrated again with acetonitrile as previously and dried off in a speed vacuum for 5 minutes. 13ng/µl of trypsin was used to rehydrate the gel pieces in a minimal volume just sufficient to cover the gel pieces at 4^{o}C for 20 minutes. Unabsorbed trypsin was discarded and a minimum volume of 50mM Ambic (20-20µl) was added to cover the gel pieces and keep them wet during enzyme cleavage. The gel pieces are incubated at 37^{o}C for 2 hours then overnight at room temperature. The following

day the supernatant was decanted from gel pieces and collected into a new eppendorf tube. The gel pieces were washed with 50mM Ambic for 5 minutes at 37^{o}C, decanted and pooled into the same eppendorf from previous step (This process is repeated again). The peptide extract was then used for MS/MS analysis.

5.3 Results

5.3.1 TAB1 induces Thr185 phosphorylation

The IVK reaction was carried out by Dr Denise Eva Martin and Mass spectrometry analysis was performed by Steven Lynham.

To test our hypothesis, the first thing we needed to determine was if TAB1 caused the phosphorylation of Thr185. To investigate this, we carried out an *in-vitro* kinase assay with WTp38α and TAB1, and WTp38α and MKK6 in a kinase buffer at 37^{O}C as described in section 5.2.7. As we did not have an antibody against p-Thr185, we ran the IVK product on an SDS-PAGE gel, coomassied the gel, cut the p38 band out, which was then analysed by MS/MS Tandem mass spectrometry. The result from mass spectrometry showed the presence of phosphorylation at residue Thr185 in the IVK sample with WTp38α and TAB1 but not in the sample with WTp38α and MKK6 (Fig 5.3.1). The result suggested that TAB1 promotes the phosphorylation of Thr185 but MKK6 does not. It was an encouraging finding as it supported the first component of our hypothesis which was TAB1 induces phosphorylation of Thr185.

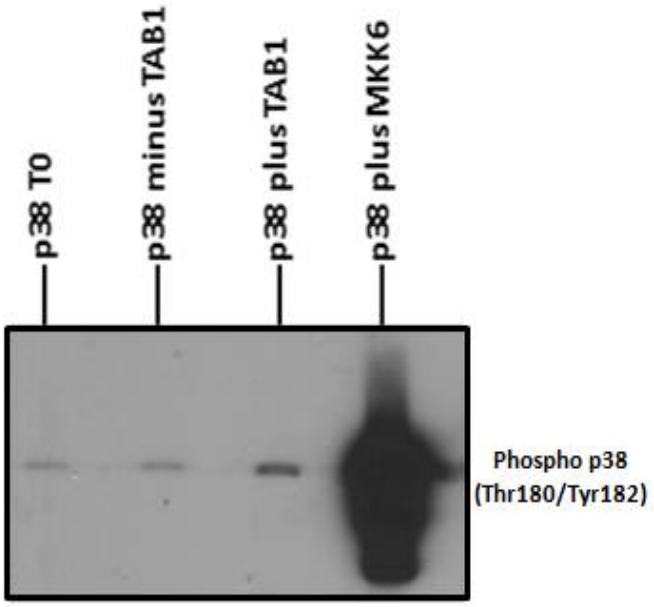

5.3.1A TAB1 induces Thr185 phosphorylation: *The western blot shows the IVK product probed with phospho p38α (Thr180/Tyr182) antibody. TAB1 caused a small increase in phospho p38α signal, whereas MKK6 caused a huge increase in phospho p38 signal. A duplicate gel was run with same samples in parallel which was used for mass spectrometry analysis.*

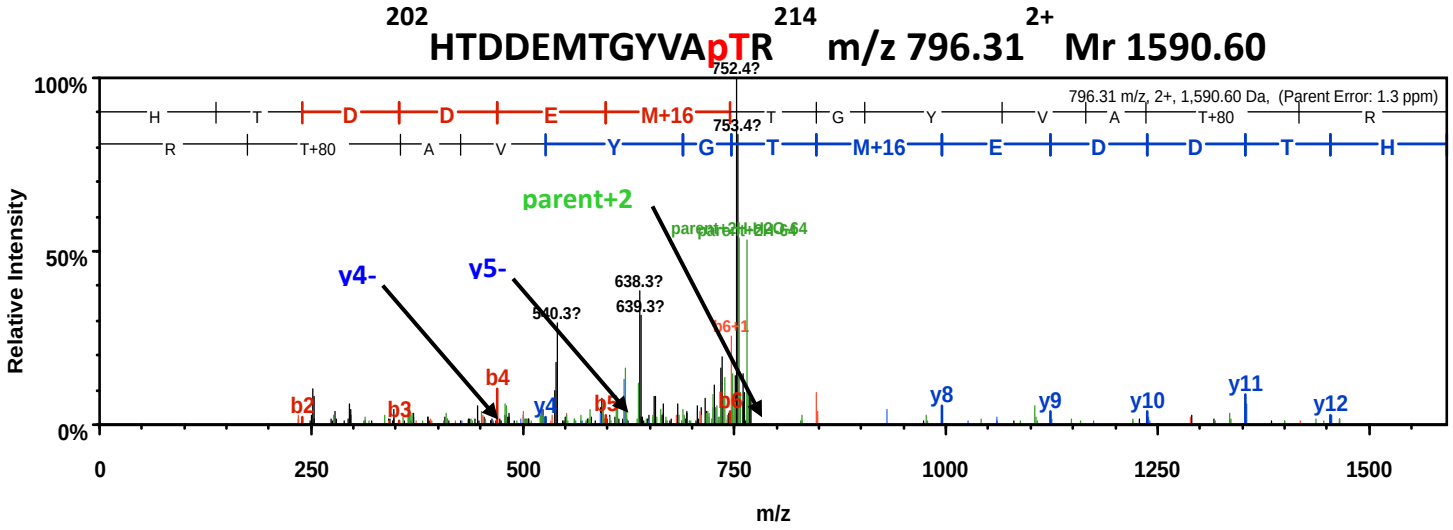

Sample	Sequence	Parent Ion m/z	Peptide mass	Phosphorylated residue	TIC Intensity
Wtp38 minus TAB1	^{174}HTDDEMpTGYVATR^{186}	788.31^{2+}	1574.61	T180	293500
	^{174}HTDDEMTGpYVATR^{186}	788.31^{2+}	1574.61	T182	197100
WTp38 plus TAB	^{174}HTDDEMpTGYVATR^{186}	788.31^{2+}	1574.61	T180	432400
	^{174}HTDDEMTGpYVATR^{186}	788.31^{2+}	1574.61	Y182	73120
	^{174}HTDDEMTGYVApTR^{186}	796.31^{2}	1574.61	T185	40450
WTp38 plus MKK	^{174}HTDDEMpTGYVATR^{186}	788.31^{2+}	1574.61	T180	52680000
	^{174}HTDDEMTGpYVATR^{186}	788.31^{2+}	1574.61	Y182	531100

5.3.1B TAB1 induces Thr185 phosphorylation: *The upper panel shows the raw spectra produced from the IVK product of WTp38α + TAB1 which were cut out from the SDS gel after they were stained with coomassie. The spectra shows the confirmation of phosphorylation of Thr185 with a phosphopeptide with m/z 796.31^{2+}. A CNL was detected from the parent ion at m/z 747.47^{2+}. A loss of phosphoric acid was not detected from the database assigned y2-ion however, there was a loss of 98 Da detected from the y4 and y5-ions. As there is not a residue that could be phosphorylated at y3, this evidence confirms the correct assignment to the threonine at T185. The table below summarizes the mass-spec result from IVK products with relative intensity observed at each residue. The phospho-p38 signal at Thr185 was only detected in the IVK product of WTp38+TAB1 (red) although the signal was low compared to the phospho signal at Thr180 and Tyr182.*

5.3.2 The effect of phosphorylation of Thr185 on p38α's cellular localization

The data above suggested that TAB1 but not MKK6 induces phosphorylation of Thr185. Next we wanted to investigate whether this TAB1 induced phosphorylation of Thr185 could cause p38α's movement into the nucleus. To test this we carried out cellular fractionation with WTp38α, p38αT185G mutant which cannot be phosphorylated at Thr185 and p38αT185D mutant which mimics phosphorylation at Thr185.

HEK293 cells were transfected with TAB1 and WTp38α, p38αT185G, or p38αT185D. 24hrs after transfection we carried out fractionation of the cells to separate the cellular and nuclear fractions as described in section 5.2.3. After fractionation, we analysed the cellular and nuclear extracts by western blotting and probed the samples with total p38 and GAPDH antibody. As seen in the figure 5.3.2, there was a similar level of p38α achieved in WTp38α, p38αT185G, and p38αT185D transfected cells in both cytosolic and nuclear fractions. The cytoplasmic fraction had a higher expression of p38α across all samples compared to the nuclear fraction, but there was no difference between the samples. To support our hypothesis, the level of p38α in p38αT185D transfected cells should have been greater in the nuclear fraction than cytoplasmic fraction compared to WTp38α transfected cells, but it was not. The co-transfection of the all p38α forms' with TAB1 caused a reduction of p38α in the nuclear fraction in all samples suggesting TAB1 promotes p38α's localization into the cytoplasm, but again there was no difference between the samples. This result is contrary to our hypothesis, since the transfection of WTp38α+TAB1 should have caused the expression of p38α to increase in the nuclear fraction and the transfection of p38αT185G+TAB1 to cause no change, however, in both cases the p38α level in nuclear fraction went down suggesting Thr185 does not play a role in p38α's cellular localization.

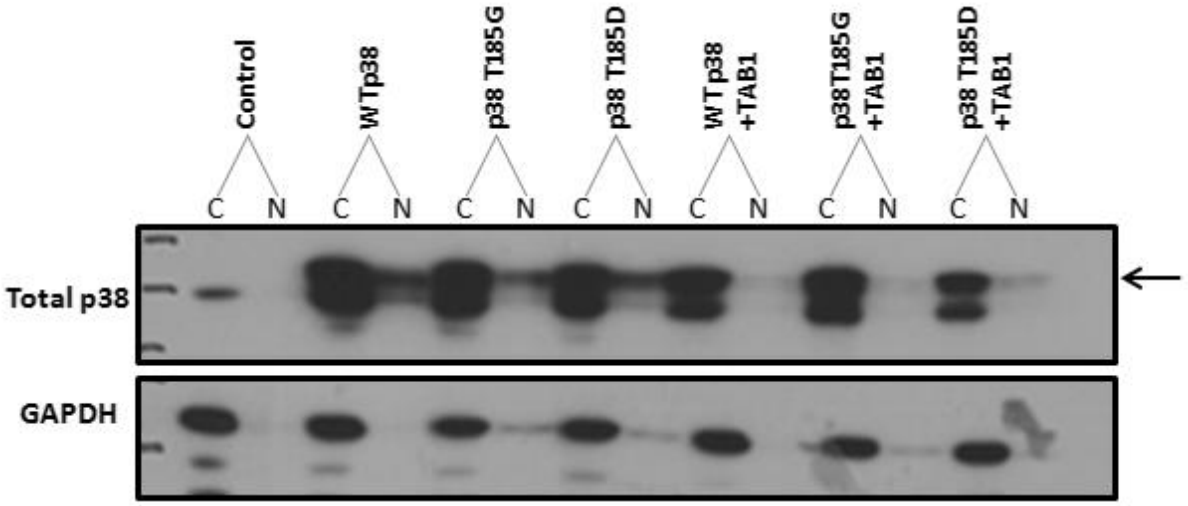

5.3.2 Phosphorylation of Thr185does not affect p38α's cellular localization: *The western blot figure shows the fractionation of HEK293 cells transfected with TAB1 and WTp38α, p38αT185G, or p38αT185D. Fractions were probed with total p38 antibody (top) and GAPDH (bottom). There was no difference in the cytoplasmic and nuclear expression level of p38α between WTp38α, p38αT185G and p38αT185D samples. Co-expression with TAB1 caused a reduction in the expression level of p38 in the nuclear fraction from all cells transfected with WTp38α, p38αT185G, and p38αT185D, but there was no difference between p38 forms. C= cytoplasmic fraction, N= nuclear fraction, arrow indicates ectopic band.*

5.3.3 Thr185 does not affect p38α's cellular localization

The cellular fractionation experiment in 5.3.2 showed no difference in the differential location of WTp38α, p38αT185G or p38αT185D in cells with or without TAB1, suggesting the phosphorylation of Thr185 plays no role in p38α's cellular localization. We wanted to investigate whether this negative result may result from the artificial nature of TAB1 co-expression, so we used the more physiologically relevant stimulus of simulated ischaemia. To achieve this, we transfected the HEK293 cells with WTp38α and p38αT185G, then subjected them to simulated ischaemia using ischaemic buffer. Under control conditions, we saw similar expression of p38α between WTp38α and p38αT185G forms. After 10 minutes of exposure to ischaemia buffer, the expression level of p38α decreased in the nuclear fraction in both WTp38α and p38αT815G transfected cell which was reversed by the SB203580 treatment. Again this result is not compatible with our hypothesis. To support our hypothesis, ischaemia buffer should

have increased the expression of WTp38α, but not p38αT815G, in the nuclear fraction. The result mirrors the outcome from experiment in 5.3.2 which indicates that Thr185 does not play a role in p38α's cellular localization.

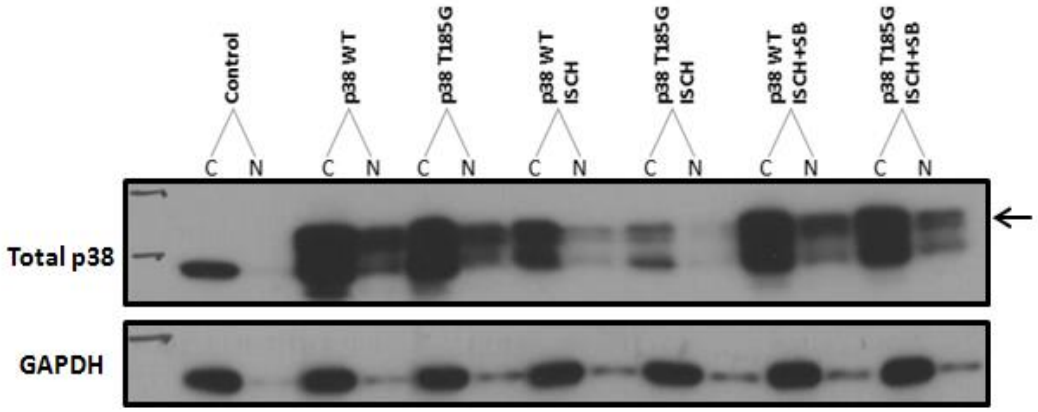

5.3.3 Thr185 does not affect p38α's cellular localization: *The western blot figure shows the HEK293 cells transfected with WTp38α and p38αT185G, subjected to 10 minutes of simulated ischaemia prior to harvest and cellular fractionation. Membranes were probed with total p38 antibody (top) or GAPDH (bottom). There were similar levels of p38α in both WTp38α and p38αT185G transfections, with greater expression in the cytoplasmic fraction compared to the nuclear fraction. After 10 minutes of simulated ischaemia, p38α levels went down in nuclear fraction in both WTp38α and p38T185G, which was reversed by SB203580 treatment. C= cytoplasmic fraction, N= nuclear fraction, arrow indicates ectopic band.*

5.3.4 Thr185 does not impact p38α's cellular localization in HELA cells

The cellular fractionation data in HEK293 cells demonstrated that Thr185 has no impact on p38α's cellular localization so we investigated our hypothesis in a different cell line. We used another mammalian cell line to test if the result would persist and carried out immunocytochemistry in HELA cells. We used an over-expression system to transfect WTp38α+TAB1 and p38αT185G+TAB1 in HELA cells. 24hrs after transfection, cells were fixed and prepared for immunostaining as described in section 5.2.5 and observed using a confocal microscope. The confocal images showed no difference between HELA cells transfected with WTp38α+TAB1 and p38αT185G+TAB1. p38α appeared to reside throughout the cell in all samples with no marked difference between WTp38α+TAB1, and

p38αT185G+TAB1 expressing cells. The expression of p38α was greater in the cytoplasm compared to the nucleus; however it was the same for both samples. The immunofluorescence data seems to mirror the cellular fractionation data from HEK293 cells, and confirm Thr185 does not affect p38α's cellular localization.

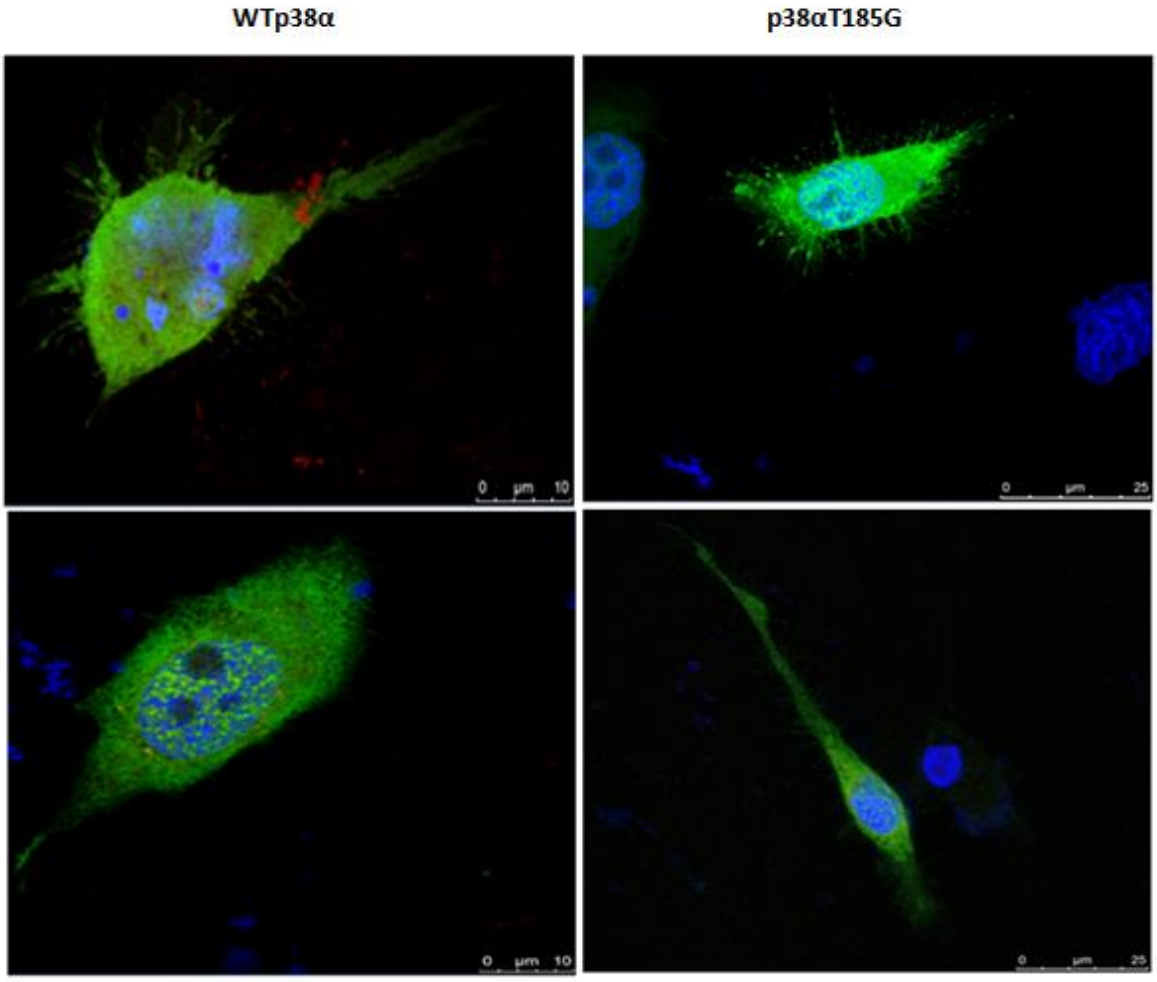

5.3.4 Immunofluorescence in HELA cells: *The HELA cells were transfected with WTp38α+TAB1 (left top/bottom)) and p38αT185G+TAB1 (right top/bottom), fixed and stained with anti-HA antibody (p38 is HA tagged) and detected with Mouse-Cy3 secondary antibody as described in section 5.2.6. The expression of p38α (HA tag) was observed in the green channel which showed no difference between WTp38α+TAB1 and p38αT185G+TAB1 samples. The p38α expression was greater in cytoplasm than in the nucleus in all samples. Blue colour indicates DAPI staining of the nucleus.*

5.4 Discussion

In this chapter we investigated if Thr185 played any role in the cellular localization of p38α.

5.4.1 TAB1 induces Thr185 phosphorylation

Based on the ERK theory described in the introduction, we proposed that the interaction with TAB1 results in p38α autophosphorylation not only at the T-G-Y motif but also at the Thr185 residue. The Thr185 phosphorylation then causes the p38α to localize into the nucleus to phosphorylate its nuclear targets. As we did not have a good p-Thr185 antibody, we decided to use mass spectrometry analysis as a readout tool to find whether Thr185 gets phosphorylated or not. We ran an IVK assay with p38α in the presence of TAB1 or MKK6. The TAB1 augmented p38α phosphorylation as seen in western blot (Fig 5.3.1A) but not as much as MKK6, which caused a huge increase in phospho p38 signal. The mass spectrometry analysis of the same samples showed that Thr185 was phosphorylated in the presence of TAB1, but not in the presence of MKK6 (Fig 5.3.1B). The result revealed that although MKK6 phosphorylated p38α at T-G-Y motif, it did not phosphorylate p38α at residue Thr185. This suggests that the first component of our hypothesis may be correct and TAB1 interaction causes the Thr185 phosphorylation. However, the phosphorylation signal seen at Thr185 was very low compared to the phosphorylation signal seen at Thr180/Tyr182, as represented by the total ion current (TIC) intensity of 40450 and 432400/73120 respectively. Furthermore, compared to the TIC intensity observed at Thr180/Tyr182 caused by MKK6 of 52680000/531100, the phosphorylation at Thr185 appears to be extremely minute, which makes it uncertain whether such a low signal could have any impact on the regulation of p38α's vital functionality such as its cellular location. Nevertheless, the initial findings were encouraging enough and we proceeded onto investigate the second part of our hypothesis which was whether the phospho Thr185 causes p38α to localize into the nucleus.

5.4.2 Thr185 does not cause p38α to localize into the nucleus

After the mass spectrometry data suggested TAB1 causes Thr185 phosphorylation, we went on to investigate whether this would impact p38α's cellular location. To test this, we created a p38α mutant that cannot be phosphorylated at Thr185 in p38αT185G, and another mutant that mimics p38α phosphorylation at Thr185 in p38αT185D. We transfected WTp38α, p38αT185G, and p38αT185D in HEK293 cells and 24 hours later analysed their cellular location with cellular fractionation. With our proposed hypothesis we expected the expression of p38αT185D to be greater in the nucleus compared to the expression of WTp38α and p38αT185G. However, contrary to our prediction we observed a similar expression of all forms of p38αs', with greater expression of p38α in the cytoplasm than in the nucleus. The result suggests that the phosphorylation of Thr185 does not cause p38α to localize into the nucleus. Similarly, we also expected the cells co-transfected with WTp38α and TAB1, and p38αT185D and TAB1 to produce a greater p38α expression in the nucleus compared to the cells co-transfected with p38αT185G and TAB1. However co-transfection of all forms of p38αs' with TAB1 produced similar p38α expression, with almost complete disappearance of p38α from the nuclear fraction. The western blot showed that TAB1 causes p38α to localize into the cytoplasm from the nucleus and Thr185 does not seem to play a role in it.

We also carried out immunocytochemistry in HELA cells to investigate whether phosphorylation of Thr185 induced p38α's movement into the nucleus. We co-transfected HELA cells with TAB1 and WTp38α or p38αT185G. 24hours after transfection we stained the cells with anti-HA antibody, as transfected p38α were HA tagged. The immunofluorescence images illustrated similar p38α expression pattern between the WTp38α and p38αT185G. Both WTp38α and p38αT185G appeared to be heavily expressed in the cytoplasm compared to the nucleus with no difference between them. The result showed that TAB1 did not cause p38α to translocate into the nucleus which is similar to the outcome we achieved from the cellular fractionation data, and suggests that Thr185 does not determine p38α's cellular location.

5.4.3 Ischaemia buffer changes p38α's cellular location

Previous results from cell fractionation and immunofluorescence suggest that the TAB1 induced Thr185 phosphorylation does not cause p38α translocation into the nucleus. However, the system we used could have been too artificial with co-transfection of TAB1, which perhaps contributed to the negative result. To address this, we transfected WTp38α and p38αT185G in HEK293 cells, and instead of co-transfecting TAB1 we used a more physiologically relevant stimulus in simulated ischaemia. Ischaemia is a well-known stimulus that induces TAB1 to interact with p38α to cause its autoactivation (Tanno et al, 2006; Ge et al, 2002; Li et al, 2005). 24hours after transfecting WTp38α, and p38αT185G, the cells were exposed to ischaemia buffer for 10 minutes. The transfection of WTp38α and p38αT185G produced similar expression levels as before with greater expression of p38α in the cytoplasm than in the nucleus. 10 minutes of simulated ischaemia reduced the expression of p38α in the nuclear fraction in both WTp38α and p38αT185G transfected cells, contrary to what we predicted. To support our hypothesis the ischaemia buffer should have induced TAB1 to phosphorylate p38α at Thr185 that would increase its expression in the nucleus. But the result suggests that TAB1's interaction with p38α promotes the p38α's localization into the cytoplasm. It supports the previous result in 5.3.2 which suggests that association with TAB1 seems to drive p38α out of the nucleus into the cytoplasm. Cells transfected with p38αT185G produced the same result indicating Thr185 does not play a role in nuclear translocation. Interestingly this effect caused by simulated ischaemia was reversed by 10μM SB203580 treatment. It means that rather than Thr185, it's the phosphorylation of T-G-Y motif, i.e p38α activation status that seems to affect p38α's cellular location. This supports several studies in the literature that claim that p38 activation status, stimulus involved, and its environment determines its cellular location (Brand *et al*, 2002; Ito *et al*, 2010; Gong *et al*, 2010; Wood *et al*, 2009;). Repeating our experiment with p38α mutant that cannot be activated should provide a better understanding. Another explanation is p38α's cellular localization is dependent on one of its substrates, as SB203580 makes p38α catalytically inactive. In fact there is evidence for this in the literature; following phosphorylation of mitogen activated protein kinase –activated protein kinase 2 by p38, it formed a complex with p38 to

drive it out of the nucleus (Ben-Levy *et al*, 1998). One puzzling observation was that although the p38α expression disappeared in the nuclear fraction with ischaemia buffer in cells transfected with p38αT185G, the expression did not increase in the cytoplasmic fraction. More cell death in the cells treated with ischaemia buffer could explain the result but the GAPDH level was not altered indicating that this is unlikely. Additionally, this conundrum was not observed in cells transfected with WTp38α which makes is even harder to explain, and further experiments are required to investigate this.

5.4.4 Conclusion

To summarise, although TAB1 appears to cause phosphorylation of Thr185, that phosphorylation does not seem to cause p38α to translocate into the nucleus. The cell fractionation and immunofluorescence data from the transfection and simulated ischaemia experiments suggest that Thr185 plays no role in p38α cellular location, instead it appears to be the activation status of p38α that does. However, the mass spectrometry analysis of IVK product showed that the phosphorylation event at Thr185 is minimal relative to the phosphorylation event at the T-G-Y motif. And we cannot confirm whether the TAB1 transfection or ischaemia buffer has caused p38α phosphorylation at Thr185 in the HEK293 and HELA cells, due to the lack of an anti-p-Thr185 antibody. So, further experiments are required with evidence of Thr185 phosphorylation in these cells before we conclude that Thr185 has no impact on p38α's cellular location. Another important point to consider is that although we have ectopically transfected WTp38α and p38αT185G, there is still endogenous p38α present in the cells which can influence the result. The endogenous p38α could make the ectopic p38α functionally redundant which could produce a negative result. One thing that appears to be concrete though, is that TAB1 seems to promote p38α localization in the cytoplasm. Both ectopically expressed TAB1, and endogenous TAB1 activated via ischaemia buffer seemed to cause nuclear export of p38α, which is in line with previous finding from Lu and co-workers who showed that TAB1 promotes p38α autophosphorylation and prevents its nuclear localization (Lu *et al*, 2005). However there are also studies in the literature which suggests that once activated, p38 goes into

the nucleus to phosphorylate transcription factors (Wood *et al*, 2009). In conclusion, the evidence gathered in this chapter suggests that although TAB1 may seem to cause the phosphorylation of Thr185, this phosphorylation does not appear to be the signal that drives p38α into the nucleus. Hence, the Thr185 of p38α does not have a similar function as the Thr188 of ERK2 with regards to nuclear localization, and this may be because of a lack of nuclear localization signal in p38α, unlike ERK2.

6 Characterization of TAB1 KI mice and preliminary data

6.1 Introduction

In previous chapters, I have extensively discussed the autoactivation mechanism of p38α induced by TAB1. During an ischaemic event in the heart, TAB1 interacts with p38α through a bipartite binding motif involving the canonical and non-canonical sites. This binding event is thought to cause the approximation of the N-terminal and C-terminal lobes of p38α. This structural rearrangement brings Glu71 and Lys53 in close proximity to each other to form a salt bridge, typical of an active kinase, which facilitates ATP binding. This is accompanied by the parallel movement of the activation loop (Leu171-Val183) which swings towards the catalytic site, and Tyr182-Thr185 form an extension of an α-helical segment, which is stabilised by the hydrogen bond between the side chains of Thr185 and Asp150 of the HRD domain. This new helical extension at the C-terminal portion of the activation loop brings Thr180/Tyr182 10Å closer to the bound ATP which we believe promotes ATP γ-phosphate transfer onto the T-G-Y motif to cause autophosphorylation, resulting in p38α's autoactivation in cis.

There is overwhelming evidence in the literature that the TAB1-induced mode of p38α activation aggravates myocardial injury during cardiac ischaemia (Barancik, 2000; Li, 2005; Ma, 1999; Kaiser, 2004; Mackay, 1999; Nagarkatti, 1998; Schneider, 2001; Tanno, 2003). As a result, preventing the interaction of p38α and TAB1 would be therapeutically desirable. Based on the findings in chapter 3, we know that TAB1 interacts with p38α in a bipartite manner at the canonical and non-canonical site. We created a mutant TAB1 containing four point mutations; V390A, Y392A (which binds to the non-canonical site), V408G and M409A (which binds to the canonical site), and showed that these residues are necessary for the interaction, as mutation of these residues prevented TAB1 binding to p38α and prevented its consequent autoactivation. We showed this using recombinant proteins in *in-vitro* kinase assays and using an over-expression system in a mammalian cell line. However, we have not yet tested this in an *in-vivo*

model to determine the effect this would have physiologically. From the studies in our lab and a plethora of studies in the literature, we predict that preventing the TAB1-induced p38α autoactivation in the ischaemic heart should reduce myocardial injury in an *in-vivo* model.

To test this, we created a gene-targeted mouse with the four point mutations in TAB1 (V390A/Y392A/V408G/M409A). We commissioned a global knock-in TAB1 mouse from Cyagen Biosciences. The TAB KI mice were viable, fertile and with no obvious developmental defects.

6.2 Specific methods

6.2.1 Generation of TAB KI mice

The TAB1 KI mice were created by Cyagen Biosciences. In brief, the mTAB1 gene (NM_025609.2) was identified on mouse chromosome 15. The gene contains eleven exons with the ATG start codon in exon 1 and the TAG stop codon in exon 11. The four amino acids to be mutated (V390, Y392, V408, M409) are located in exon 10. The mutations V390A, Y392A, V408G, and M409A were introduced into exon 10 by site-directed mutagenesis with the QuickChange™ Site-Directed Mutagenesis Kit. In the targeted vector, the Neo cassette was flanked by LoxP sites and diphtheria toxin A (DTA) was used for negative selection. The constitutive KI allele was obtained by Cre-recombination and C57BL/6 ES cells were used for gene targeting.

```
  1   MAAQRRSLLQ SEQQPSWTDD LPLCHLSGVG SASNRSYSAD GKGTESHPPE
 51   DNWLKFRSEN NCFLYGVFNG YDGNRVTNFV AQRLSAELLL GQLNTEHTEA
101   DVRRVLLQAF DVVERSFLES IDDALAEKAS LQSQLPEGVP QHQLPPQYQK
151   ILERLKALER EISGGAMAVV AVLLNSKLYV ANVGTNRALL CKSTVDGLQV
201   TQLNMDHTTE NEDELFRLSQ LGLDAGKIKQ MGVICGQEST RRIGDYKVKY
251   GYTDIDLLSA AKSKPIIAEP EIHGAQPLDG VTGFLVLMSE GLYKALEAAH
301   GPGQANQEIA AMIDTEFAKQ TSLDAVAQAV VDRVKRIHSD TFASGGERAK
351   FCPRHEDMTL LVRNFGYPLG EMSQPTPTPA PGGRVYPVSV PYSSAQSTSK
401   TSVTLSLVMP SQGQMVNGSH SASTLDEATP TLTNQSPTLT LQSTNTHTQS
451   SSSSSDGGLF RSRPAHSLPP GEDGRVEPYV DFAEFYRLWS VDHGEQSVMT
501   AP
```

The amino acid sequence of TAB1 protein with the four amino acids mutated highlighted in red.

Overview of the Targeting Strategy

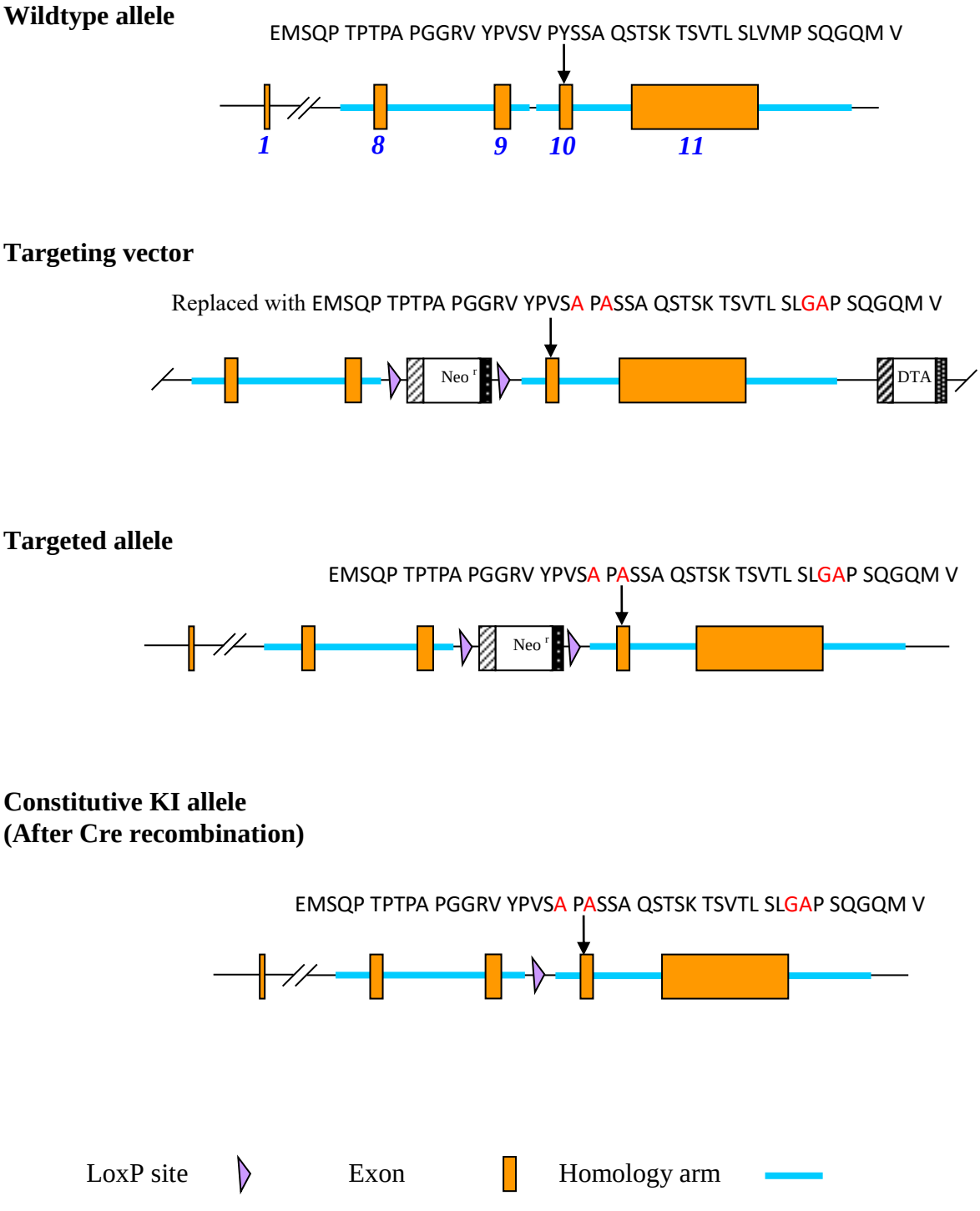

Figure 6.2.1 Overview of the targeting strategy to produce TAB KI mice: *The diagram illustrates the targeting strategy to generate the TAB1 KI mice. The DNA sequences for 4 amino acids to be mutated reside in exon 10 and were mutated by site-directed mutagenesis. The constitutive KI allele was obtained after Cre-mediated excision of the Neo selection cassette between LoxP sites.*

6.2.2 Breeding

All experiments were carried out in accordance with the United Kingdom Home Office Guidance on the operation of Animals (Scientific Procedures) Act 1986.

5 heterozygous (Hets) (2 males and 3 females) mice were received from Cyagen Bioscience and housed in the Biological Service Unit (BSU) at St Thomas' Hospital campus, King's College London. The care of the colony, feeding, setting up the breeding, weaning, ear sampling, and culling were done by the BSU staff under our instructions. The mouse litters were ear clipped at 21 days of age and used for analysis by PCR to confirm the genotype of each mouse prior to their use in breeding or in experiments.

6.2.3 Genotyping

6.2.3.1 DNA isolation and purification

Ear clips from mice were processed to collect the genomic DNA using a DNeasy Blood & Tissue kit (69506) from Qiagen. The ear clip was re-suspended in 180µl of Buffer ATL (lysis buffer), 20µl of proteinase K solution and incubated at 56^{o}C for 1 hour. After the ear clip dissolved completely in the buffer, 200µl of Buffer AL was added and mixed by vortexing. 200µl of ethanol was added, mixed by vortex and poured into DNeasy Mini Spin column in a 2ml collection tube, and centrifuged at 6,000g for 1 minute. The DNeasy Mini Spin column was transferred into a new 2ml collection tube, washed with 500µl of Buffer AW1 (wash buffer) and centrifuged for 1 minute at 6,000g. The DNeasy Mini Spin column was transferred into a new 2ml column, washed with 500µl of Buffer AW2 (wash buffer) and centrifuged at 20,000g for 3 minute. The DNeasy Mini Spin column was transferred into a 1.5ml eppendorf tube and DNA was eluted with 50µl of nuclease free water by centrifuging at 6,000g for 1 minute. The DNA was stored at -20^{o}C until further use.

6.2.3.2 Polymerase Chain Reaction (PCR)

Once genomic DNA was collected, PCR was carried out using primers provided by Cyagen Biosciences. As seen in figure below (Fig 6.2.3.2A), the forward and reverse primers (black arrows) are on either side of the LoxP site which is only present in the KI allele, therefore the KI allele is heavier than the WT allele, which lacks a LoxP site.

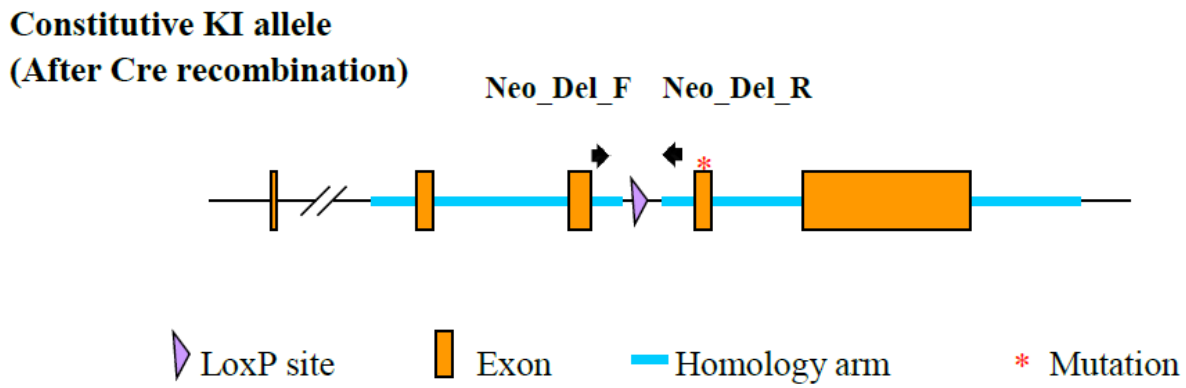

Figure 6.2.3.2A Primers for PCR reaction to genotype the mice: *The diagram illustrates the forward and reverse primers (black arrows) for genotyping.*

Forward primer: GCTGGCCTTGCTCAACTCCAG

Reverse primer: GACCATCTGTCTCATACCTGACCTCAC

Annealing Temp: 60^{o}C

Mutated allele: 405bp

WT allele: 261bp

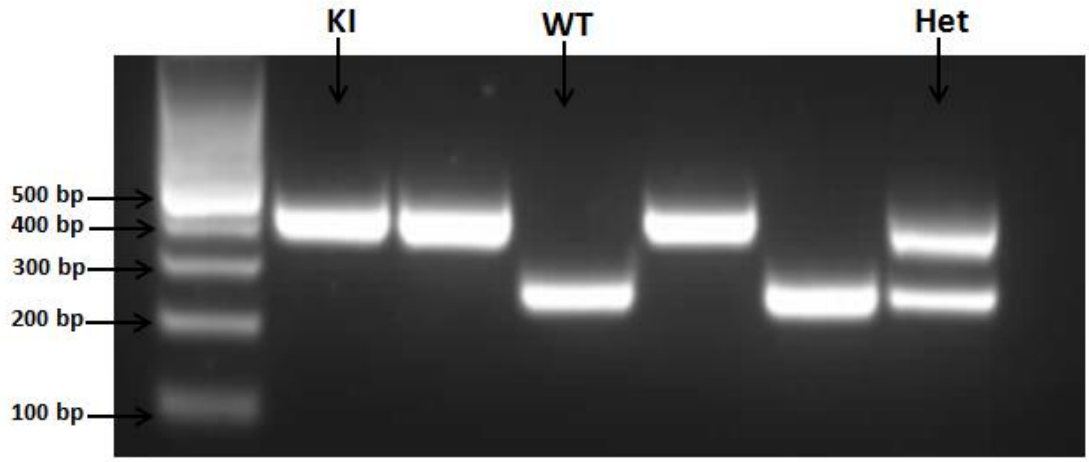

Figure 6.2.3.2B Genotyping of TAB KI and WT mice: *The image shows the PCR product run on an agarose gel. The KI product appears around 405bp, the WT product appears around 261bp and the Hets harbour one of each allele with bands appearing at both molecular weights.*

The PCR products used for genotyping do not contain the site where the mutations have been introduced in exon 10, and as a result these PCR products cannot be sequenced to screen for the mutations. Therefore, new primers (blue arrows on figure below) were designed to flank exon 10 and amplify the segment for sequencing (Fig 6.2.3.2B).

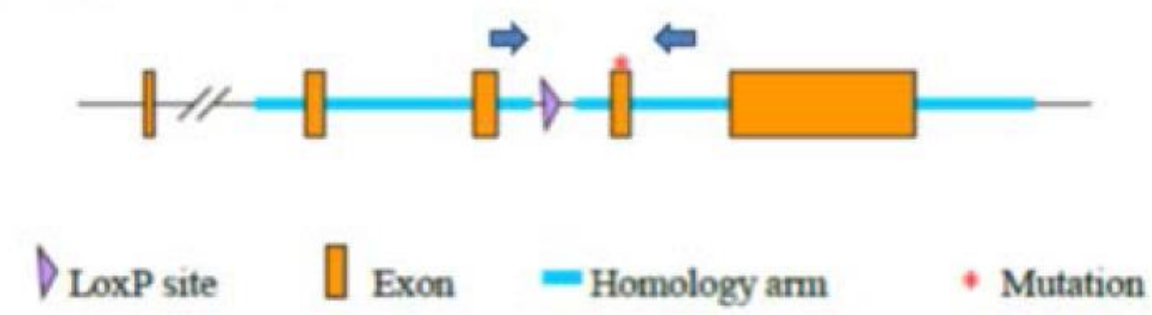

Figure 6.2.3.2C Primers to amplify the region containing the mutated sites: *The diagram illustrates the forward and reverse primers (blue arrows) to amplify the DNA sequence containing the 4 residues that have been mutated.*

Forward primer: GGCTGGCCTTGCTCAACTCCA

Reverse primer: GCTGTTTCTCTCCAGGTTCCCAT

Annealing Temp: 65^{o}C

Mutated allele: 1170bp

WT allele: 1026bp

Sequencing primer: TTATTCCACTCCCACCTTGA

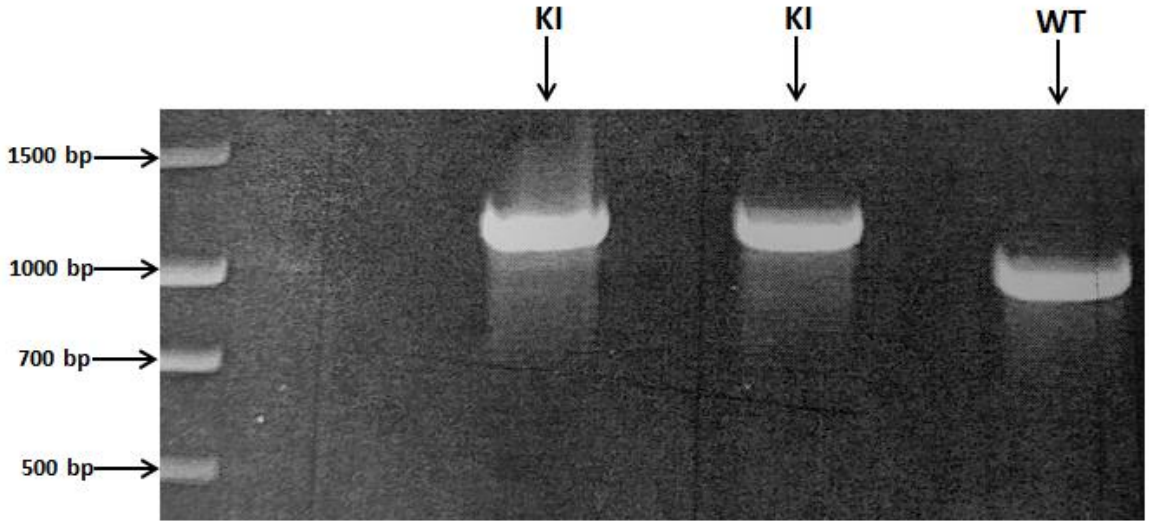

Figure 6.2.3.2D PCR to sequence the TAB KI allele and the WT allele: *The image shows the PCR product run on an agarose gel. The KI product appears around 1170bp, the WT product appears around 1026bp. The PCR products were excised from the agarose gel, purified, and sent for sequencing to confirm the presence of mutated residues in the KI sample.*

The PCR reaction mix was prepared as set out in table A below. A master mix was prepared which contained nuclease free water, forward and reverse primers, and TAQ polymerase with dNTPs. The master mix was aliquoted into PCR tubes and DNA was added before starting the PCR reaction. The PCR reaction for genotyping and sequencing the KI allele was run on the settings as described in table 6.2.3.2B and 6.2.3.2C respectively.

Component	Volume (µl)
ddH_2O	9.4
Forward Primer	0.8
Reverse Primer	0.8
Premix Taq	12.5
DNA	1.5
Total	25

Table 6.2.3.2A PCR components for genotyping: *Table shows the PCR reaction components in a 25µl mixture.*

Step	Temperature (^oC)	Time (min)	Number of cycles
Initial denaturation	94^oC	3	1
Denaturation	94^oC	0.5	33
Annealing	60^oC	0.5	
Extension	72^oC	0.25	
Additional Extension	72^oC	5	1

Table 6.2.3.2B PCR setting for genotyping: *Table shows the settings used to run the PCR for genotyping.*

Step	Temperature (^oC)	Time (min)	Number of cycles
Initial denaturation	94^oC	3	1
Denaturation	94^oC	0.5	33
Annealing	65^oC	0.58	
Extension	72^oC	1.58	
Additional extension	72^oC	5	1

Table 6.2.3.2C PCR setting for sequencing: *Table shows the settings used to run the PCR to amplify the gene section for sequencing the mutated sites.*

6.2.3.3 Agarose gel electrophoresis

Once the PCR was completed, the PCR products for genotyping (250-405bp) were prepared to run on a 2% agarose gel electrophoresis. 4µl of 6X gel loading dye was added to the PCR product, and 5µl was loaded into the gel. The electrophoresis was run at a constant voltage of 100 volts for 1 hour and visualised using a UV dual intensity transilluminator (UVP).

6.2.4 Langendorff Perfusion of isolated mouse hearts

All Langendorff experiments were performed by Dr Rekha Bassi, and I assisted her with perfusion and blinding to mouse genotype.

Langendorff perfusion of isolated mouse hearts was carried out on 10 week old male mice. Mice were anesthetized and anti-coagulated by intraperitoneal injection with pentobarbital (300mg/kg) and heparin (150 units). The body weight was measured and the heart was rapidly excised and placed in an ice cold modified KREBS-Henseleit buffer (K-HB) (See chapter 2 for constituents). The excess fatty tissue was carefully removed to reveal the aorta between the thymus and trachea. The aorta was then cannulated with a 23G blunt ended/grooved stainless steel needle. The hearts were perfused at a constant pressure of 80mmHg with KREBs buffer, equilibrated with 95% O_2 and 5% CO_2 and maintained at a constant temperature of 37+/- 0.3^{o}C. The temperature of the heart was maintained at 37^{o}C by immersing the heart 1/3 in a water jacketed chamber.

A fluid-filled compliant balloon was inserted into the left ventricular cavity by carefully removing the left atrial appendage and the balloon passed through the mitral valve. The balloon was attached to a catheter with a pressure transducer coupled to a 4S Powerlab (AD Instruments, UK) that monitored and recorded contractile function; left ventricular systolic and diastolic pressures and left ventricular developed pressure (LVDP) and coronary flow. Once in position and secured with clamps, the balloon was gently inflated until the end diastolic pressure

measured between 1 and 10mmHg. The hearts were electrically paced at 600bpm with a 0.05mm silver wire (Advent, UK). The wire and the aortic cannula were attached to an SD9 stimulator (Grass Instruments, USA) delivering a square wave pulses of 5ms duration and 1V amplitude.

The Langendorff technique was used to carry out two different experiments

1. Activation of p38α during ischaemia.
2. Measurement of infarct size resulting from ischaemia.

The protocol for each experiment is outlined below

Figure 6.2.4A Schematic representation of mouse heart perfusion to investigate p38α activation caused by ischaemia: *The isolated hearts were subjected to 40 minutes of stabilization with KREBs buffer, followed by 10 minutes of global zero-flow ischaemia. The control hearts were subjected to continuous perfusion of KREBs buffer for 50 minutes. At the end, the hearts were snap frozen in liquid nitrogen and stored at -80^{o}C until further use.*

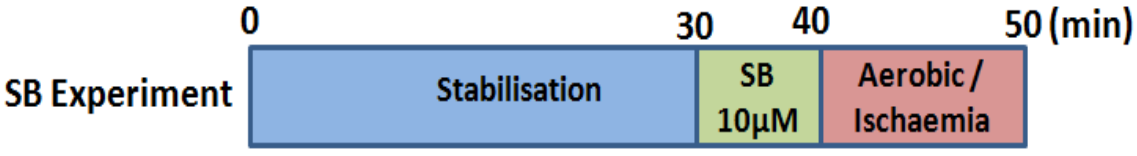

Figure 6.2.4B Schematic representation of mouse heart perfusion to investigate SB sensitive-p38α activation caused by ischaemia: *The isolated hearts were subjected to 40 minutes of stabilization with KREBs buffer, followed by 10 minutes of global ischaemia. The control hearts were subjected to continuous perfusion with KREBs buffer for 50 minutes. At the 30 minute time-point during stabilization, 10µM SB203580 was added to the KREBs buffer. At the end of all protocols, the hearts were snap frozen in liquid nitrogen and stored at -80^{o}C until further use.*

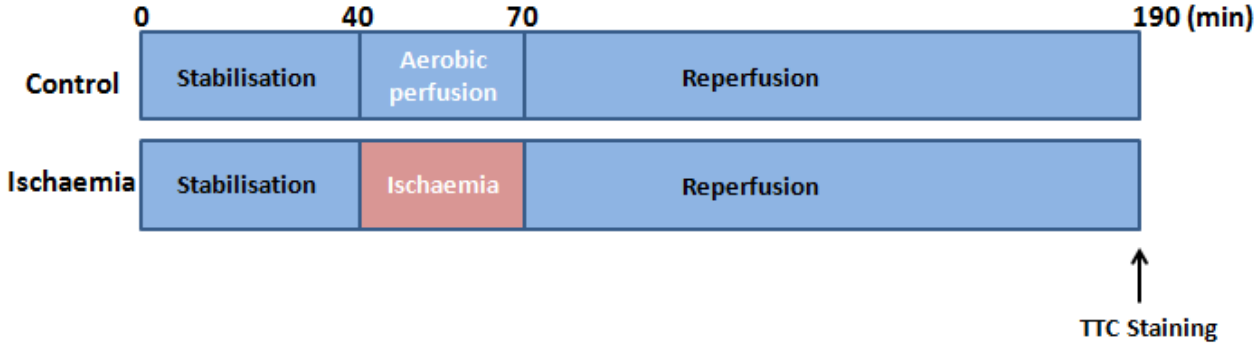

Figure 6.2.4C Schematic representation of mouse heart perfusion to investigate infarct size caused by ischaemia: *The isolated hearts were subjected to 40 minutes of stabilization with KREBs buffer, followed by 30 minutes of global ischaemia and 2 hours of reperfusion. The control hearts were subjected to continuous perfusion with KREBs buffer for 3 hours. At the end of both protocols the hearts were prepared for TTC staining to measure the infarct size.*

6.2.5 Infarct size assessment

After the hearts were perfused using the Langendorff technique, they were stained with triphenyl tetrazolium chloride (TTC) to measure the infarct size. TTC is a redox indicator that differentiates metabolically active tissue from inactive/dead tissue. TTC, a white compound, is reduced to a red TPF (1,3,5-triphenylformazan) by the activity of dehydrogenase enzymes present within cells in viable tissue. However, in dead tissues these enzymes are degraded and denatured, and as a result TTC cannot be reduced and remains white.

The hearts were perfused with 5ml of warm 1% TTC in PBS for 5 min. The heart was then completely immersed in 1% TTC solution and incubated at 37^{o}C for 10 minutes. After 10 minutes incubation, the heart was blotted dry, the atria were removed, and remnants weighed and stored at -80^{o}C.

After TTC staining, the hearts were fixed and sectioned to measure the infarct size. The hearts were fixed by placing in 2.5% gluteraldehyde for 1 minute and mounted in 5% agarose in PBS with the apex uppermost. The agarose embedded heart blocks were sectioned from apex to base

in 0.75mm slices using a vibratome (Series 1000, Agar Scientific, UK). The heart slices were placed in a 6-well plate in PBS and scanned at a high resolution by placing them on a flat bed scanner compressed between perspex plates (separation gap = 0.75mm). The images were then analysed using the ImageJ software to quantify the infarct volume as a percentage of total LV volume. The experiments and analyses were carried out by an investigator that was blind to the mouse genotype.

6.2.6 Homogenization of hearts

The hearts were removed from -80^{o}C storage and thawed on ice. Once pat dried on a paper towel, hearts were weighed before being homogenized with 100mg/ml of homogenization buffer in a mortar using a pestle. Homogenization buffer was made up of 20mM HEPES, pH 7.4, 150mM NaCl, 1mM EDTA, 1mM EGTA, 1mM Na_2VO_4, 5mM NaF, 1mM DTT, 0.5% (v/v) Triton X-100 and 1X Protease Inhibitor Tablet (Roche)/50ml buffer. The hearts were homogenized for 3 minutes by the shearing force generated at the interface of the mortar and pestle. Homogenate was transferred to 1.5ml eppendorf tube and centrifuged at 10,000g for 10 minutes at 4^{o}C. The supernatant was collected and stored at -80^{o}C to analyse by western blotting. The liver and thymus were also homogenized in the same manner.

6.2.7 Isolation of MEFs

A pregnant mouse 13 or 14 d.p.c (day post-coitum) was culled by neck dislocation. The uterine horn was dissected out, briefly rinsed in 70% ethanol, and placed on a petri dish with sterile PBS. Individual embryos were isolated and carefully removed from its embryonic sac. The embryo was separated from placenta, and head and red organ were dissected off. The heads were stored at 4^{0}C and used for genotyping each embryo. Then with a sterile razor blade, the embryo was minced finely until it was possible to pipette with a 1ml pipette tip. 1ml of 0.25% trypsin/EDTA was used to collect the minced embryo and transferred into a falcon tube to incubate at 37^{o}C for 20 minutes. During incubation, cells were pipetted up and down thoroughly every 5 minutes to help with the digestion. 9ml of full growth medium (Dulbecco's

modified Eagle's medium containing 584mg/l L-glutamine, 10% v/v foetal bovine serum, 1% v/v penicillin/streptomycin) was added into the falcon tube to neutralize the trypsin. The cells were passed through 0.75µm cell strainer and centrifuged at 500g for 5 minutes. The supernatant was removed and pellet was re-suspended in 2ml full growth medium and plated onto a gelatine pre-coated 6-well plate (plates were coated with 0.2% gelatine in PBS for 2 hours prior to addition of cells). After 24hrs, the cells are usually 80-90% confluent and transferred into a T75 flask.

6.3 Results

6.3.1 Testing TAB1 antibodies

The first experiment we carried out was to test the expression of mutated TAB1 protein in the KI mouse and whether the TAB1 antibody would be able to pick it up. To investigate this, we sacrificed a KI mouse and harvested the key organs where TAB1 is most abundant; heart, liver, and thymus. The organs were homogenized using mortar and pestle as described in 6.2.6. After homogenization, the supernatant was run on western blot and probed with the Total TAB1 antibody (Santacruz) and compared against the WT protein. The antibody picked up two bands around 60kDa and 50kDa which we believe are the alpha and beta isoforms respectively, of the TAB1 protein. The antibody detected a strong signal with the WT protein and a very faint signal with the KI protein as seen on the western blot below (Fig 6.3.1A). One interesting observation was the fact that the KI protein appeared to run slightly lower than the WT protein in all of the organs. The WT protein is only slightly heavier (54.581kDa) than the KI protein (54.359kDa), and the western blot seems to confirm this but it is still surprising to see that shift on the gel with such a small molecular weight difference.

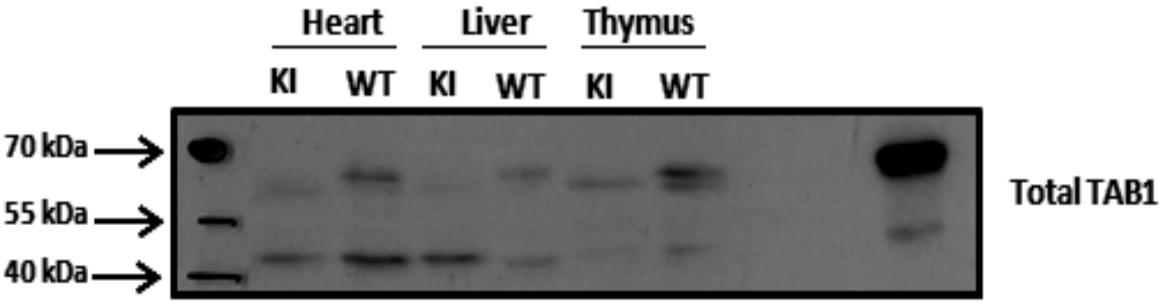

Figure 6.3.1A Testing anti-TAB1 antibody: *The western blot shows the homogenate from the heart, liver and thymus probed with Total TAB1 antibody from Santacruz. The antibody was able to pick up both the alpha (60kDa) and beta (50kDa) isoforms of the TAB1 protein. The WT protein appeared to run higher than the KI protein in all organs confirming the fact that the WT TAB1 is slightly heavier than the KI TAB1. On the right hand is the ectopically expressed TAB1 protein in 293 cells run as a positive control.*

Next, we used another total TAB1 antibody (obtained from Phil Cohen's group in Dundee) to probe the same samples again to test if we would be able to reproduce the result. The western blot figure shows that the second TAB1 antibody was also able to detect the WT protein more easily than the KI protein (Fig 6.3.1B). Similarly, WT TAB1 appeared to run slightly higher than the KI protein although the difference in the shift appeared less compared to the Santacruz antibody depicted in figure 6.3.1A. These results confirm that TAB1 antibody can detect the total TAB1 protein in the KI mouse albeit weakly compared to the WT, and the expression of TAB1 is not markedly affected by the mutation. Later in the project, we received a new fresh TAB1 antibody from Phil Cohen which showed no difference in the expression of TAB1 and the shift on the western blot between the WT and the KI samples. We concluded that the result in 6.3.1A/B were due to antibodies being old, and proceeded with using the new antibody from Phil Cohen for the rest of the project from 6.3.2.

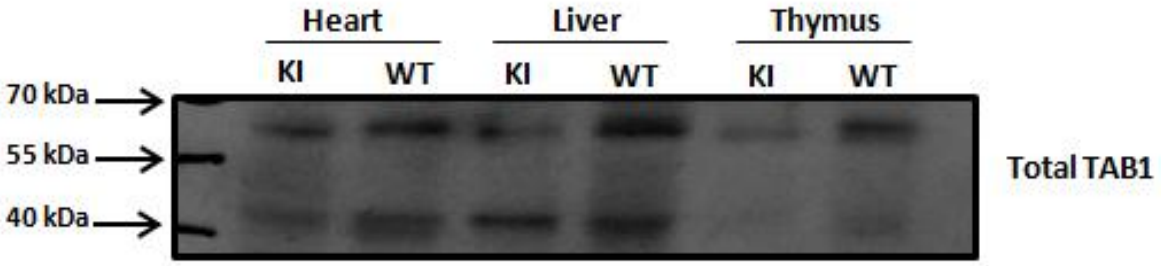

Figure 6.3.1B Testing proprietary anti-TAB1 antibody: *The western blot figure shows the homogenate from heart, liver and thymus probed with Total TAB1 antibody from Dundee. The antibody was able to pick up both the alpha (60kDa) and beta (50kDa) isoforms of the TAB1 protein.*

6.3.2 p38α activation in KI ischaemic hearts

To investigate the TAB1-induced activation of p38α in the KI mice, we carried out Langendorff perfusion on the hearts. The hearts were subjected to 40 minutes of stabilization with KREBs buffer followed by 10 minutes of ischaemia, as described in section 6.2. The heart homogenates were analysed by western blotting and probed with phospho p38 antibody to examine the activation of p38α. Contrary to our expectation, 10 minutes of global ischaemia caused activation of p38α in the KI mouse. As seen in western blot 6.3.2, following ischaemia there was a significant increase in the phospho p38 signal at the T-G-Y motif compared to the control. This could be attributed to the activation of MKK3, which appeared to be higher in the KI hearts, perhaps compensating for the disabled TAB1 pathway. In the WT hearts, ischaemia caused a significant increase in the phospho p38α signal as expected, but interestingly the increment in the phospho p38 signal compared to the control seemed to be less than in the KI hearts. An intriguing observation was the fact that the p38α activation at baseline seemed to be greater in the WT hearts compared to the KI hearts. Also, the phospho TAB1 signal did not change with ischaemia in the WT hearts. The phospho TAB1 signal in the KI hearts was not detectable as expected as TAB1 cannot dock to p38α. Our results suggest that p38α activation, at both baseline and during ischaemic stress, is not abolished in the TAB1 KI hearts.

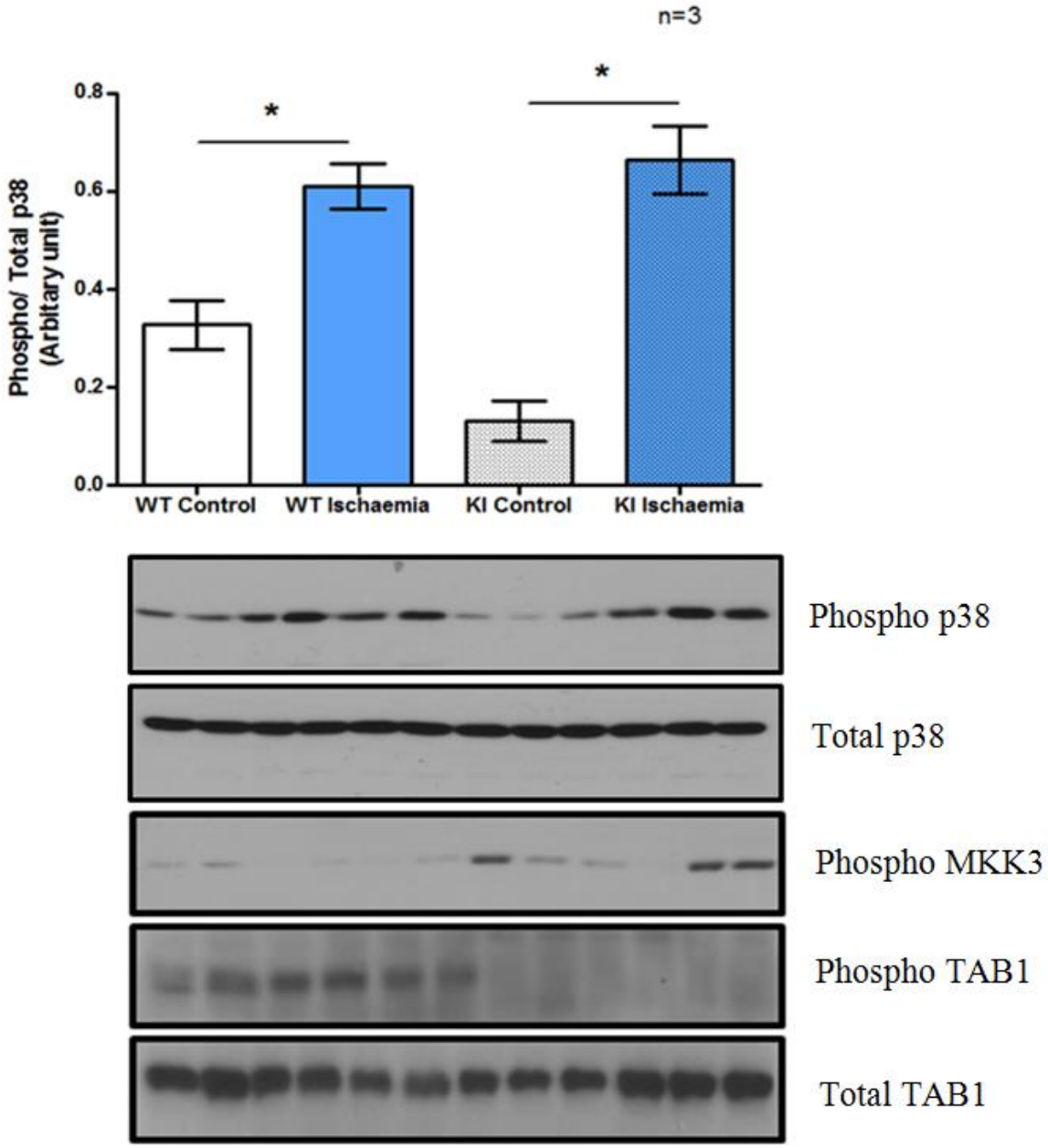

Figure 6.3.2 Western blot analysis of TAB1 KI and WT hearts at baseline and during global ischaemia: *The western blot shows the heart homogenates probed with phospho p38 (T-G-Y), total p38, phospho MKK3, phospho TAB1 and Total TAB1 antibody. The graph above shows the quantification of blots with significant difference in p38α activation between the control and ischaemic hearts for both genotypes, however no significant difference in p38α activation was observed between the WT and KI hearts with ischaemia. (Graph was analysed by One-way ANOVA with post-hoc Tukey test, $p<0.05$)*

6.3.3 p38α auto-activation in KI ischaemic hearts

The experiment above suggests that p38α activation during ischaemia is not impaired in the KI hearts, contrary to our prediction. To test the mode of p38α activation in the KI hearts during ischaemia, we carried out Langendorff perfusion on the KI hearts in the presence of SB203580. SB203580 is an ATP-mimetic and should inhibit the autophosphorylation of p38α. As seen in the western blot figure below, there was a varied level of p38α activation in different hearts in the presence of SB with ischaemia. In all hearts, the p38α activation appeared to be inhibited by the SB treatment, some more than others. However this effect was also seen in the presence of DMSO, the control solvent in which SB203580 was dissolved, indicating that the effect observed may not be due to the SB203580 alone. The result suggests that SB203580 in this experiment might have not blocked the activation of p38α indicating the mode of p38α activation was not by autoactivation. The most likely interpretation is that p38α is being activated via the canonical activation pathway involving MKK3/6 (see figure 6.3.2).

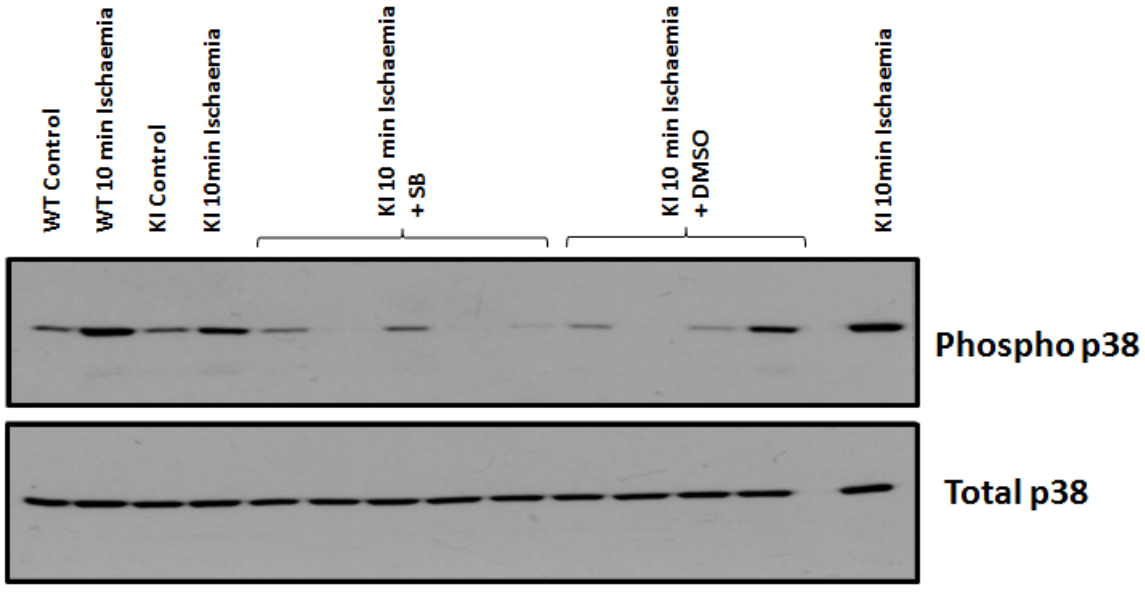

Figure 6.3.3 Western blot analysis of TAB1 KI hearts at baseline and during global ischaemia in the presence of SB203580: *The western blot shows the KI heart homogenates probed with phospho p38 (T-G-Y) antibody and total p38 antibody.*

6.3.4 Morphometric characteristics and hemodynamic function

The Morphometric characteristics of the WT and KI mice are illustrated in the graphs below. 10 week old male mice were used for experiments with n=12 in each group of WT and KI. The WT appeared to be heavier with a mean weight of 28.1g compared to the KI mice whose mean weight was 26.3g. Similarly, the isolated hearts were also weighed, and the KI hearts tended to be heavier with a mean weight of 138mg compared to the WT hearts with a mean weight of 120mg.

A)

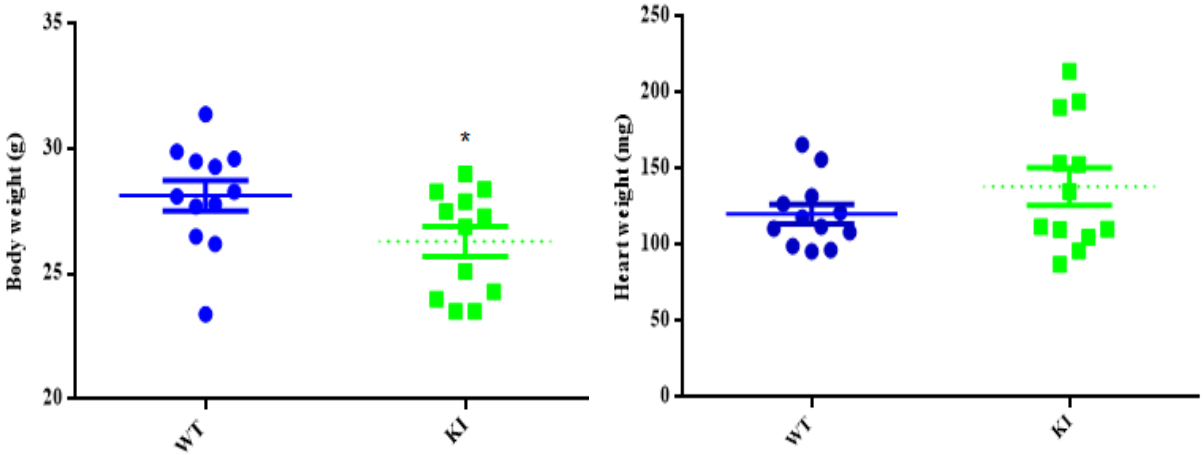

Figure 6.3.4A Morphometric characteristics: *The graphs show the body weight and the heart weight of the WT and KI mice selected for experiments. There was a significant difference in the body weight between the WT and KI mice with WT slightly heavier than the KI. There was no significant difference between the WT and KI mice in heart weight. (n=12, unpaired t-test with p<0.05)*

The WT and KI mice were grouped into two subgroups of control and ischaemia in a random fashion, and the ischaemia-reperfusion protocol was implemented which is described in 6.2.

1. WT Control (6)
2. WT Ischaemia (6)
3. KI Control (5)
4. KI Ischaemia (7)

The coronary flow, end diastolic pressure and left ventricular pressure were recorded just before the induction of ischaemia at 40 minutes, then during 5, 10, 20 and 30 minutes of global ischaemia, and finally at the end after 120 minutes of reperfusion. The coronary flow, as expected went down to zero with ischaemia and returned back to towards the baseline level at the end of reperfusion in both genotypes. The end diastolic pressure went up with ischaemia in both WT and KI hearts with significant difference from baseline appearing after 10 minutes of ischaemia. There was a significant difference between the WT and the KI hearts only at the 10 minute time-point of ischaemia. The left ventricular pressure went down after induction of ischaemia with a significant difference in both WT and KI hearts but there was no significant difference between the WT and the KI hearts.

B)

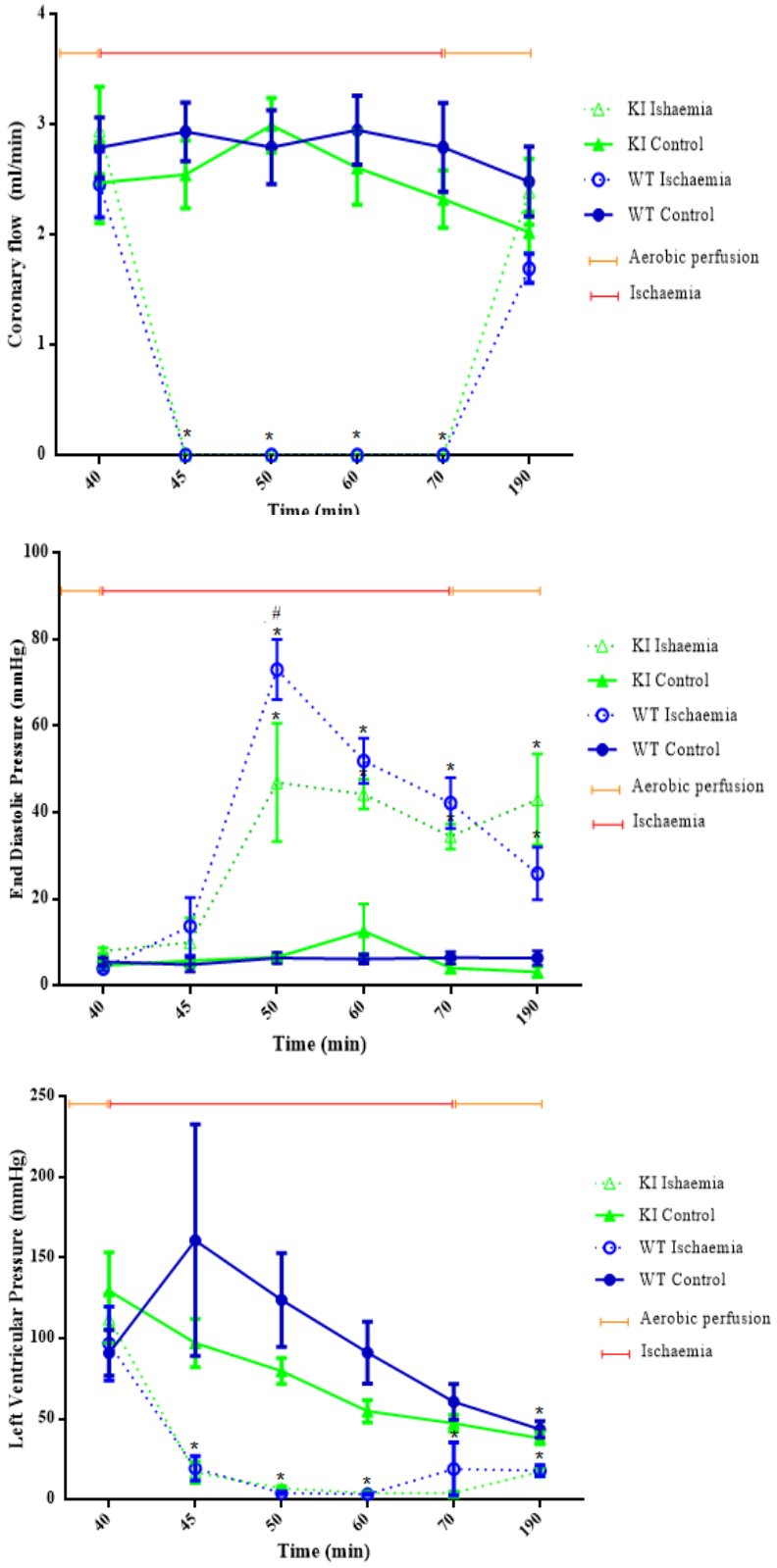

Figure 6.3.4B Hemodynamics of the perfused hearts: *The graphs above show the coronary flow, EDP, and LVP of the isolated perfused hearts under ischaemia-reperfusion protocol which consists of 40 minutes of stabilization, and 30 minutes of ischaemia/aerobic perfusion, followed by 120 minutes of reperfusion. The measurements were taken at following times; just prior to ischaemia (40 minutes), during 30 minutes of ischaemia (45, 50, 60, 70 minutes) and then finally at the end of reperfusion (190 minute). (Graphs were analysed by Two-way ANOVA with post-hoc Tukey test, $p<0.05$, *=against baseline, #=against genotype at that time-point)*

6.3.5 Infarct size in the TAB1 KI and WT hearts

To assess myocardial infarction in WT and KI hearts resulting from ischaemia, the Langendorff technique was performed with an ischaemia-reperfusion protocol. The hearts were subjected to 40 minutes of stabilization, followed by either 30 minutes of global ischaemia or continuous aerobic perfusion, which was then followed by 120 minutes of reperfusion. At the end of the experiment, the hearts were stained with TTC for infarct assessment as described in section 6.2. After the analysis, to our surprise the infarction caused by ischaemia tended to be greater in the KI hearts compared to the WT hearts (Fig 6.3.5A), although there was no significant difference between the two genotypes. Ischaemia caused a significant increase in the infarction to the heart in both WT and KI as expected. However, interestingly the infarction caused by prolonged aerobic perfusion tended to be less in the KI hearts compared to the WT hearts; which correlates with the p38α activation we observed in figure 6.3.2.

A)

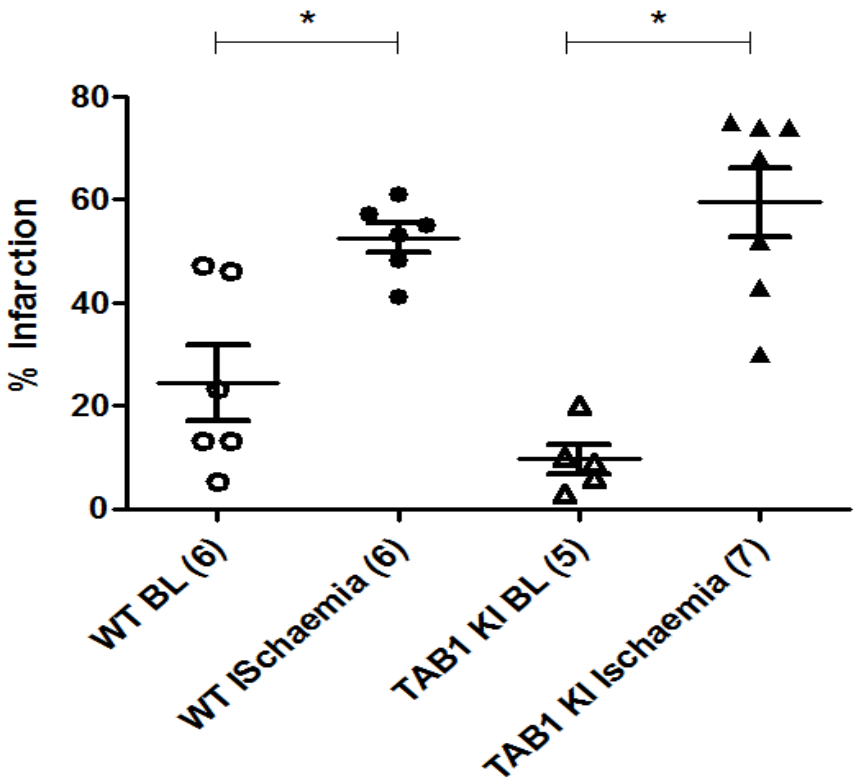

Figure 6.3.5A Graph illustrating the infarct size assessment in TAB KI and WT hearts during 190 min of perfusion with and without 30 minutes of global ischaemia: *30 minutes of global ischaemia caused extensive infarction in both WT and KI hearts. At the baseline, the KI hearts tended to have less infarction compared to the WT hearts, whereas with ischaemia the KI hearts tended to have more infarction compared to the WT hearts. There was no significant difference in infarct size between genotypes. Graphs were analysed by One-way ANOVA with post-hoc Tukey test, $p<0.05$)*

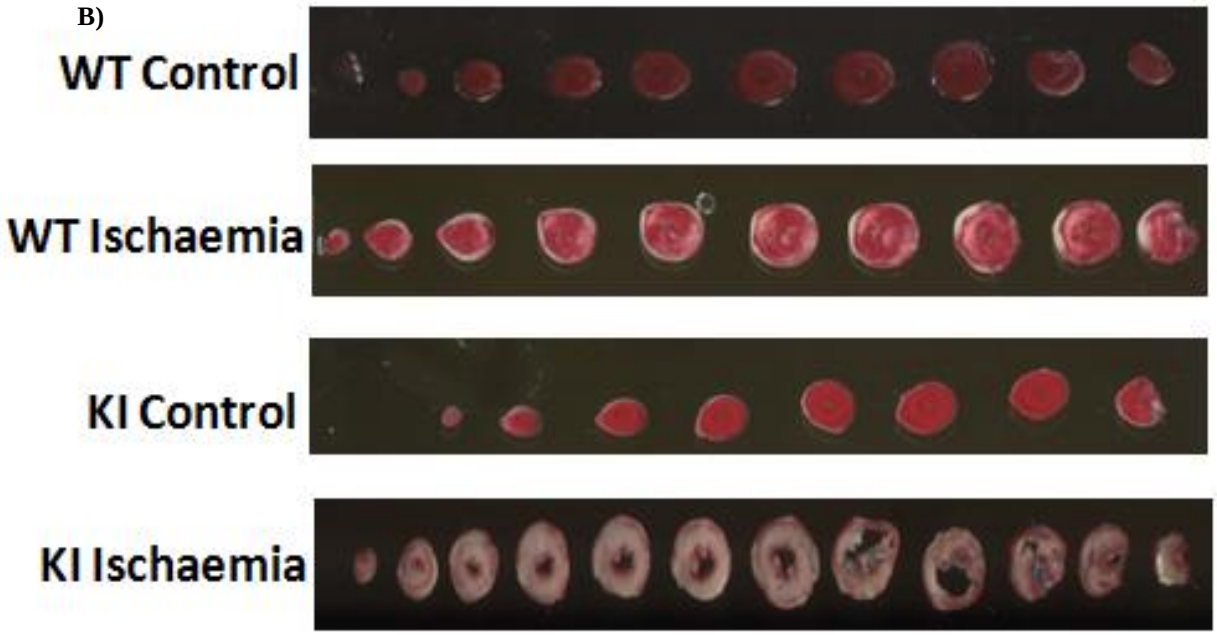

Figure 6.3.5B Image shows the heart sections scanned for infarct analysis: *The heart sections (0.75mm) are representative images of the WT and KI mice after TTC staining, scanned for infarct analysis using image J. The red stain shows the viable tissues whereas the white stain shows the dead myocardium.*

6.3.6 p38α autoactivation in mouse embryonic fibroblasts

We used fibroblasts isolated from the WT and KI embryos as a tool to investigate the effect of ischaemia on p38α activation. The fibroblasts were subjected to simulated ischaemia using the ischaemic buffer as described in chapter 4. The WT and KI cells were incubated in serum starved growth medium for 2 hours prior to the addition of ischaemic buffer. To induce ischaemia, the serum-free medium was aspirated and replaced with 2ml of simulated ischaemia buffer. The cells were incubated in the buffer for 20 minutes, washed with PBS, collected with 2X SDS buffer and analysed by western blotting. As seen in western blot below, the ischaemic buffer slightly increased the phospho p38 signal in the WT cells and SB203580 treatment completely abolished the phospho p38 signal. In the KI cells, the phospho p38 signal was very high at baseline and the ischaemia buffer did not increase the signal further. However, the SB203580 treatment greatly reduced the signal. The high phospho p38 signal seen in the control

cells could be the reason ischaemic buffer was unable to cause further increase as the signal was already at maximum.

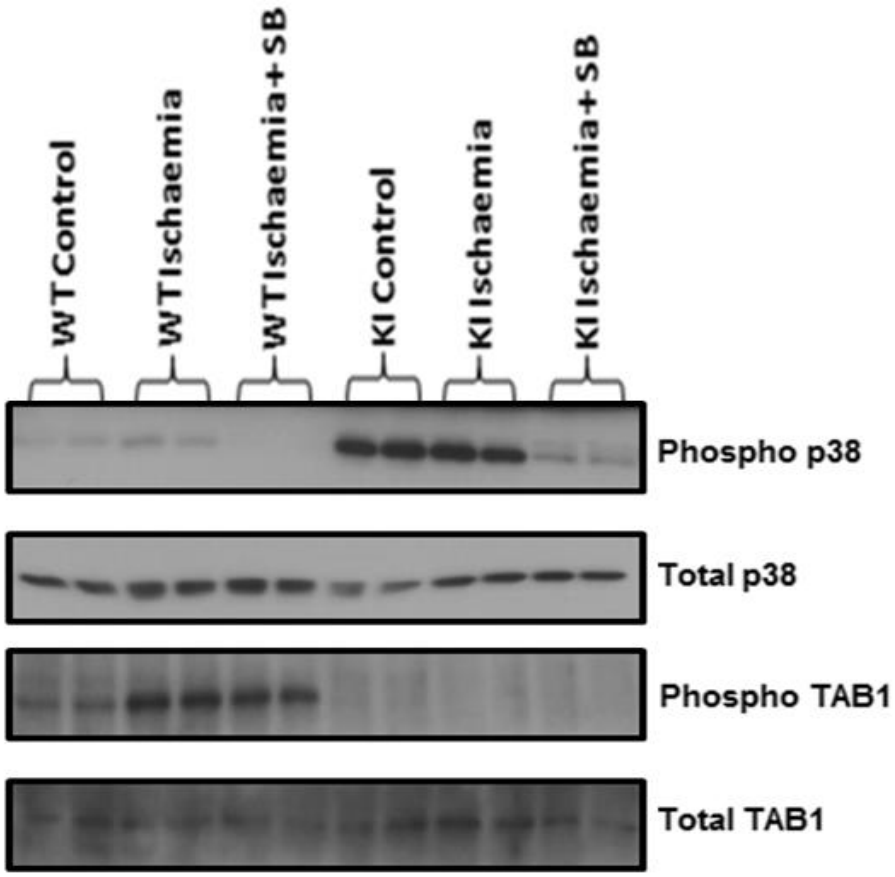

Figure 6.3.6 Mouse embryonic fibroblasts subjected to simulated ischaemia: *Western blot shows the effect of simulated ischaemia buffer on the WT and the KI cells. The phospho-p38 signal in the WT cells under basal condition was low and the addition of ischaemia buffer appeared to increase it slightly which was then reversed by the addition of 10µM SB203580. The phospho p38 signal in the KI cells was very high under basal condition and the addition of ischaemia buffer did not increase the signal further. The addition of 10µM SB203580 however markedly inhibited the phospho p38 signal.*

6.4 Discussion

6.4.1 Expression of TAB1 protein in the KI mice

To investigate the TAB1-induced p38α activation caused by ischaemia, we created transgenic TAB1 KI mice with four point mutations in the TAB1 protein (V390A, Y392A, V408G, and M409A) which prevents TAB1 from interacting with p38α. The four mutated residues reside on the C-terminal end of TAB1 in the p38α binding domain, and prior to the start of our investigation, we needed to confirm that the mutation did not affect the expression of the protein in the KI mice. To test this, we homogenized 3 organs; heart, liver, and thymus, and compared the expression of TAB1 in the KI and the WT mice.

The commercially available anti-TAB1 antibody from Santacruz detected a stronger TAB1 band in the WT organs compared to the KI organs suggesting that the TAB1 expression is higher in the WT mice than in the KI mice (Fig 6.3.1A). The anti-TAB1 antibody from Phil Cohen's group in Dundee reproduced similar result (Fig 6.3.1B) providing further evidence that there is more TAB1 expression in the WT mice. The result suggests that the four point mutations introduced at the C-terminal end of the TAB1 protein has diminished its expression in the cells. The other explanation could be that the antibody is not able to recognize the KI TAB1 as efficiently because of the mutations. The 4 point mutations could have altered the folding of the protein and its structure ever so slightly that the antibodies' affinity may have gone down. However, when we probed the Langendorff perfused hearts with the new fresh batch of TAB1 antibody from the Cohen group, there was no difference in the expression of TAB1 between the WT and the KI mice. In addition, the MEFs probed with the same antibody produced no difference in the TAB1 expression level between the WT and KI either (Fig 6.3.6). So, the result produced in 6.3.1 could be due to the fact that those two antibodies were old and not as good, and might have degraded, but we need to test the samples in 6.3.1 with the fresh TAB1 antibody from Cohen's group before we conclude this. Another interesting result in 6.3.1 was

that the TAB1 from the WT mice appeared to run higher than the TAB1 from the KI mice. This was produced by both Santacruz and the Cohen group's old TAB1 antibody. The result confirmed that the WT TAB1 (54.581kDa) is heavier than the KI TAB1 (54.359kDa). However the difference in molecular weight is a mere 0.222kDa and it is very surprising to see a shift in the western blot for such small difference. The result would be more plausible if the WT TAB1 was to undergo more post-translational modifications such as phosphorylation and ubiquitination than the KI TAB1 that would make it heavier. The new batch of TAB1 antibody from the Cohen group did not produce the shift between the WT and KI TAB1 band with both running at same molecular weight. To conclude, although the old antibodies detected a small difference in the expression of the WT and KI TAB1, the new fresh antibody did not detect any differences. From these results, we conclude that the expression of the mutated TAB1 in the KI mice is not impaired, and it should not affect our investigation to compare its function between the WT and the KI mice.

6.4.2 p38α activation in the KI mice

6.4.2.1 p38α activation is not impaired in the KI mice

After confirming that the mutated TAB1 protein is expressed in the KI mice, we investigated the TAB1-induced activation of p38α caused by ischaemia. We carried out Langendorff perfusion of the WT and KI hearts and subjected them to 40 minutes of stabilization followed by 10 minutes of global ischaemia. These hearts were then homogenised and analysed by western blotting to look at the activation of p38α. As the TAB1 protein in the KI mice has its 4 residues involved in binding to p38α mutated, we expected a lack of p38 activation in the KI mice during ischaemia. However, as seen in western blot 6.3.2 there was a clear activation of p38α in the KI hearts. In fact, p38α activation appeared to be more in the KI mice compared to the WT mice. In the WT hearts, ischaemia caused an increase in p38α activation as expected but to see p38α activation in the KI hearts was a surprise. Interestingly, there was also more MKK3 activation in the KI hearts compared to the WT hearts which could help to explain the phospho

p38 signal seen in the KI hearts. p38α is a vital signalling protein and it seems the MKK pathway may have been switched on to compensate for the lack of TAB1 pathway. Additionally, we know that MKK3/6 activates p38α significantly more strongly than the TAB1 activates p38α, and it could explain the stronger phospho p38 signal we see in the KI hearts compared to the WT hearts where there is minimum active MKK3. Intriguingly in a reversal study where MKK3 pathway was knocked out, the p38α activation induced by tumour necrosis factor (TNF)-α (activator of canonical pathway) did not seem to be compensated via the TAB1 pathway (Tanno *et al,* 2003).

The p38α activation at the baseline condition appeared to be less in the KI hearts compared to the WT hearts. This result suggests that in heart the TAB1-induced p38α autoactivation pathway could also play a role in baseline condition in addition to the ischaemic event. There was no change in the phospho TAB1 signal with ischaemia in the WT hearts. The result was surprising as with increased activation of p38α following ischaemia, we expected the phospho TAB1 signal to go up as well, since it is the downstream target of p38α. The phospho TAB1 signal in the KI hearts could not be detected either at baseline or during ischaemia. This was expected as the mutated TAB1 in the KI mice is unable to bind to p38α and as a result TAB1 cannot dock to p38α and become phosphorylated.

6.4.2.2 p38α auto-activation is impaired in the KI mice

The result in 6.3.2 showed that p38α gets activated during ischaemia in the KI hearts as opposed to our prediction. It suggests that the canonical MKK pathway may be compensating for the lack of TAB1 pathway. To confirm this, we carried out Langendorff perfusion of the KI hearts that were subjected to global ischaemia in the presence of SB203580. SB203580 is an ATP-mimetic inhibitor that competes with ATP for p38α's catalytic site and as a result inhibits the p38α's activation caused via TAB1 (Cohen, 1997; Young *et al*, 1997). SB203580 does not inhibit enzymes involved in the canonical pathway so it does not prevent the activation of p38α via trans-activation mechanism (Kumar *et al*, 1999). If p38α activation is inhibited in the

presence of SB203580, it means that p38α must be getting activated via the TAB1-induced autoactivation mechanism. The western blot analysis in 6.3.3 showed that in the KI hearts treated with 10μM SB203580, the phospho p38 signal was reduced in some hearts by various degrees. The result suggests that SB203580 is preventing the p38 auto-activation during ischaemia, i.e. p38α must be getting activated via the TAB1 pathway. However, that is not possible, as TAB1 cannot bind to p38α in the KI animal, and the only other known autoactivation mechanism of p38α not involving TAB1 is specific to T-cells (Salvador *et al*, 2005). In the presence of DMSO, the vehicle solvent in which the SB203580 was dissolved, p38α activation was also reduced; producing very similar result to the SB203580 treated hearts. This result indicates that it was not in fact the SB203580 that caused the inhibition of p38α activation, but DMSO. However, DMSO itself should not inhibit the p38 activation. It is something we cannot explain at this stage and it requires further tests, for example running the experiments with water-soluble SB203580 and also running the experiments alongside WT hearts. To conclude, the results so far suggest that the p38α auto-activation in the KI hearts seems to be impaired but the p38α trans-activation is not, as the canonical MKK pathway appears to take over for the lack of the TAB1 pathway.

6.4.3 Infarct volume assessment in the KI hearts

As discussed in previous chapters and the introduction of this chapter, the TAB1-induced p38α autoactivation in ischaemic heart aggravates the lethal injury to the heart. p38α autoactivation causes biochemical signalling in the myocardium that drives the damage to the heart which results in myocardial death and heart failure (Barancik *et al*, 2000; Ma *et al*, 1999; Martin *et al*, 2015). From the results in 6.3.2 and 6.3.3, we know p38α activation is not affected in the TAB1 KI mice, as the canonical pathway takes over the impaired TAB1 pathway. The p38α activation that causes the damage in ischaemic heart takes place via the TAB1 pathway not the canonical pathway, however p38α is activated nevertheless. Whether the contrasting mode of p38α activation from two different pathways reflects in phosphorylation of different substrates to

produce distinct outcomes is not known. We tested this by carrying out Langendorff perfusion of these hearts with ischaemia-reperfusion protocol and quantifying the infarct sizes.

The result in 6.3.6 showed that ischaemia caused a significant infarction in the KI hearts similar to the WT hearts. In fact the average infarct volume in the KI hearts tended to be greater (60%) than in the WT hearts (50%). The result suggests that the KI hearts are not protected during ischaemia contrary to our prediction. The result is not entirely surprising considering our previous results which showed p38α activation is not impaired in the KI hearts, and the findings from previous study which has shown that only a complete inhibition of p38α elicits a protective phonotype (Kumphune *et al*, 2010). In fact the infarction result correlates with the p38α activation result in 6.3.2 where we observed greater p38α activation in the KI hearts which produced a higher infarction from ischaemia in 6.3.5. Similarly, in the control hearts of the KI mice, we observed less infarction compared to the control hearts of the WT mice, which also correlates with the p38α activation result in 6.3.2 where we observed less p38α activation in the KI baseline hearts compared to the WT baseline hearts. However, the infarction of around average of 25% in the WT control hearts is a surprise. Under the aerobic perfusion, the infarction should be at minimal level as seen in the KI control hearts. The 2 out of 6 hearts in the WT control showed big infarction which could have resulted from individual experimental error on those particular hearts, so repeating the experiment with another 2 control WT hearts would be a good future experiment. Nevertheless, the infarction study has confirmed that p38α is the main determinant that orchestrates the catastrophic biochemical signalling in the heart which contributes to infarction and heart failure.

To summarise, our results have demonstrated that p38α activation during ischaemia aggravates the injury to the heart, to support hundreds of other studies in the literature (Barancik *et al*, 2000; Ma *et al*, 1999; Mackay *et al*, 1999; Liu *et al*, 2005; Kaiser *et al*, 2004). However, our study at this stage has suggested one novel finding, which is, the mode of p38α activation does not seem to determine the detrimental outcome as long as p38α is activated. After 20 years of

failure in clinical trials, the circumstance selective inhibition of p38α had provided a promising outlook and looked to be the way forward in p38α therapeutics. We hoped to contribute to that research with our study of TAB1 KI mice and aimed to achieve selective inhibition of TAB1 pathway during ischaemia that would translate into protective phenotype of the heart. However, the results so far from the TAB1 KI mice seem to suggest that even if the TAB1 pathway is targeted, the MKK3/6 pathway could be switched on to activate p38α to cause damage in the ischaemic heart. But having said that, this is a preliminary data collected from one *ex-vivo* technique and we need to carry out significant amount of further studies on these animals before coming to any conclusion. Additionally, knocking out TAB1 pathway genetically is completely different to selectively inhibiting TAB1 pathway using an inhibitor. Using a drug to inhibit the TAB1 pathway will not necessarily activate the MKK pathway.

7 General discussions and future work

p38α is a serine/threonine kinase belonging to a family of MAPKs which plays a vital role in a myriad of cellular cascades. Also known as stress activated protein kinase (SAPK), several studies in the literature in past twenty years have shown that ischaemic stress in myocardium causes an activation of p38α, which exacerbates the injury (Tanno *et al*, 2003; Nagarkatti *et al*, 1998; Ren *et al*, 2005). Significantly, the studies have also established that inhibiting the activation of p38α prevents the injury to the heart (Barancik *et al*, 2000; Cain *et al*, 1999; Martin *et al, 2001*; Kumphune *et al*, 2009; See *et al*, 2004). As a result, a huge amount of time and resources have been poured into elucidating p38α's activation mechanism that accelerates injury to the heart in ischaemic heart disease. Several p38α inhibitors have been tested but unfortunately none have passed through the phase III stage of clinical trials, attributed to severe side effects (Martin *et al*, 2012; Marber *et al*, 2011). In early 2000, Ge and co-workers made a major observation and discovered the activation mechanism of p38α during ischaemia, which surprisingly was not via the classical activation pathway but via a scaffold protein known as TAB1 (Ge *et al*, 2002). This finding has become critical in the development of a new type of p38α inhibitor that bypasses the activation of p38α via classical activation pathway but inhibits the p38α activation induced by TAB1. This, in theory, should reduce the incidence of side effects seen with the p38α inhibitors in the clinical trials by avoiding a blanket inhibition. However, in order to develop such a drug, a better understanding of the activation of p38α by TAB1 is required in atomic detail. This was the aim of my thesis in which I investigated the structural aspects of TAB1-mediated p38α activation.

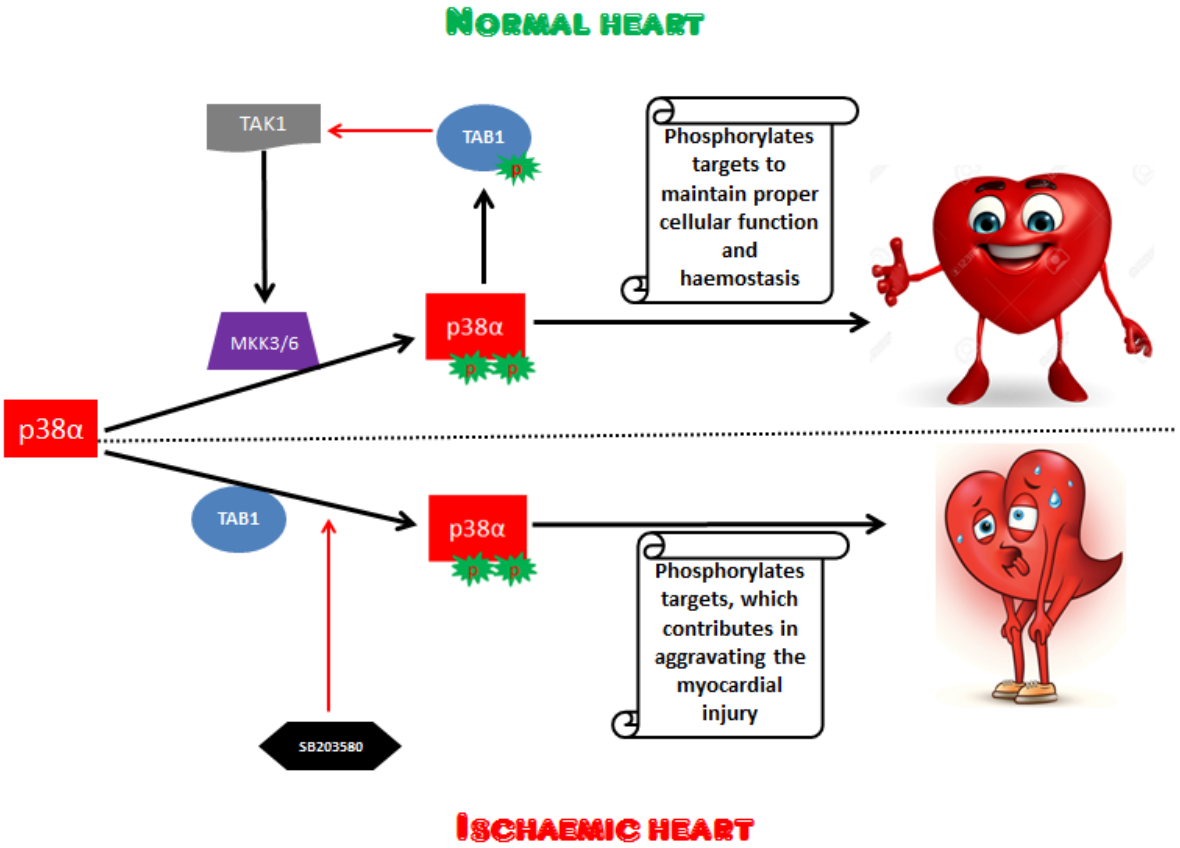

Figure 7 p38α activation pathways: *The cartoon describes the activation pathways of p38α. The classical activation pathway involving the TAK1/MKK3&6/p38α cascade helps to maintain proper cellular function and physiological homeostasis. The TAB1/p38α pathway is activated during ischaemia and aggravates myocardial injury. The therapeutic strategy is to prevent the TAB1-mediated p38α activation pathway, without affecting the classical activation pathway. (The black arrow indicates activation, the red arrow indicates inhibition).*

7.1 Chapter 4

7.1.1 Summary

In chapter 3, using an *in-vitro* kinase assay and the living system of a mammalian cell line, I confirmed the TAB1-mediated activation mode of p38α**.** I showed that TAB1 caused autoactivation of p38α which was sensitive to an ATP-mimetic inhibitor, SB203580. This supported the original findings from Ge *et al* in 2002. With that confirmation, I went on to address the main aim of my thesis; to study the structural details of TAB1-mediated p38α activation. In 2013 our lab resolved the crystal structure of a p38α-TAB1 complex which

revealed many key findings of the autoactivation mechanism of p38α (De Nicola *et al*, 2013). The significant findings were; TAB1 interacts with p38α in a bipartite manner, interaction leads to structural changes that increase affinity for ATP, the activation loop swings towards the catalytic site bringing Thr180 in proximity to the bound ATP which facilitates the T-G-Y autophosphorylation. On a closer inspection of the crystal structure, we observed that the C-terminal end of the activation loop (Tyr182-Thr185) extended to form an α-helical segment, which caused the activation loop to swing towards the catalytic site. This extension appeared to be stabilized by the formation of a hydrogen bond between the side chains of Thr185 and Asp150. Based on this observation, we hypothesised that if this hydrogen bond between Thr185 and Asp150 was disrupted then this would deprive the system of the free energy that is required to hold the activation loop in this new orientation and disturb the structural changes that favour autophosphorylation of the T-G-Y motif. To test this hypothesis, we created a mutant p38αT185G and compared its biophysical and biochemical properties with WTp38α. Using an *in-vitro* kinase assay and several stimuli in the living system of HEK293 cells, we produced robust data to show that the hydrogen bond between the side chains of Thr185 and Asp150 does indeed play a significant role in the structural changes induced by TAB1 and without it the autoactivation of p38α is impaired. We showed this with purified recombinant protein in in-vitro kinase assay (Fig 4.3.6) and by transfecting p38αT185G in to HEK293 cells with TAB1 (Fig 4.3.7). Additionally, we also showed that ischaemia, a prominent activator of TAB1-mediated activation of p38α, was unable to cause autoactivation of p38αT185G. These results collectively support our hypothesis that the autoactivation of p38αT185G is impaired, and it was not due to the inability of the mutant p38αT185G to bind and interact with TAB1. We verified this using ITC and showed that p38αT185G was indeed able to interact with TAB1 similar to the WTp38α. Finally, we resolved the crystal structure of the p38αT185G-TAB1 complex which confirmed the interaction and the lack of hydrogen bond between residues 185 and 150. This in-turn caused the C-terminal end of the activation loop (Tyr182-Thr185) to be more relaxed, which in-turn destabilized and prevented the swing of activation loop toward the

catalytic site. Due to this, the activation loop was too mobile which was depicted by the high B factor and could not be resolved in the crystal structure (Fig 4.3.5).

7.1.2 Implications

The results gathered in chapter 4 highlighted a key feature; that the hydrogen bond between Thr185 and Asp150 plays a vital role in the successful activation of p38α induced by TAB1. Unfortunately however, a hydrogen bond cannot be targeted by a drug or an inhibitor, so this is not an observation that can be easily translated to disrupt p38α activation during ischaemia *in-vivo*. Nevertheless we know that the hydrogen bond stabilizes the extension of the C-terminal end of the activation loop (Tyr182-Thr185), one of the key structural changes that takes place during the activation mechanism, and this region can perhaps be targeted for disruption. A definite line of future work would be to create a transgenic mouse based on this mutation. Our results suggest that the mutation has not impacted p38α's ability to interact with TAB1, which means it is highly likely that its ability to bind to other binding partners is not affected either. Although the classical activation mechanism, and the catalytic ability, of the p38αT185G mutant appeared to be disrupted at low nanomolar concentrations, we speculate the higher differential sensitivity of the auto-activation mechanism would provide a high therapeutic index. These results suggest that the transgenic mice should be viable and healthy without any major complications. Once created, the hearts from these mice could be investigated under ischaemic stress to assess p38α's activation status and whether they present a protective phenotype. If the results are positive, this model can be exploited in several ways to elucidate p38α's role in ischaemia. For example, any difference in the activation of substrates compared to WT mice can be investigated to compile potential hits for p38α's substrates that are activated during ischaemia. The p38αT185G knock-in mice therefore have the potential to both validate our target and identify relevant and harmful downstream signals during myocardial ischaemia.

7.2 Chapter 5

7.2.1 Summary

In chapter 5 I investigated if Thr185 also played a role in determining p38α's cellular location. The underlying rationale behind this prediction was related to the role of Thr188, the corresponding residue in ERK2, in determination of cellular location (Lorenz *et al*, 2008). In pathological cardiac hypertrophy, autophosphorylation of Thr188 drives ERK2 into the nucleus to phosphorylate pro-hypertrophic genes which exacerbate hypertrophy. p38α is a close family member of ERK2 and we wondered whether TAB1-mediated autophosphorylation extends to Thr185 and that in turn translocates p38α during ischaemia. We showed using mass spectrometry analysis that TAB1 induced phosphorylation at Thr185, however, this did not result in p38α localizing to the nucleus. We found no different in the cellular location of WTp38α compared to p38αT185G, suggesting that phosphorylation of Thr185 had no impact on p38α's cellular location. Therefore, Thr185 of p38α does not have a similar functional role to the Thr188 of ERK2.

7.2.2 Implications

Our hypothesis was based on the 50% shared homology between p38α and ERK2 that warranted this investigation (Cargnello *et al*, 2011). However, despite the similarity, one major difference between them with regards to their regulation of cellular location was that; ERK2 has a nuclear localization signal, whereas p38α does not. Therefore our negative result is not a total surprise. The regulation of p38α's cellular location has been the subject of debate with several studies publishing contrasting results as discussed in 5.4. So, more work needs to be done in this area, but based on our study, we can conclude that Thr185 does not play a major role in determining cellular location under our conditions.

7.3 Chapter 6

7.3.1 Summary

The final chapter contains the preliminary data collected from the TAB1 KI mice, where four residues (V390A/Y392A/V408G/M409A) in TAB1 involved in the interaction with p38α have been mutated. As a result, TAB1 is unable to bind to and auto-activate p38α in the TAB1 KI mice. Using a Langendorff technique, we perfused the KI hearts and subjected them to 10 minutes of ischaemia to determine the p38α activation status. To our surprise, ischaemia caused similar p38α activation in the KI hearts to that observed in the WT hearts. The result was completely the opposite of what was expected. We also observed a greater activation of MKK3 by the classical activation pathway in the KI hearts compared to the WT hearts, and concluded that the MKK3/6 pathway appeared to be compensating for the lack of the TAB1 pathway. If this is indeed the case, it would not be a total surprise since p38α is a vital signalling molecule, especially in a stressful environment such as ischaemia. The key question was whether this activation of p38α via a different activation pathway resulted in a similar detrimental outcome. To find out, we subjected Langendorff-perfused hearts to an ischaemia-reperfusion protocol. After 30 minutes of ischaemia and 2 hours of reperfusion, we observed that the ischaemia tended to cause more substantial infarction in the KI hearts compared to the WT hearts. This result correlated with the activation level of p38α, as higher phospho p38α level was observed in the KI hearts compared to the WT hearts. The result suggested that the injury to the heart is determined by the level of p38α activation and the mechanism of activation may have no impact on it. It is an interesting result because MKK3/6 activates p38α significantly more strongly than TAB1. So, the fact that p38α get activated via TAB1 during ischaemia could be an adaptive mechanism to protect the cell, thereby minimizing the activation of p38α and consequent injury during myocardial ischaemia.

7.3.2 Implications

To observe p38α activation and greater infarction in the TAB1 KI hearts compared to the WT hearts was a very disappointing outcome. We created the TAB1 KI mice in the hope that it would produce a protective phenotype during ischaemia by preventing the detrimental TAB1-mediated p38α activation pathway. However, such is the elegance of a cellular system to adapt for survival that the MKK3/6 pathway seems to have been switched on to maintain the activity of p38α, which further demonstrates p38α's importance as a signalling protein. Ironically, this compensative mechanism has led to greater infarction resulting from higher p38α activation by MKK3/6. However, this does not mean we cannot target the TAB1 pathway with a drug. Using an inhibitor to target p38α-TAB1 pathway is not going to evoke the same cellular response as genetically ablating the pathway, i.e. a small molecule that targets TAB1-p38α complex will not necessarily cause an activation of the classical MKK3/6 pathway. Furthermore, our observations may reflect the germline KI of p38α and the compensatory activation of MKK3/6 may not happen with short-term inhibition of the association between TAB1 and p38α that would be achieved with a small molecule. So, the work to create a drug to prevent TAB1 and p38α interaction must continue. Additionally, the data presented in this chapter are preliminary from an ex-vivo technique. A more relevant in-vivo technique, such as transverse aortic constriction (TAC) should be performed to further validate the observation. Similarly, these mice can be studied in a different disease setting in order to discover other roles of TAB1/p38α pathway.

7.4 Conclusion

The aim of this thesis was to study the TAB1-mediated autoactivation of p38α in the hope we can reveal key structural features that are vital to this process. I investigated the structural features, and consequence of activating and disrupting this pathway. Determining how exactly p38α mediates its signalling to aggravate myocardial injury is a challenging task. So many variables- such as different isoforms of p38, signalling networks, feedback loops, status of MKK3/6 and TAB1, p38 cell location, availability of substrates- will have an impact on p38α signalling. In this thesis, the two models I investigated, p38αT185G and TAB1 KI (V390A/Y392A/V408G/M409A) have provided promising preliminary results in respect to understanding the p38α signalling in more details and how to target TAB1-mediated p38α activation. However, it warrants further investigations so that we can achieve the ultimate aim of reducing myocardial ischaemic injury caused by p38α that may contribute to heart failure, the biggest cause of death in the world.

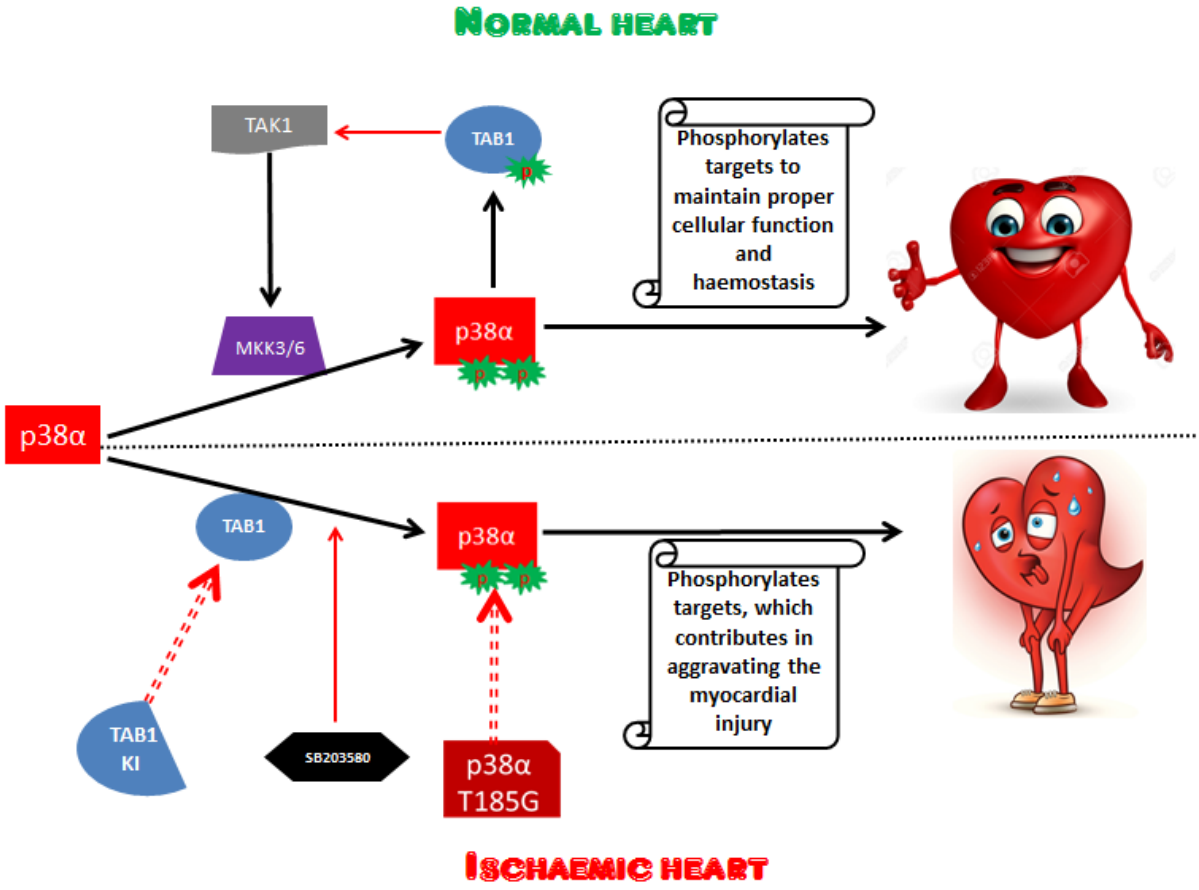

Figure 7.4 Targeting TAB1-mediated p38α activation: *The p38αT185G and the TAB1 KI model can be exploited to unravel p38α's functionality during ischaemia that contributes to myocardial injury. The black arrow indicates activation and the red arrow indicates inhibition.*

REFERENCES

Adams, RH., Porras, A., Alonso, G., Jones, M., Vintersten, K., Panelli, S., Valladares, A., Perez, L., Klein, R., Nebreda, AR. (2000). Essential role of p38alpha MAP kinase in placental but not embryonic cardiovascular development. *Molecular cell, 6*(1), 109-16.

Aicher, A., Shu, GL., Magaletti, D., Mulvania, T., Pezzutto, A., Craxton, A., Clark, EA. (1999). Differential role for p38 mitogen-activated protein kinase in regulating CD40-induced gene expression in dendritic cells and b cell. *Journal of immunology, 163*, 5786-5795.

Arabacilar, P., Marber, M. (2015). The case for inhibiting p38 mitoen-activated protein kinase in heart failure. *Frontiers in pharmacology, 6*, 102.

Arbustini, E., Brega, A., Narula, J. (2008). Ultrastuctural definition of apoptosis in heart failure. *Heart failure reviews, 13*, 121-135.

Armstrong, J., Harbron, C., Lea, S., Booth, G., Cadden, P., Wreggett, KA., Singh, D. (2011). Synergistic effects of p38 mitogen-activated protein kinase inhibition with a corticosteroid in alveolar macrophages from patients with chronic obstructive pulmonary disease. *Journal of pharmacology and experimental therapeutics, 338*(8), 732-40.

Barancik, M., Htun, P., Strohm, C., Kilian, S., & Schaper, W. (2000). Inhibition of the cardiac p38-MAPK pathway by SB203580 delays ischemic cell death. *Journal of cardiovascular pharmacology, 35*(3), 474–83.

Bartlett, JM., Stirling, D. (2003). A short history of the polymerase chain reaction. *Methods in molecular biology, 226*, 3-6.

Bassi, R., Heads, R., Marber, MS., Clark, JE. (2008). Targeting p38-MAPK in the ischaemic heart: kill or cure. *Current opinion in pharmacology, 8*(2), 141-6.

Beardmore, V. A., Hinton, H. J., Eftychi, C., Apostolaki, M., Armaka, M., Darragh, J., … Arthur, J. S. C. (2005). Generation and characterization of p38beta (MAPK11) gene-targeted mice. *Molecular and cellular biology, 25*(23), 10454–64. Bell, RM., Mocanu, MM., Yellon, DM. (2011). Retrograde heart perfusion: the Langendorff technique of isolated heart perfusion. *Journal of molecular and cellular cardiology, 50*(6), 940-50.

Bell, RM., Mocanu, MM., Yellon, DM. (2011). Retrograde heart perfusion: the Langendorff technique of isolated heart perfusion. *Journal of molecular and cellular cardiology, 50*(6), 940-50.

Ben-Levy, R., Hooper, S., Wilson, R., Paterson, HF., Marshall, CJ. (1998). Nuclear export of the stress-activated protein kinase p38 mediated by its substrate MAPKAP kinase-2. *Current biology, 8*(19), 1049-57.

Bernardo, BC., Weeks, KL., Pretorius, L., McMullen, JR. (2010). Molecular distinction between physiological and pathological cardiac hypertrophy: Experimental findings and therapeutic strategies. *Pharmacology & therapeutics, 128*, 191-227.

Bernet, JD., Doles, JD., Hall, JK., Kelly, Tanaka, K., Carter, TA., Olwin, BB. (2014). p38 MAPK signaling underlies a cell-autonomous loss of stem cell self-renewal in skeletal muscle of aged mice. *Nature medicine, 20*(3), 265-71.

BHF. BHF coronary artery heart disease statistics, 2010

Bing, RJ., Gudbjarnason, S., Tschopp, H., Braasch, W. (1969). Molecular changes in myocardial infarction in heart muscle. *Annals of the new york academy of sciences, 156*(1), 583-93.

Brand, P., Plochmann, S., Valk, E., Zahn, S., Saloga, J., Knop, J., Becker, D. (2002). Activation and translocation of p38 mitogen-activated protein kinase after stimulation of monocytes with contact sensitizers. *The journal of investigative dermatology, 119*(1), 99-106.

Brown, K., Vial, SC., Dedi, N., Long, JM., Dunster, NJ., Cheetham, GM. (2005). Structural basis for the interaction of TAK1 kinase with its activating protein TAB1. *Journal of molecular biology, 354*(5), 1013-20.

Brownlee, KA. (1955). Statistics of the 1954 polio vaccine trials. *Journal of American statistical association, 50*(272), 1005-1013.

Bulavin, DV., Higashimoto, Y., Popoff, IJ., Gaarde, WA., Basrur, V., Potapova, O., Appella, E., Fornace, AJ. (2001). Initiation of a G2/M checkpoint after ultraviolet radiation requires p38 kinase. *Nature, 411*(6833), 102-7.

Cain, BS., Meldrum, DR., Meng, X., Dinarello, CA., Shames, BD., Banerjee, A., Harken, AH. (1999). p38 MAPK inhibition decreases TNF-alpha production and enhances postischemic human myocardial function. *The journal of surgical research, 83*(1), 7-12.

Cargnello, M., Roux, PP. (2011). Activation and function of the MAPKs and their substrates, the MAPK-activated protein kinases. *Microbiology and molecular biology reviews, 75*(1), 50-83.

Chen, BX., Ma, FY., Luo, W., Ruan, JH., Zhao, XZ., Xie, WL., Sun, SH., Guo, XM., Wang, F., Tian, T., Chu, XW. (2009). Characterization of atherosclerotic plaque in patients with unstable angina pectoris and stable angina pectoris by optical coherence tomography. *Zhonghua Xin Xue Guan Bing Za Zhi, 37*(5), 422-5.

Cheung, PC., Nebreda, AR., Cohen, P. (2004). TAB3, a new binding partner of the protein kinase TAK1. *Biochemical journal, 378*(Pt 1), 27-34.

Cheung, PC., Campbell, DG., Nebreda, AR., Cohen, P. (2003). Feedback control of the protein kinase TAK1 by SAPK2a/p38alpha. *EMBO, 22*(21), 5793-805.

Clark, JE., Sarafraz, N., Marber, MS. (2007). Potential of p38-MAPK inhibitors in the treatment of ischaemic heart disease. *Pharmacology and therapeutics, 116*(2), 192-206.

Clarkson, PB., Halim, M., Ray, KK., Doshi, S., Been, M., Singh, H., Shiu, MF. (1999). Coronary artery stenting in unstable angina pectoris: a comparison with stable angina pectoris. *Heart, 81*(4), 393-7.

Cohen, P. (1997). The search for physiological substrates of MAP and SAP kinases in mammalian cells. *Trends in cell biology, 7*(9), 353-61.

Cohen, S. B., Cheng, T.-T., Chindalore, V., Damjanov, N., Burgos-Vargas, R., Delora, P., … Caulfield, J. P. (2009). Evaluation of the efficacy and safety of pamapimod, a p38 MAP kinase inhibitor, in a double-blind, methotrexate-controlled study of patients with active rheumatoid arthritis. *Arthritis and rheumatism, 60*(2), 335–44.

Cohen, SB., Cheng, TT., Chindalore, V., Damjanov, N., Burgos-Vargas, R., Delora, P., Zimanya, K., Travers, H., Caulfield, JP. (2009). Evaluation of the efficacy and safety of pamapimod, a p38 MAP kinase inhibitor, in a double-blind, methotrexate-controlled study of patients with active rheumatoid arthritis. *Arthritis and rheumatism, 60*(2), 335-44.

Cohn, JN., Ferrari, R., Sharpe, N. (2000). Cardiac remodeling- concepts and clinical implications: a consensus paper from an international forum on cardiac remodeling. Behalf of an international forum on cardiac remodeling. *Journal of the American college of cardiology, 35*(3), 569-82.

Cruchten, SV., Broeck, VD. (2002). Morphological and biochemical aspects of apoptosis, oncosis and necrosis. *Anatomia, Histologia, Embryologia, 31*, 214-223.

Cuadrado, A., & Nebreda, A. R. (2010). Mechanisms and functions of p38 MAPK signalling. *The Biochemical journal, 429*(3), 403–17.

Damjanov, N., Kauffman, RS., Spencer-Green, GT. (2009). Efficacy, pharmacodynamics, and safety of VX-702, a novel p38 MAPK inhibitor, in rheumatoid arthritis: results of two randomized, double-blind, placebo-controlled clinical studies. *Arthritis and rheumatism, 60*(5), 1232-41.

Davidson, SM., Morange, M. Hsp25 and the p38 MAPK pathway are involved in differentiation of cardiomyocytes. 2000. *Dev Biol, 218*(2), 146-60.

DeMello, WC. (1982). Cell-to-cell communication in heart and other tissues. *Progress in biophysics and molecular biology, 39*(3), 147-82.

De Nicola, GF., Martin, ED., Chaikuad, A., Bassi, R., Clark, J., Martino, L., Verma, S., Sicard, P., Tata, R., Atkinson, RA., Knapp, S., Conte, MR., Marber, MS. (2013). Mechanism and consequence of the autoactivation of p38α mitogen-activated protein kinase promoted by TAB1. *Nature structure molecular biology, 20*(10), 1182-90.

Dingar, D., Merlen, C., Grandy, S., Gillis, MA., Villeneuve, LR., Mamarbachi, AM., Fiset, C., Allen, BG. (2010). Effect of pressure overload-induced hypertrophy on the expression and localization of p38 MAP kinase isoforms in the mouse heart. *Cellular signalling, 22*(11), 1634-44.

Diskin, R., Lebendiker, M., Engelberg, D., & Livnah, O. (2007). Structures of p38alpha active mutants reveal conformational changes in L16 loop that induce autophosphorylation and activation. *Journal of molecular biology, 365*(1), 66–76.

Domon, B., Aebersold, R. (2006). Mass spectrometry and protein analysis. *Science, 312*(5771), 212-7.

Duff MR, Jr., Grubbs, J., Howell, EE. (2011). Isothermal titration calorimetry for measuring macromolecule-ligand affinity. *Journal of visualized experiments, 55*, 2796

Esumi, K., Nishida, M., Shaw, D., Smith, TW., Marsh, JD. (1991). NADH measurements in adult rat myocytes during simulated ischemia. *The American journal of physiology, 260*(6), 1743-52.

Eyers, P. A., van den IJssel, P., Quinlan, R. A., Goedert, M., & Cohen, P. (1999). Use of a drug-resistant mutant of stress-activated protein kinase 2a/p38 to validate the in vivo specificity of SB 203580. *FEBS letters, 451*(2), 191–6.

Faas, MM., Moes, H., Fije, JW., Muller Kobold, AC., Tulleken, JE., Zijlstra, JG. (2002). Monocyte intracellular cytokine production during human endotoxaemia with or without a second in vitro LPS challenge: effect of RWJ-67657, a p38 MAP-kinase inhibitor, on LPS-hyporesponsiveness. *Clinical and experimental immunology, 127*(2), 337-43.

Ferrari, R. (2000). Ischaemic heart disease: clinical improvement with metabolic approach. *Rev Port Cardiolo, 19*(5), 7-20

Fiedler, B., Feil, R., Hofmann, F., Willenbockel, C., Drexler, H., Smolenski, A., Lohmann, SM., Wollert, KC. (2006). cGMP-dependent protein kinase type I inhibits TAB1-p38 mitogen-activated protein kinase apoptosis signaling in cardiac myocytes. *The journal of biological chemistry, 281*(43), 32831-40.

Fijen, JW., Zijlstra, JG., De Boer, P., Spanijersberg, R., Tervaert, JW., Van Der Werf, TS., Ligtenberg, JJ., Tulleken, JE. (2001). *Clinical and experimental immunology, 124*(1), 16-20.

Fozzard, HA., Makielski, JC. (1985). The electrophysiology of acute myocardial ischaemia. *Annual reviews medicine, 36*, 275-84.

Ge, B., Gram, H., Di Padova, F., Huang, B., New, L., Ulevitch, R. J., … Han, J. (2002). MAPKK-independent activation of p38alpha mediated by TAB1-dependent autophosphorylation of p38alpha. *Science (New York, N.Y.), 295*(5558), 1291–4.

Genovese, MC. (2009). Inhibition of p38: has the fat lady sung? *Arthritis and rheumatism, 60*(2), 317–20.

Genovese, MC., Cohen, SB., Wofsy, D., Weinblatt, ME, Firestein, GS., Brahn, E., Strand, V., Baker, DG., Tong, SE. (2011). A 24-week, randomized, double-blind, placebo-controlled, parallel group study of the efficacy of oral SCIO-469, a p38 mitogen-activated protein kinase inhibitor, in patients with active rheumatoid arthritis. *The journal of rheumatology, 38*(5), 846-54.

Gong, X., Ming, X., Deng, P., Jiang, Y. (2010). Mechanisms regulating the nuclear translocation of p38 MAP kinase. *Journal of cellular biochemistry, 110*(6), 1420-9.

Gorog, DA., Jabr, RI, Tanno, M, Sarafrz, N., Clark, JE, Fisher, SG., Cao, XB., Bellahcene, M., Dighe, K., Kabir, AM., Quinlan, RA., Kato, K., Gaestel, M., Marber, MS., Heads, RJ. (2009). MAPKAPK-2 modulates p38-MAPK localization and small heat shock protein phosphorylation but does not mediate the injury associated with p38-MAPK activation during myocardial ischaemia. *Cell stress and chaperones, 14*(5), 477-89.

Graham, FL., Smiley, J., Russell, WC., Nairn, R. (1977). Characteristics of a human cell line transformed by DNA from human adenovirus type 5. *The journal of general virology, 36*(1), 59-74.

Gray, WD., Che, P., Brown, M., Ning, X., Murthy, N., Davis, ME. (2011). N-acetylglucosamine conjugated to nanoparticles enhances myocyte uptake and improves delivery of a small molecule p38 inhibitor for post-infarct healing. *Journal of cardiovascular translational research, 4*(5), 631-43.

Gum, RJ., McLaughlin, MM., Kumar, S., Wang, Z., Bower, MJ., Lee, JC., Adams, JL., Livi, GP., Goldsmith, EJ., Young, PR. (1998). Acquisition of sensitivity of stress-activated protein kinases to the p38 inhibitor, SB203580, by alteration of one or more amino acids within the ATP binding pocket. *The journal of biological chemistry, 273*(25), 15605-10.

Guth, BD., Wisneski, JA., Neese, RA., White, FC., Heusch, G., Mazer, CD. (1990). Myocardial lactate release during ischaemia in swine. Relation to regional blood flow. *Circulation, 81,* 1948-58.

Gutierrez, J., Ramirez, G., Rundek, T., Sacco, RL., (2012). Statin therapy in the prevention of recurrent cardiovascular events: a sex-based meta-analysis. *Arch Intern Med, 172*(12), 909-19.

Haddad, JJ. (2001). VX-745 Vertex pharmaceuticals. *Current opinion in investigational drugs, 2*(8), 1070-6.

Haddad, EB., Birrell, M., McCluskie, K., Ling, A., Webber, SE., Foster, ML., Belvisi, MG. (2001). Role of p38 MAP kinase in LPS-induced airway inflammation in the rat. *British journal of pharmacology, 132*(8), 1715-24.

Halestrap, AP. (2009). What is the mitochondrial permeability transition pore. *Journal of molecular and cellular cardiology, 46,* 821-831.

Halestrap, AP., Pasdois, P. (2008). The role of the mitochondrial permeability transition pore in heart disease. *Biochimica et biophysica acta, 1787,* 1402-1415.

Hammaker, D., Firestein, GS. (2010). "Go upstream, young man": lessons learned from the p38 saga. *Annals of the rheumatic disease, 77,* i77-82.

Han, J., Lee, JD., Bibbs, L., & Ulevitch, RJ. (1994). A MAP kinase targeted by endotoxin and hyperosmolarity in mammalian cells. *Science (New York, N.Y.), 265*(5173), 808–11.

Han, J., Lee, JD., Jiang, Y., Li, Z., Feng, L., Ulevitch, RJ. (1996). Characterization of the structure and function of a novel MAP kinase kinase (MKK6). *The journal of biological chemistry, 271*(6), 2886-91.

Heineke, J., Molkentin, JD. (2006). Regulation of cardiac hypertrophy by intracellular signalling pathways. *Nature review molecular cell biology, 7*(8), 589-600.

Heschelere, J., Meyer, R., Plant, S., Krautwurst, D., Rosenthal, W., Schultz, G. (1991). Morphological, biochemical, and electrophysiological characterization of a clonal cell (H9C2) line from rat heart. *Circulation research, 69*(6), 1476-86.

Hollander, W., Kirkpatrick, B., Paddock, J., Colombo, M., Nagraj, S., Prusty, S. (1979). Studies on the progression and regression of coronary and peripheral atherosclerosis in the cynomolgus monkey. I. Effects of dipyridamole and aspirin. *Exp Mol Patholo, 30*(1), 55-73.

Honndorf, VS., Coudevylle, N., Laufer, S., Becker, S., Griesinger, C. (2008). Dynamics in the p38αMAP kinase-SB203580 complex observed by liquid-state NMR spectroscopy. *Agnew Chem. Int. Ed Engl. 47*, 3548-3551.

Huber, JD., Bentzien, J., Boyer, SJ., Burke, J., De Lombaert, S…Eldrup, AB. (2012). Identification of a potent sodium hydrogen exchanger isoform 1 (NHE1) inhibitor with a suitable profile for chronic dosing and demonstrated cardioprotective effects in a preclinical model of myocardial infarction in the rat. *J Med Chem, 55*(16), 7114-40.

Itakura, K., Hirose, T., Crea, R., Riggs, AD., Heyneker, HL., Bolivar, F., Boyer, HW. (1977). Expression in Escherichia coli of a chemically synthesized gene for the hormone somatostatin. *Science, 198*(4321), 1056-63.

Ito, M., Miyado, ., Nakagawa, K., Muraki, M., Imai, M., Yaakawa, N., Qin, J., Hosoi, Y., Saito, H., Takahashi, Y. (2010). Age-associated changes in the subcellular localization of phosphorylated p38 MAPK in human granulose cells. *Molecular human reproduction, 16*(12), 928-37.

James, TN. (1998). The variable morphological coexistence of apoptosis and necrosis in human myocardial infarction: significance for understanding its pathogenesis, clinical course, diagnosis and prognosis. *Coron Artery Dis, 9*(5), 291-307.

Jennings, RB., Reimer, KA. (1991). The cell biology of acute myocardial ischaemia. *Annual reviews medicine, 42*, 225-46.

Johnson, G. (2002). Signal transduction. Scaffolding proteins – more than meets the eye. *Science, 295*(5558), 1249-50.

Kaiser, RA., Bueno, OF., Lips, DJ., Doevendans, PA., Jones, F., Kimball, TF., Molkentin, JD. (2004). Targeted inhibition of p38 mitogen –activated protein kinase antagonizes cardiac injury and cell death following ischaemia-reperfusion in vivo. *The journal of biological chemistry, 279*(15), 15524-30.

Kang, YJ., Seit-Nebi, A., Davis, RJ., Han, J. (2006). Multiple activation mechanisms of p38alpha mitogen-activated protein kinase. *The journal of biological chemistry, 281*(36), 26225-34.

Kerkela, R., Force, T. (2006). Recent insights into cardiac hypertrophy and left ventricular remodeling. *Current heart failure reports, 3*, 14-18.

Kimes, BW., Brandt, BL. (1976). Properties of a clonal muscle cell line from rat heart. *Experimental cell research, 98*(2), 367-81.

Kishida, S., Sanjo, H., Akira, S., Matsumoto, K., Ninomiya, TJ. (2005). TAK1-binding protein 2 facilitates ubiquitination of TRAF6 and assembly of TRAF6 with IKK in the IL-1 signalling pathway. *Genes cells, 10*(5), 447-54.

Klerber, AG. (1983). Resting membrane potential, extracellular potassium activity, and intracellular sodium activity during acute global ischemia in isolated perfused guinea pig hearts. *Circulation research, 52*(4), 442-50.

Komatsu, Y., Shibuya, H., Takeda, N., Ninomiya-Tsuji, J., Yasui, T., Miyado, K., Sekimoto, T., Uneno, N., Matsumoto, K., Yamada, G. (2002). Targeted disruption of the Tab1 gene causes embryonic lethality and defects in cardiovascular and lung morphogenesis. *Mechanism of development, 119*(2), 239-49.

Konstam, MA., Kramer, DG., Patel, AR., Maron, MS., Udelson, JE. (2011). Left ventricular remodeling in heart failure: current concepts in clinical significance and assessment. *JACC cardiovascular imaging, 4*(1), 98-108.

Korup, E. Dalsgaard, D., Nyvad, O., Jensen, TM., Toft, E., Berning, J. (1997). Comparision of degrees of left ventricular dilation within three hours and up to six days after onset of first acute myocardial infarction. *American journal of cardiology, 80*(4), 449-53.

Kumar, S., Jiang, MS., Aams, JL., Lee, JC. (1999). Pyridinylimidazole compound SB203580 inhibits the activity but not the activation of p38 mitogen-activated protein kinase. *Biochemical and biophysical research communications, 263*(3), 825-31.

Kumphune, S., Bassi, R., Jacquet, S., Sicard, P., Clark, J. E., Verma, S., … Marber, M. S. (2010). A chemical genetic approach reveals that p38alpha MAPK activation by diphosphorylation aggravates myocardial infarction and is prevented by the direct binding of SB203580. *The Journal of biological chemistry*, *285*(5), 2968–75.

Kumphune, S., Chattipakorn, S., & Chattipakorn, N. (2012). Role of p38 inhibition in cardiac ischemia/reperfusion injury. *European journal of clinical pharmacology*, *68*(5), 513–24. doi:10.1007/s00228-011-1193-2

Lambers, C., Roth, M., Zhong, J., Campregher, C., Binder, P., Burian, B., … Block, L.-H. (2013). The Interaction of Endothelin-1 and TGF-β1 Mediates Vascular Cell Remodeling. *PloS one*, *8*(8), e73399.

Lee, JC., Kumar, S., Griswold, DE., Underwood, DC., Votta, BJ., Adams, JL. (2000). Inhibition of p38 MAP kinase as a therapeutic strategy. *Immunopharmacology, 47*(2-3), 185-201.

Li, J., Miller, EJ., Ninomiya-Tsuji, J., Russell, RR., Young, LH. (2005). AMP-activated protein kinase activates p38 mitogen-activated protein kinase by increasing recruitment of p38 MAPK to TAB1 in the ischemic heart. *Circulation research, 97*(9), 872-9.

Liu, YH., Wang, D., Rhaleb, NE, Yang, XP., Xu, J., Sankey, SS., Rudolph, AE., Carretero, OA. (2011). Inhibition of p38 mitogen –activated protein kinase protects the heart against cardiac remodelling in mice with heart failure resulting from myocardial infarction. *Journal of cardiac failure, 11*(1), 74-81.

Lochhead, PA. (2009). Protein kinase activation loop autophosphorylation in cis: overcoming a catch-22 situation. *Science signalling, 2*(54), pe4.

Lozano, R., Naghavi, M., Foreman, K., Lim, S., Shibuya, K., Aboyans, V., Abraham, J., Adair, T., Aggarwal, R., Ahn SY., Lopez, AD., Murray, CJ., AlMazroa, MA., Memish, ZA. (2012) Global and regional mortality from 235 causes of death for 20 age groups in 1990 and 2010: a systematic analysis for the global burden of disease study 2010. *Lancet, 380*(9859), 2095-128.

Lorenz, K., Schmitt, JP., Schmitteckert, EM., Lohse, MJ. (2008). A new type of ERK1/2 autophosphorylation causes cardiac hypertrophy. *Nature medicine, 15*(1), 75-83.

Lu, G., Kang, YJ, Han, J., Herschman, HR., Stefani, E., Wang, Y. (2006). TAB-1 modulates intracellular localization of p38 MAP kinase and downstream signalling. *The journal of biological chemistry, 281*(9), 6087-95.

Ma, X. L., Kumar, S., Gao, F., Louden, C. S., Lopez, B. L., Christopher, T. A., … Yue, T. L. (1999). Inhibition of p38 mitogen-activated protein kinase decreases cardiomyocyte apoptosis and improves cardiac function after myocardial ischemia and reperfusion. *Circulation, 99*(13), 1685–91.

Mackay, K., & Mochly-Rosen, D. (1999). An inhibitor of p38 mitogen-activated protein kinase protects neonatal cardiac myocytes from ischemia. *The Journal of biological chemistry*, *274*(10), 6272–9.

Mao, Z., Bonni, A., Xia, F., Nadal-Vicens, M., Greenberg, ME. (1999). Neuronal activity-dependent cell survival mediated by transcription factor MEF2. *Science, 286*(5440), 785-90.

Marber, MS., Molkentin, JD., Force, T. (2010). Developing small molecules to inhibit kinases unkind to the heart: p38MAPK as a case in point. *Drug discovery today. Disease mechanisms, 7*(2), 123-127.

Marber, M. S., Rose, B., & Wang, Y. (2011). The p38 mitogen-activated protein kinase pathway--a potential target for intervention in infarction, hypertrophy, and heart failure. *Journal of molecular and cellular cardiology*, *51*(4), 485–90.

Marshall, RC., Nash, WW., Shine, KI., Phelps, ME., Ricchiuti, N. Glucose metabolism during ischemia due to excessive oxygen demand or altered coronary flow in the isolated arterially perfused rabbit septum. *Circ Res, 49,* 640-48.

Martin, ED., Bassi, R., Marber MS. (2015). p38 MAPK in cardioprotection – are we there yet. *British journal of pharmacology, 172*(8), 2101-13.

Martin, JL., Avkiran, M, Quinlan, RA., Cohen, P., Marber, MS. (2001). Antiischemic effects of SB203580 are mediated through the inhibition of p38alpha mitogen-activated protein kinase: Evidence from ectopic expression of an inhibition-resistant kinase. *Circulation research, 89*(9), 750-2.

Mayor, F Jr., Jurado-Pueyo, M., Campos, PM., Murga, C. (2007). Interfering with MAP kinase docking interactions: implications and perspective for the p38 route. *Cell cycle, 6*(5), 528-33.

McGill, HC., McMahan, CA., Gidding, SS. (2008). Preventing heart disease in the 21st century: implications of the pathobiological determinants of atherosclerosis in youth (PDAY) study. *Circulation, 117*(9), 1216-27.

McMullen, JR., Jennings, GL. (2007). Differences between pathological and physiological cardiac hypertrophy: novel therapeutic strategies to treat heart failure. *Clinical and experimental pharmacology and physiology, 34*(4), 255-62.

Medicherla, S., Fitzgerald, MF., Spicer, D., Woodman, P., Ma, JY., Kapoun, AM., Chakravarty, S., Dugar, S., Protter, AA., Higgins, LS. (2008) p38 alpha-selective mitogen-activated protein kinase inhibitor SD-282 reduces inflammation in a subchronic model of tobacco smoke-induced airway inflammation. *Journal of pharmacology and experimental therapeutics, 324*(3), 921-9.

Mendoza, H., Campbell, DG., Burness, K., Hastie, J., Ronkina, N., Shim, JH., Arthur, JS., Davis, RJ., Gaestel, M., Johnson, GL., Ghosh, S., Cohen, P. (2008). Roles for TAB1 in regulating the IL-1 dependent phosphorylation of the TAB3 regulatory subunit and activity of the TAK1 complex. *The biochemical journal, 409*(3), 711-22.

Mitchell, GF., Lamas, GA., Vaughan DE., Pfeffer, MA. (1992). Left ventricular remodeling in the year after first anterior myocardial infarction: a quantitative analysis of contractile segment lengths and ventricular shape. *Journal of the American college of cardiology, 19*(6), 1136-44.

Morioka, S., Broglie, P., Omori, E., Ikeda, Y., Takaesu, G., Matsumoto, K., Ninomiya, TJ. (2014). TAK1 kinase switches cell fate from apoptosis to necrosis following TNF stimulation. *Journal of cell biology, 204*(4), 607-23.

Murphy, MP. (2009). How mitochondria produce reactive oxygen species. *Biochemical journal, 417*, 1-13.

Murphy, E., Cross, HR., Steenbergen, C. (2002). Is Na/Ca exchange during ischemia and reperfusion beneficial or detrimental?. *Ann N Y Acad Sci, 976,* 421-30.

Nagai, H., Noguchi, T., Takeda, K., Ichijo, H. (2007). Pathophysiological roles of ASK1-MAP kinase signaling pathway. *J Biochem Mol Biol, 40*(1), 1-6.

Nagarkatti, DS., Sha'afi, RI. (1998). Role of p38 MAP kinase in myocardial stress. *Journal of molecular and cellular cardiology, 30*(8), 1651-64.

Ninomiya-Tsuji, J., Kishimoto, K., Hiyama, A., Inoue, J., Cao, Z., Matsumoto, K. (1999). The kinase TAK1 can activate the NIK-I kappaB as well as the MAP kinase cascade in the IL-1 signalling pathway. *Nature, 398*(6724), 252-6.

O'Donoghue, ML., Glaser, R., Cavender, MA., Aylward, PE., Bonaca, MP., Budaj, A., Davies, RY., Dellborg, M., Fox, KA., Gutierrez, JA., Hamm, C., Kiss, RG., Kovar, F., Kuder, JF., Im, KA., Lepore, JJ., LATITUDE-TIMI 60 Investigators. (2016). Effects of Losmapimod on cardiovascular outcomes in patients hospitalized with acute myocardial infarction: a randomized clinical trial. *The journal of American medical association, 315*(15), 1591-9.

Ono, K., & Han, J. (2000). The p38 signal transduction pathway: activation and function. *Cellular signalling, 12*(1), 1–13.

Ota, A., Zhang, J., Ping, P., Han, J., Wang, Y. (2010). Specific regulation of noncanonical p38alpha activation by Hsp90-Cdc37 chaperone complex in cardiomyocytes. *Circulation research, 106*(8), 1404-12.

Parasrampuria, DA., de Boer, P., Desai-Krieger, D., Chow, AT., Jones, CR. (2003). Single-dose pharmacokinetics and pharmacodynamics of RWJ67657, a specific p38 mitogen-activated protein kinase inhibitor: a first-in-human study. *The journal of clinical pharmacology, 43*(4), 406-13.

Park, JM., Greten, FR., Li, ZW., Karin, M. (2002). Macrophage apoptosis by anthrax lethal factor through p38 MAP kinase inhibition. *Science, 297*(5589), 2048-51.

Perregaux, DG., Dean, D., Cronan, M., Connely, P., Gaebl, CA. (1995). Inhibition of interleukin-1 bta production by SKF86002: evidence of two sites of in vitro activity and of a time and system dependence. *Molecular pharmacology, 48*(3), 433-42.

Pierce, MM., Raman, CS., Nall, BT. (1999). Isothermal titration calorimetry of protein-protein interactions. *Methods, 19*(2), 213-21.

Pietersma, A., Tilly, BC., Gaestel, M., de Jong, N., Lee, JC., Koster, JF., Sluiter, W. (1997). p38 mitogen activated protein kinase regulates endothelial VCAM-1 expression at the post-transcriptional level. *Biochemical and biophysical research communication, 230*(1), 44-48.

Porras, A., Zuluaga, S., Black, E., Valladares, A., Alvarez, AM., Ambrosino, C., Benito, M., Nebreda, AR. (2004). p38 alpha mitogen-activated protein kinase sensitizes cells to apoptosis induced by different stimuli. *Molecular biology of the cell, 15*(2), 922-33.

Prickett, TD., Ninomiya-TJ., Broglie, P., Muratore-Schroeder, TL., Shabanowitz, J., Hunt, DF., Brautigan, DL. (2008). TAB4 stimulates TAK1-TAB1 phosphorylation and binds polyubiquitin to direct signalling to NF-kappaB. *Journal of biological chemistry, 283*(28), 19245-54.

Raingeaud, J., Gupta, S., Rogers, JS., Dickens, M., Han, J., Ulevitch, RJ., Davis, RJ. (1995). Pro-inflammatory cytokines and environmental stress cause p38 mitogen-activated protein kinase activation by dual phosphorylation on tyrosine and threonine. *The journal of biological chemistry, 270*(13), 7420-6.

Rajpurohit, N., Ayaz, SZ., Yee, J., Khan, MA., Stys, A. (2015). Review of acute coronary syndromes: diagnosis and management of unstable angina and non ST-elevation myocardial infarction. *S D Med, 68*(2), 71-3.

Ren, J., Zhang, S., Kovacs, A., Wang, Y., Muslin, AJ. (2005). Role of p38alpha MAPK in cardiac apoptosis and remodelling after myocardial infarction. *Journal of molecular and cellular cardiology, 38*(4), 617-23.

Risco, A., & Cuenda, A. (2012). New Insights into the p38γ and p38δ MAPK Pathways. *Journal of signal transduction, 2012*, 520289.

Ross, R. (1999). Atherosclerosis – an inflammatory disease. *New England Journal of Meidcine, 349*(2), 115-26.

Ross, R., Glomset, JA., (1973). Atherosclerosis and the arterial smooth muscle cell: Proliferation of smooth muscle is a key event in the genesis of the lesions of atherosclerosis. *Science, 180*(4093), 1332-9.

Rubin, SA., Fishbein, MC., Swan, HJ. (1983). Compensatory hypertrophy in the heart after myocardial infarction in the rat. *Journal of the American college of cardiology, 1*(6), 1435-41.

Ruwald, AC., Gang, U., Thomsen, PE., Jorgensen, RM., Ruwald, MH., Huikuri, HV., Jons, C. The predictive value of CHADS2 risk score in post myocardial infarction arrhythmias – a cardiac arrhythmias and risk stratification after myocardial infarction (CARISMA) substudy. *Int J Cardiol, 173*(3), 441-6.

Salvador, J. M., Mittelstadt, P. R., Guszczynski, T., Copeland, T. D., Yamaguchi, H., Appella, E., … Ashwell, J. D. (2005). Alternative p38 activation pathway mediated by T cell receptor-proximal tyrosine kinases. *Nature immunology*, *6*(4), 390–5.

Sarkar, D., Su, ZZ., Lebedeva, IV., Sauane, M., Gopalkrishnan, RV., Valerie, K., Dent, P., Fisher, PB. (1999). Mda-7 (IL-24) mediates selective apoptosis in human melanoma cells by

inducing the coordinated over-expression of the GADD family of genes by means of p38 MAPK. *Proc Natl Acad Sci, 99*(15), 10054-9.

Saurin, A. T., Martin, J. L., Heads, R. J., Foley, C., Mockridge, J. W., Wright, M. J., … Marber, M. S. (2000). The role of differential activation of p38-mitogen-activated protein kinase in preconditioned ventricular myocytes. *FASEB journal : official publication of the Federation of American Societies for Experimental Biology, 14*(14), 2237–46.

Scherer, WF., Syverton, JT., Gey, GO. (1953). Studies on the propagation in vitro of poliomyelitis viruses. IV. Viral multiplication in a stable strain of human malignant epithelial cells (strain HeLa) derived from an epidermoid carcinoma of the cervix. *The journal of experimental medicine, 97*(5), 695-710.

Schneder, S., Chen, W., Hou, J. Steenbergen, C., Murphy, E. (2001). Inhibition o p38 MAPK alpha/beta reduces ischemic injury and does not block protective effects of preconditioning. *American journal of physiology. Heart and circulatory physiology, 280*(2), 499-508.

Schreiber, S., Feagan, B., D'Haens, G., Colomel, JF., Geboes, K., Yurcov, M., Isakov, V., Golovenko, O., Bernstein, CN., Ludwig, D., Winter, T., Meier, U., Yong, C., Steffgen, J., BIRB796 study group. (2006). Oral p38 mitogen-activated protein kinase inhibition with BIBR796 for active Crohn's disease: a randomized, double-blind, placebo-controlled trial. *Clinical gastroenterology and hepatology, 4*(3), 325-34.

See, F., Thomas, W., Way, K., Tzanidis, A., Kompa, A., Lewis, D., Itescu, S., Krm, H. (2004). p38 mitogen-activated protein kinase inhibition improves cardiac function and attenuates left ventricular remodelling following myocardial infarction in the rat. *Journal of the American college of cardiology, 44*(8), 1679-89.

Seidlmayer, LK., Juettner, VV., Kettlewell, S., Pavlov, EV., Blatter, LA., Dedkova, EN. (2015. Distinct mPTP activation mechanisms in ischaemia-reperfusion: contribution of Ca2+, ROS, pH, and inorganic polyphosphate. *Cardiovasc Res, 106*(2), 237-48.

Shibuya, H., Yamaguchi, K., Shirakabe, K., Tonegawa, A., Gotoh, Y., Ueno, N., … Matsumoto, K. (1996). TAB1: an activator of the TAK1 MAPKKK in TGF-beta signal transduction. *Science (New York, N.Y.), 272*(5265), 1179–82.

Shimizu, I., Minamino, T. (2016). Physiological and pathological cardiac hypertrophy. *J Mol Cell Cardiol. 97*¸245-62.

Shin, MS., Shinghirunnusorn, P., Sugishima, Y., Nishimura, M., Suzuki, S., Koizumi, K., Saiki, I., Sakurai, H. (2009). Cross interference with TNF-alpha-induced TAK1 activator via EGFR-mediated p38 phosphorylation of TAK1-binding protein1. *Biochimica et biophysica acta-molecular cell research, 1973*(7), 1156-64.

Shrestha, A., Hamilton, G., O'Neill, E., Enapp, S., Elkins, JM. (2012). Analysis of conditions affecting auto-phosphorylation of human kinases during expression in bacteria. *Protein expression and purification, 81*(1), 136-43.

Sicard, P., Clark, JE., Jacquet, S., Mohammadi, S., Arthur, JS., O'Keefe, SJ., Marber, MS. (2010). The activation of p38 alpha, and not p38 beta, mitogen-activated protein kinase is required for ischemic preconditioning. *Journal of molecular and cellular cardiology, 48*(6), 1324-8.

Stanley, WC. (2001). Changes in cardiac metabolism: a critical step from stable angina to ischaemic cardiomyopathy. *European Heart Journal Supplements, 3*(O), O2-7.

Stanley, WC., Lopaschuk, GD., Hall, JL., McCormack, JG. (1997). Regulation of myocardial carbohydrate metabolism under normal and ischaemic conditions. Potential for pharmacological interventions. *Cardiovascular Research, 33*(2), 243-57.

Takaesu, G., Kishida, S., Hiyama, A., Yamaguchi, K., Shibuya, H., Irie, K., Ninomiya-Tsuji, J., Matsumoto, K. (2000). TAB2, a novel adaptor protein, mediates activation of TAK1 MAPKKK by linking TAK1 to TRAF6 in the IL-1 signal transduction pathway. *Molecular cell, 5*(4), 649-58.

Tanno, M., Bassi, R., Gorog, D. A., Saurin, A. T., Jiang, J., Heads, R. J., … Marber, M. S. (2003). Diverse mechanisms of myocardial p38 mitogen-activated protein kinase activation: evidence for MKK-independent activation by a TAB1-associated mechanism contributing to injury during myocardial ischemia. *Circulation research, 93*(3), 254–61.

Vanderkerken, K., Medicherla, S., Coulton, L., De Raeve, H., Willems, A., Lawson, M., Van Camp, B., Protter, AA., Higgins, LS., Menu, E., Croucher, PI. (2007). Inhibition of p38alpha mitogen –activated protein kinase prevents the development of osteolytic bone disease, reduces tumor burden, and increases survival in murine models of multiple myeloma. *Cancer research, 67*(10), 4572-7.

Ventura, JJ., Tenbaum, S., Perdiguero, E., Huth, M., Guerra, C., Barbacid, M., Pasparakis, M., Nebreda, AR. (2007). p38 alpha MAP kinase is essential in lung stem and progenitor cell proliferation and differentiation. *Nature genetics, 39*(6), 750-8.

Volders, PG., Willems, IE., Cleutjens, JP., Arends, JW., Havenith, MG., Daemen MJ. (1993). Interstitial collagen is increased in the non-infarcted human myocardium after myocardial infarction. *Journal of molecular and cellular cardiology, 25*(11), 1317-23.

Wang, Y. (2007). Mitogen-activated protein kinases in heart development and disease. *Circulation, 116*(12), 1413-23.

Webster, KA. (2012). Mitochondrial membrane permeabilization and cell death during myocardial infarction: roles of calcium and reactive oxygen species. *Future cardiology, 8*(6), 863-884.

Westra, J., Limburg, PC., de Boer, P., van Rijswijk, MH. (2004). Effects of RWJ67657, a p38 mitogen activated protein kinase (MAPK) inhibitor, on the production of inflammatory mediators by rheumatoid synovial fibroblasts. *Annals of the rheumatic disease, 63*(11), 1453-1459.

Wilson, KP., Fitzgibbon, MJ., Caron, PR., Griffith, PJ., Chen, W., McCaffrey, PG., Chambers, SP., Su, MS. (1996). Crystal structure of p38 mitogen-activated protein kinase. *The journal of biological chemistry, 271*(44), 27696-700.

Wood, CD., Thornton, TM., Sabio, G., Davis, RA., Rincon, M. (2009). Nuclear localization of p38 MAPK in response to DNA damage. *International journal of biological sciences.*

Wolf, A., Beuerlein, K., Eckart, C., Weiser, H., Dickkopf, B., Müller, H., … Kracht, M. (2011). Identification and functional characterization of novel phosphorylation sites in TAK1-binding protein (TAB) 1. *PloS one, 6*(12), e29256.

Wolff, T., Miller, T., Ko, S., (2009). Aspirin for the primary prevention of cardiovascular events: an update of the evidence for the U.S. Preventive services task force. *Ann Intern Med, 150*(6), 405-410.

Wong, ND. (2014). Epidemiological studies of CHD and the evolution of preventive cardiology. *Nature reviews. Cardiology, 11*(5), 276-89.

Young, P. R., McLaughlin, M. M., Kumar, S., Kassis, S., Doyle, M. L., McNulty, D., … Lee, J. C. (1997). Pyridinyl imidazole inhibitors of p38 mitogen-activated protein kinase bind in the ATP site. *The Journal of biological chemistry*, *272*(18), 12116–21.

Yoshida, H., Kisugi, R., (2010). Mechanisms of LDL oxidation. *Clin Chim Acta, 411*(23-24), 1875-82.

Yurtsever, Z., SCheaffer, SM., Romero, AG., Holtzman, MJ., Brett, TJ. (2015). The crystal structure of phosphorylated MAPK13 reveals common structural features and differences in p38 MAPK family activation. *Acta Crystallogr D Biol Crystallogr, 71*(4), 790-9.

Zaino, EC., Tabor, SH. (1963). Cardiac hypertrophy in acute myocardial infarction. A study based on 100 autopsied cases. *Circulation, 28*, 1081-3.

Zarubin, T., & Han, J. (2005). Activation and signaling of the p38 MAP kinase pathway. *Cell research*, *15*(1), 11–8.

Zetser, A., Gredinger, E., Bengal, E. (1999). p38 mitogen-activated protein kinase pathway promotes skeletal muscle differentiation. Participation of the Mef2c transcription factor. *The journal of biological chemistry, 274*(8), 5193-200.

Zhang, J., Shen, B., Lin, A. (2007). Novel strategies for inhibition of the p38 MAPK pathway. *Trends in pharmacological sciences, 28*(6), 286-95.

Zhang, M., Zhu, H., Ding, Y., Liu, Z., Cai, Z., Zou, MH. (2017). AMP-activated protein kinase α1 promotes atherogenesis by increasing monocyte-to-macrophage differentiation. *J Biol Chem, 117*(9), 44-47.

Zhao, F., Li, YW., Pan, HJ., Shi, CB., Luo, XC., Li, AX., Wu, SQ. (2014). TAK1-binding proteins (TAB1 and TAB2) in grass carp (Ctenopharyngodon idella): identification, characterization, and expression analysis after infection with Ichthyophthirius multifiliis. *Fish and Shellfish Immunology, 38*(2), 389-99.

Zhou, H., Zheng, M., Chen, J., Xie, C., Kolatkar, A. R., Zarubin, T., … Han, J. (2006). Determinants that control the specific interactions between TAB1 and p38alpha. *Molecular and cellular biology*, *26*(10), 3824–34.